Biological evaluation of novel peptidic vectors for transmembrane delivery of intracellularly targeted probes for molecular imaging

Biologische Studien an neuartigen peptidischen Vektoren für die transmembrane Aufnahme intrazellulärer Kontrastmittel zur molekularen Bildgebung

der Fakultät für Biologie
der EBERHARD KARLS UNIVERSITÄT TÜBINGEN

zur Erlangung des Grades eines Doktors
der Naturwissenschaften

von

Ritu Mishra
aus Bathinda

vorgelegte

DISSERTATION

2009

Tag der mündlichen Prüfung:	9. Oktober 2009
Dekan:	Prof. Dr. Hanspeter A. Mallot
1. Berichterstatter	Prof. Dr. Alfred Nordheim
2. Berichterstatter	Prof. Dr. Roland Brock

To

My father

who sparked the flame of science in me, and

My husband

who kept this flame burning…

This PhD thesis was prepared at the Max-Planck Institute for Biological Cybernetics (Chemical Biology Laboratory of the Department of High Field Magnetic Resonance Center, Dr. Joern Engelmann) in collaboration with the Department of Molecular Biology, Interfaculty Institute for Cell Biology, Eberhard-Karls-University, Tübingen under the guidance of Prof. Dr. Alfred Nordheim during the period from April 2004 to June 2009.

Hereby I declare the fact that I wrote this work and no different than the indicated aids have been used.

Tübingen, June, 2009

Acknowledgements

The accomplishment of my PhD work would be partial without expressing a word of appreciation for the people who helped and supported me for the successful completion of my thesis.

First of all I would like to thank Dr. Joern Engelmann, who unconditionally supervised as well as advised me all these years. Through his inexhaustible enthusiasm, optimism and patience I learnt to continue to endeavor under any circumstances. I greatly appreciate his meticulous participation in preparation of work presentations followed by endless discussions. I admire his understanding nature and ability to ignore serious mistakes committed by me.

I wish to express my deepest reverence to Prof. Dr. Kamil Ugurbil and Dr. Josef Pfeuffer for considering me suitable to undertake a crucial role in the freshly conceived department. I owe deep gratitude for their help and advice at the beginning of this project and still after they advanced from MPI for other ventures.

Special thanks to Prof. Dr. Roland Brock for thought provoking discussions and critical comments. His suggestions steered new directions in the project. Also I am grateful to him for keeping our long distance alliance alive over these years. I appreciate him for devoting time to read my thesis and coming all the way from Nijmegen for conducting the exam.

I express my heartfelt gratitude to Prof. Dr. Alfred Nordheim for gladly agreeing to examine my thesis. I certainly thank him for his time and co-operation while going through my thesis, helping with the submission and conducting my official PhD examimation.

I sincerely gratify the support, hard work and assistance of Dr. Wu Su, Deepti Jha, Dr. Rajendra Joshi and Aneta Brud. Without the efforts of all these chemists my PhD thesis would not have materialized. I greatly enjoyed the wonderful scientific and non-scientific discussions and thank them for their trust and help in the experiments as well as in personal concerns. Another special person worthy acknowledgement is Hildegard Schulz. I owe her sincere gratitude for all the assistance provided and appreciate her never ending passion for work and science.

I am very thankful to Dr. Rolf Pohmann and Dipl.-Ing. Michael Beyerlein for performing MRI measurements. I deeply appreciate the enormous help by Mihai Vintiloiu for computer related issues especially his quick backups every time the microscope computer broke down. Special thanks to Tina Schroeder for all the help on the administrative as well as personal arrangements.

I feel lacunae of words to express sentiments for Ranganathan family, Gunomany family, Suryadeep Dash, Vikram Alva and Dr. Kirti Dhingra for sharing many light moments together and giving me moral support and resilience during critical times.

Finally, most of all, I thank my family members for their unconditional love, and encouragement. I appreciate the deep faith my parents, Meenakshi and Om Prakash Kamboj, and my parents-in law, Pratibha and Kamlesh Kumar Misra, showed in all my deeds. I could have never come so far if my mother, in spite of her sickness, would not have checked me in examination nights if I was learning.

Words are insufficient to convey my gratefulness to my wonderful husband, Dr. Anurag Mishra. He patiently accompanied me through these PhD years, which were not always enjoyable, and at times also clarified Chemistry concepts. A smile of my darling daughter, Arshiya Mishra, was enough for me to forget all the stress on the days I came home disappointed with results. I owe you both all my achievements and to be able to give back all your love.

I also thank all those who could not find a separate name but have helped directly and indirectly.

Table of Contents

Chapter 1: General introduction

1.1 Preamble

1.1.1 Molecular imaging

The completion of the Human Genome Project lead to the outburst of research related to gene and cell based therapies (*1*). These therapies promise progress for the treatment of numerous genetic metabolic diseases, cancers as well as neurological, cardiovascular, immunological or inherited disorders. In spite of the effort for several years, no human gene therapy product has yet been approved by the Food and Drug Administration (FDA). This necessitated the development of modalities to decipher the reasons for successes and failures of these therapies by direct visualization of biological processes at the sub-cellular level. The available traditional diagnostic methods have limited application in this case. These conventional ways are primarily based on the macroscopic observations of morphological and physiological changes appearing as a result of underlying molecular processes. However, a recent biomedical discipline emerged that allows the possibility to directly evaluate the differences at the molecular level in intact living organisms (*2*). Appropriately designated as "Molecular Imaging", this discipline has been defined as 'the *in vivo* characterization and measurement of biological processes at the cellular and molecular level' (*3*). Other variations to the definition are also proposed for the field but all of them emphasize on the same theme (*4, 5*). Apart from gene imaging, molecular imaging proposes the utilization of diverse imaging modalities for evaluating molecular events like protein-protein interactions, optimize drug therapy and observe their effects at sub-cellular levels, to assess the progression of diseases starting at the molecular level and to traffic and target cells *in vivo*.

Molecular imaging offers several benefits over routine *in vitro* or cell culture methods. An interesting aspect of molecular imaging is that by using specific probes it can follow biological processes in intact living organism using minimum invasive techniques. This, in addition, permits repeated measurements on the same object at different time points. Also a combination of different imaging modalities could be applied to gain insight into the temporal and spatial biodistribution of a specific probe in the midst of complex network of several other biological processes. These developments would facilitate the extrapolation of observations from whole laboratory animals to use in human scenario. The most widely used imaging technologies include radionuclide imaging (positron emission tomography (PET), single photon emission computed tomography (SPECT), etc.), optical imaging (fluorescence,

bioluminescence), computed tomography imaging (CT) and magnetic resonance imaging (MRI) (*3*, *5*) (Fig. 1). Depending on the final application, each of these techniques possesses some benefits and some drawbacks. On one hand PET is a highly sensitive method but has a poor spatial resolution. Fluorescence imaging is time–efficient but limited by depth penetration and MRI offers excellent three-dimensional resolution but needs improvement in sensitivity. Recent advancements involve the coupling of two or more techniques leading to multi-modality molecular imaging which improves their distinct advantages (*4*, *6-8*).

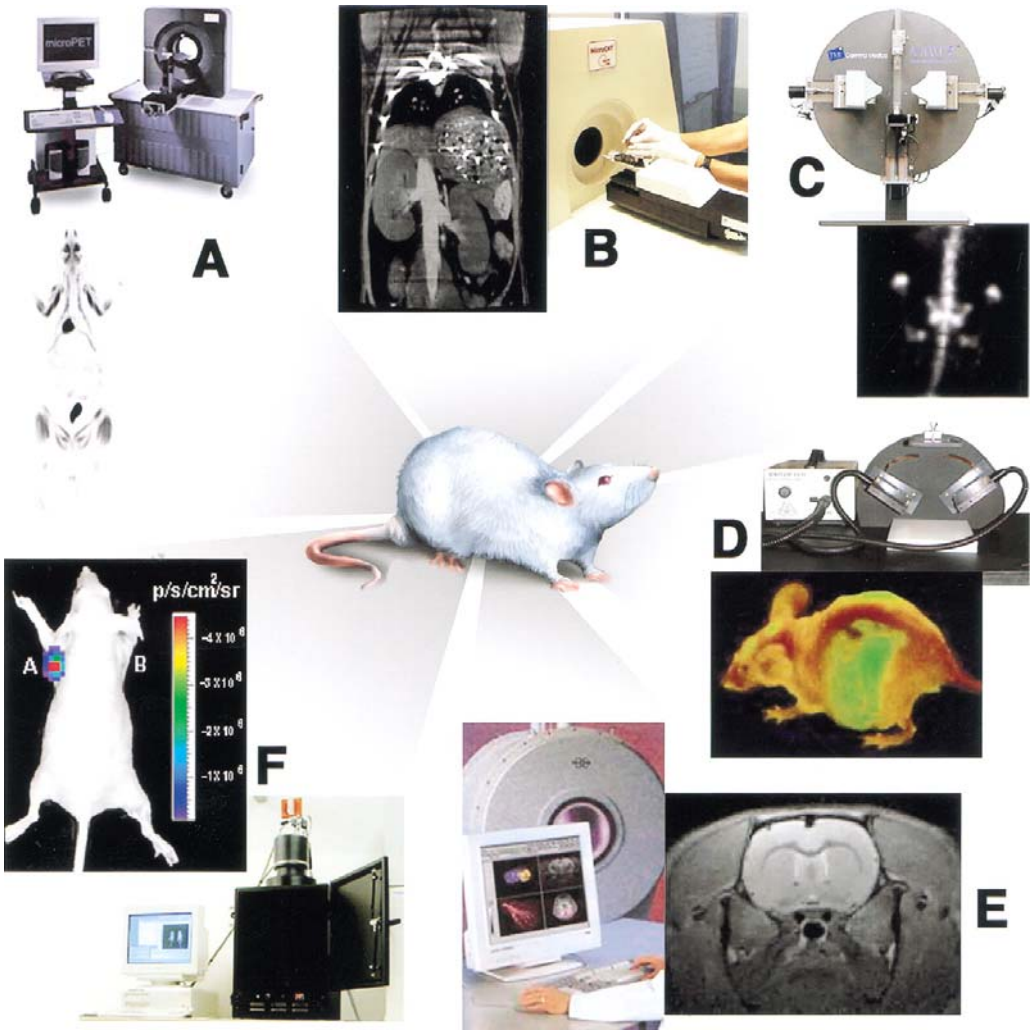

Figure 1. Overview of multiple imaging modalities available for molecular imaging of small laboratory animals (A) microPET, (B) microCT, (C) microSPECT, (D) optical reflectance fluorescence, (E) microMRI (F) optical bioluminescence image. (adapted from Massoud *et al.* (*5*).

Amongst the various biological imaging techniques, advances in MRI have revolutionized the way in which biological processes are being investigated. It offers a noninvasive means to chart structure and function with high spatial resolution without use of harmful radiations. Through MRI, three-dimensional imaging of soft tissues is performed by assessing the amount, flow and environment of water protons *in vivo*. The signal intensity of the image obtained depends on the water content, relaxation times (T_1, the longitudinal relaxation time and T_2, the transverse relaxation time) and/or diffusion characteristics (*9*). MRI is not limited by light scattering, as optical microscopic techniques and offers a resolution in the range of tens of μm. However, the low sensitivity of this technique needs longer imaging times and therefore, slow acquisition of data, thus compromising the temporal resolution.

The intrinsic signal generated in MR images can be further enhanced by contrast agents (CAs) to better visualize regions, tissues and cells that are magnetically similar but histologically distinct (*10*). The effect of CA on the MR signal is indirect as it does not appear on the CA but on the surrounding water protons. The efficiency of the CAs depends on their relaxivity defined as the increase of the nuclear relaxation rate (the reciprocal of the relaxation time) of water protons produced by 1 mmol per liter of CA (expressed in $s^{(-1)}$ $mmol^{(-1)}L$). The number of water molecules in the first coordination sphere, the water exchange rate and the rotational correlation time have a strong effect on their relaxivity. Based on the changes in T_1 and T_2 relaxation rates, CAs in MRI have been categorized as positive agents, producing increased signal intensity on T_1-weighted images, or negative agents, showing decreased signal intensity on T_2-weighted images, or both (*11*). T_1 CAs mainly contain the paramagnetic metal ion gadolinium (Gd) (*12, 13*) while most of the T_2 agents are based on superparamagnetic iron oxide particles (*14*). To put in a simpler way, images of regions where the CAs are located appear brighter with Gd-based agents and those with iron-based agents appear darker.

As the free metal ion of Gd is toxic, it needs to be complexed to ensure the safety of the agent during its passage through the body of the patient. Two of the widely used CAs are the acyclic chelator diethylenetriaminepentaacetic acid (DTPA) or the more stable macrocyclic chelator 1,4,7,10-tetracarboxymethyl-1,4,7,10-tetraazacyclododecane (DOTA) (Fig. 2) (*13*). The Gd metal ion needs to be loaded into these chelators for use as a CA. As a result of their kinetic inertness and thermodynamic stability, they remain chelated in the body and are

excreted intact. Based on these chelators, a handful of CAs (like Magnevist®, DOTAREM®, etc.) are clinically approved and commercially available but most of them are exogenous, restricted to the extracellular space, non-specific and also need to be applied in a concentration range between 0.01 to 10 mM. They are marked by unselective biodistribution over the extracellular fluid and the resultant contrast is dependent on their tissue permeability versus the clearance rate.

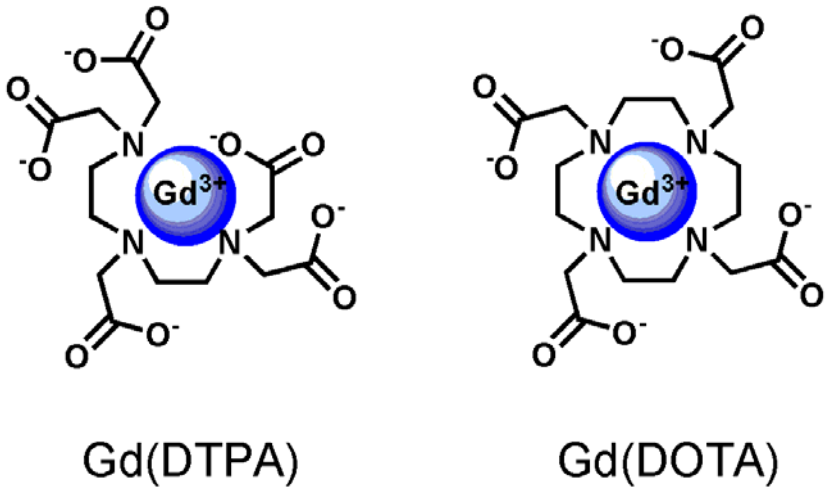

Figure 2. Chemical structures of Gd(DTPA) and Gd(DOTA).

New classes of MRI CAs are gradually emerging in the context of molecular imaging. These agents need to be designed for showing higher contrasting ability and improved specificity for characterization of cellular and molecular processes. Almost all of the available CAs till date have been compiled in an extensive review by Yoo *et al.* (*15*). Though most MR investigations for molecular imaging were based on iron nanoparticles but the issues relating to the metabolic fate of these iron-based agents and retention of their high concentrations in the cellular cytoplasm led to the exploration of Gd-based CAs for molecular imaging (*16*, *17*).

1.1.2 Targets for intracellular imaging

The cell is the most basic unit of life. It is the smallest unit of an organism that has been classified as living but is still extremely complicated. The complexity arises as a result of a myriad of biological processes simultaneously going on in the cell to maintain its function (Fig. 3). These processes, like protein synthesis, cellular metabolism, DNA replication, cell signaling, etc., are fundamental and involve intricate cascades of biochemical reactions. In

fact, cellular processes are carried out by the combined activity of numerous genes, their products, and a variety of other molecules.

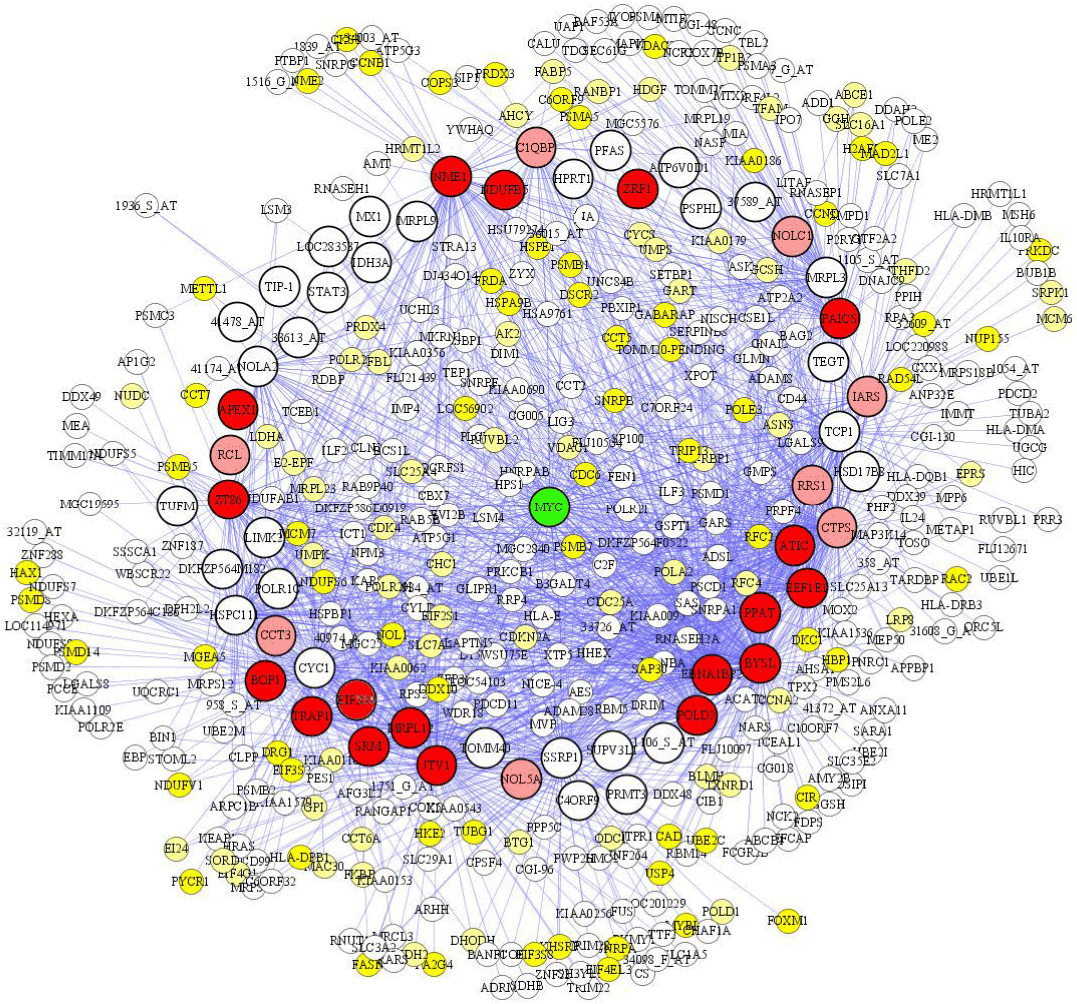

Figure 3. The complexity of biological processes essential for proper functioning of a cell. (adapted from the webpage of MAGnet, http://magnet.c2b2.columbia.edu/). The circles here indicate the collection of biomolecules which are in constant interaction with one another, depicted by the dense network of lines, for proper functioning of the cell.

Interestingly, any of these cellular components from the cellular pool could be recognized as targets keeping the final purpose of application in view. The generic cellular targets comprise of DNA, messenger RNA and proteins. In drug development, proteins, especially receptors and enzymes, have been generally exploited. The major reason for application of proteins as targets was related to their large numbers per cell (Table 1). Imaging of protein based targets, referred as "downstream imaging", has been well explored for *in vivo* molecular imaging as it requires little signal amplification (*18-20*). Apart from the ones

already used, there exists a collection of almost ten times more enzymes, receptors, antigens, etc. that are still to be tried and tested for application as targets.

Table 1. Different intracellular imaging targets and their number per cell. (adapted from Sharma *et al.* (*21*)).

Target	Number/cell
Gene (DNA)	2
Message	50-1,000
Protein	100 - 1,000,000
Function	massive

Nevertheless, to be able to directly image gene expression for the understanding of genetic defects from the origin, therapy assessment and many more applications, imaging at DNA and mRNA level is necessary. Use of DNA as a target, with only two molecules per cell (*21*), requires extraordinary mechanisms for enhancing the signal to noise ratio. Fluorescence *in situ* hybridization (FISH) exists as a method for imaging DNA at cellular level. Such technologies and methods still need to be developed for whole body imaging. Moreover, monitoring the DNA provides information on genetic alterations and not on its expression and normal or abnormal function.

The copy number for mRNA ranges from a few hundred to few thousand copies in a single cell. Although not most favorable for imaging by MR, combinations with amplification techniques are being developed to directly image mRNA and obtain information on cellular gene expression in normal and diseased conditions.

1.1.3 Antisense imaging

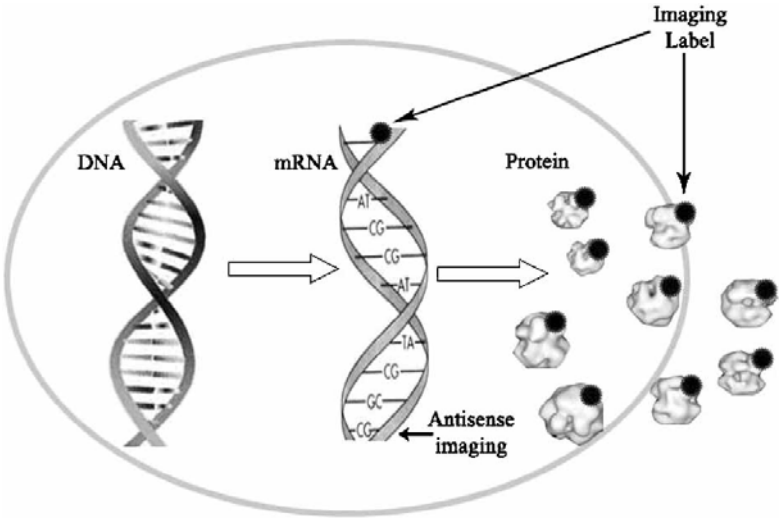

Figure 4. Schematic representation of antisense imaging in the context of cellular gene expression, contrasted with imaging of proteins and reporter protein function. (adapted from Lewis et al. (*22*)).

According to the central dogma of molecular biology, the principal role of mRNA is to transfer the genetic information contained in the DNA for translation to the protein level. Transcription is the process of RNA synthesis through which information is transferred between DNA sequence and a complementary mRNA by formation of Watson-Crick base pairs. Any synthetic short oligonucleotide with a sequence complementary to the target mRNA is referred as antisense (Fig. 4). The antisense sequence binds to the target and mostly inhibits its translation. This concept is being used for antisense chemotherapy to inhibit the translation of a defective gene for treatment of various cancers and viral diseases. Antisense drug development continues further with a drug (Vitravene, Isis) for the treatment of cytomegalovirus-induced retinitis in AIDS patients already approved by the US FDA (*23*) and some more in late-stage development.

In 1994, Dewanjee et al. presented a pioneer study to image a mouse tumor in vivo using a radiolabeled DNA sequence complementary to the initiation code of c-myc oncogene RNA (*24*). Although it is still to be verified, this study suggested the use of labeled antisense oligonucleotide analogues for imaging of gene expression and thus the conceptualization of antisense imaging (Fig. 4). Due to increased sensitivity, mostly radiolabeling has been used for antisense imaging studies (*25-27*). In spite of various efforts, until date no real-time, direct, *in vivo* imaging has been demonstrated in a conclusive manner. But the field has not been dormant and progress has been made to remove some bottlenecks by means of development of higher affinity antisense analogues, development of protocols to assess target interaction, improved cellular delivery, etc. (*22, 28*).

While a direct depiction of antisense targeting is still hard to define even in cell culture, most studies rely on indirect evidences. Increased accumulation against different targets and in different cell types compared to control suggested an involvement of antisense mechanism (*29, 30*). Another investigation demonstrated that accumulation of probe decreases with increasing concentration of (*31, 32*). This indicates that with increasing dosage binding becomes saturated.

The first antisense agents used were unmodified phosphodiester DNAs. But their fast degradation by nucleases in vivo hindered their use for imaging. The new generation of oligonucleotide analogues show improved stability and target binding. By varying the backbone of oligomers large variations can be imparted in their properties. DNA phosphorothioates show higher biological stability (*33*) and have been used for antisense therapy as they activate RNase H mediated degradation of mRNA. As only 5-6 base pairs are involved in duplex formation and therefore have a high possibility of also degrading the non-target mRNAs, it has been concluded that RNase H-independent analogs would be preferred for imaging (*28*). By introducing an artificial backbone in place of the ribose scaffold of DNA and RNA, new analogs have been developed. These analogs bind complementary DNA with greater affinity and include peptide nucleic acids (PNA) (*34*), morpholino (MORF) (*35*), trans-4-hydroxy-L-proline nucleic acid-phosphono nucleic acid (HypNA-pPNA) (*36*) and 2'-*O*-methyl small interfering RNA (siRNA) (*37*). However, the use of most of these modified analogs is limited to laboratories with a monomer synthesis facility as only PNAs and MORFs are commercially available.

As their nomenclature suggests, PNAs contain a neutral peptide backbone instead of the negatively charged sugar-phosphate backbone in DNA (*38*). PNAs have several properties that make them favorable for application. The duplexes between PNA/DNA and PNA/RNA show higher thermal stability than DNA/DNA or DNA/RNA duplexes (*39*). The absence of charge repulsion between neutral PNA and DNA or RNA leads to a stronger binding between them. Also, PNA show a greater specificity to bind to the target sequence and binding occurs at low ionic strength where normal DNA binding would not take place. Another advantage of their peptide backbone is the resistance to nucleases and proteases, thus, extending their lifetime (*40*). PNAs are being utilized for a multitude of applications (*38*) but two major problems still need to surmounted. The first is the poor solubility in aqueous solution arising from the charge-neutral backbone which, therefore, also is related to the length of oligomer (*39*). The second issue is their inadequate cellular uptake leading to a low intracellular accumulation of PNAs. This is a serious challenge for in vivo applications and new methods need to be investigated to assist the delivery of PNAs across the plasma membrane.

1.1.4 The plasma membrane

The cell evolved as a highly organized structure with barriers that define its inside and outside. The plasma membrane serves as the boundary of cells and protects it from the

surrounding environment. The eukaryotes also contain intracellular membranes that define internal organelles like nucleus, mitochondria, lysosomes, etc. Membranes are as diverse in structure as they are in function. They are dynamic structures but have a common membrane architecture composed of a lipid bilayer with proteins floating in this sea of lipids (Fig. 5). The membrane lipids are amphipathic molecules as they contain a hydrophilic polar head group pointing out and a hydrophobic moiety forming the core (*41*). The thickness of most membranes is between 60 Å (6 nm) and 100 Å (10 nm). Membranes also contain carbohydrates that are linked to lipids (glycolipids) and proteins (glycoproteins). Most cell membranes are electrically polarized, such that the inside is negative [typically -60 millivolts (mV)]. The membrane potential plays a key role in transport, energy conversion, and excitability.

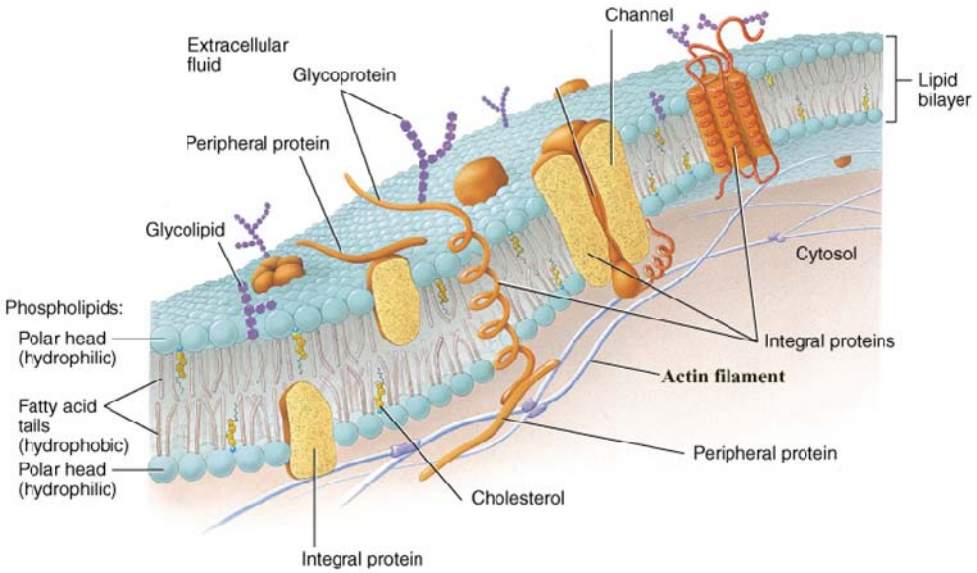

Figure 5: Diagrammatic representation of the plasma membrane. (adapted from an online representation under copyright by John Wiley & Sons, Inc.).

The lipid components of the membrane act as a permeability barrier while the proteins permit limited transport and impart selective permeability to the membrane. Membrane proteins are embedded in the lipid bilayer, which creates a suitable environment for their action. These proteins can be categorized as peripheral or integral based on the difference in their dissociability. Peripheral membrane proteins are loosely bound to membranes mainly by electrostatic and hydrogen-bond interactions with the head groups of lipids. In contrast, integral membrane proteins interact strongly with the hydrocarbon chains of membrane

lipids, and are embedded in the lipid bilayer. These embedded proteins are also amphipathic with their side chains oriented in hydrophobic and hydrophilic regions of the lipid bilayer.

Due to their own physicochemical characteristics and the functional characteristics of the embedded transmembrane proteins, the plasma membranes are selectively permeable. Their structure allows specific molecules to be taken up and unwanted compounds to be removed from the cell. All transport across cell membranes occurs by one of the following fundamental processes:

- Passive transport: Through this process, molecules are transported across the membrane barrier without spending any energy. Usually small molecules like water, oxygen gas and some ions enter into cells by passive transport. The transport is driven by a concentration gradient (diffusion) or osmotic gradient (osmosis). Movement of ions could be energy independent but assisted by channels (facilitated diffusion).
- Active transport: This procedure is also used for the transport of small molecules but depends upon the expenditure of cellular energy. The active transport can move molecules even against a concentration gradient. ATP-dependent pumps are used for active transport.
- Endocytosis and exocytosis: The movement of large sized molecules into (endocytosis) or out off (exocytosis) a cell proceeds through a more elaborate system. By pinching off or fusing together of vesicles, essential materials for nutritional uptake, receptor signaling, neurotransmission, etc. cross the plasma membrane.

1.1.5 Cellular delivery vectors

As discussed in the previous sections, neither the imaging moieties nor the targeting analogs can permeate the plasma membrane by themselves. Therefore, methods need to be developed to transport the conjugates into cells in such a way that their functionality is maintained. Perspectives of various techniques established primarily for transport of macromolecules have been reported by Stephens *et al. (42)* and Gao *et al.* (*43*).

Direct transfer assisted by capillary microinjection is widely used and shows high efficacy. However, this method is technically demanding and offers no possibility for *in vivo* applications. Another route to deliver into cells is by transient permeabilization of the plasma membrane. This methodology involves the formation of pores in the membrane by the action of detergents, toxins, UV illumination or short electrical pulses (electroporation). These

techniques are cheap, easy to use, show high efficiency and also address large numbers of cells. However, their application is limited due to the uncertainty of impact on cellular structures and organelles and also lack translation for live animal studies.

Carrier-mediated transfer is an alternative methodology that makes use of a cell permeating carrier to deliver the molecule of interest into target cells. It can easily be adapted for use in an in vivo setup. Viral vectors have been extensively investigated to efficiently transfer genes into cells (*44*). In spite of their excellent efficiency, viral vectors suffer from disadvantages like immunogenicity and cytotoxicity. Liposome-mediated transfer has been extensively used for the introduction of DNA or RNA into cells (*45*). However, the delivery efficiency by this method is low and it is also reported to affect lipid metabolism.

Another type of carrier that gained popularity over the last 15 years is a class of short peptides with the potential to translocate across the plasma membrane of eukaryotic cells (*46, 47*). These peptides are commonly designated as cell penetrating peptides (CPPs), protein transduction domains (PTDs), or cellular delivery vectors (CDVs) and have been used for transmembrane delivery of hydrophilic macromolecules. They usually consist of short, typically basic, peptide sequences of 7–34 amino acids in length that are capable of crossing the cell membrane either alone or attached to a molecular cargo (*48*). CPPs could be derived from natural sequences like HIV-1 Tat (*49*) and penetratin (*50*) or be artificial constructs designed by use of important features of natural sequences like polyarginines (*51*) and transportan (*52*). Table 2 presents a selection of the CPP families, their origin and some model cargoes delivered by their assistance.

Table 2: Selection of representative CPP families and model cargoes. (adapted from Foerg et al., (*46*)).

Name	Origin	Sequence	Cargo
Tat family			
Tat (48-60)	HIV-1 protein	GRKKRRQRRRPPQQ	β-galactosidase
Oligoarginine	Tat derivative	R_n	Cyclosporin A
Penetratin family			
pAntp	Antennapedia homeodomain	RQIKIWFQNRRMKWKK	Polo-box
pIsl	Isl-1 homeodomain	RVIRVWFQNKRCKDKK	Biotin/avidin
Chimeric CPPs			
Transportan	Galanin-mastoparan	GWTLNSAGYLLGKINLKALAALAKKIL	GalR-1 (antisense)
MPG peptides			siRNA
pβ	gp41-SV40	GALFLGFLGAAGSTMGAWSQPKKKRKV	Fluorophore
Pα	gp41-SV40	GALFLAFLAAALSLMGLWSQPKKKRKV	Fluorophore
Pep-1	Trp-rich motif-SV40	KETWWETWWTEWSQPKKKRKV	Proteins

Name	Origin	Sequence	Cargo
Antimicrobial-derived CPPs			
Buforin 2	Toad stomach	TRSSRAGLQWPVGRVHRLLRK	GFP
Bac715-24	Bactenecin family	PRPLPFPRPG	NeutrAvidin
SynB(1)	Protegrin 1	RGGRLSYSRRRFSTSTGR	Doxorubicin
Other CPPs			
pVEC	Murine VE-cadherin	LLIILRRRIRKQAHAHSK	Fluorophore
VP22	Viral protein (HSV-1)	DAATATRGRSAASRPTE- -RPRAPARSASRPRRPVE	GFP
hCT-derived peptides			
hCT(9-32)	Human calcitonin	LGTYTQDFNKFHTFPQTAIGVGAP	GFP
hCT(9-32)-br	Human calcitonin, SV40	LGTYTQDFNKFHTFPQTAIGVGAP AFGVGPDEVKRKKKP-NH_2	GFP
SAP	Modified maize	VRLPPP-VRLPPP-VRLPPP	Fluorophore
Protamin	Salmon roe	Mixture of protamin 1-4	Fluorophore

Although diverse in sequence, CPPs share some characteristics. Almost all known penetrating peptides have a dependence on cationic amino acids, primarily arginine and lysine. It has been established that guanidine head groups are a critical structural feature for interaction with the plasma membrane and for translocation (*53*). The uptake is also shown to be independent of the involvement of receptors. Delivery of penetratin (*54, 55*) and HIV-1 Tat (*56*) was unaffected by the retro-inverso sequence or when these peptides were composed entirely of D-enantiomers, indicating that the process is not mediated by receptors. Several investigations have also been conducted to elucidate the route of entry of CPPs into cells (*57, 58*). A variety of internalization mechanisms seem to be operating for breaching the membrane barrier (Fig. 6).

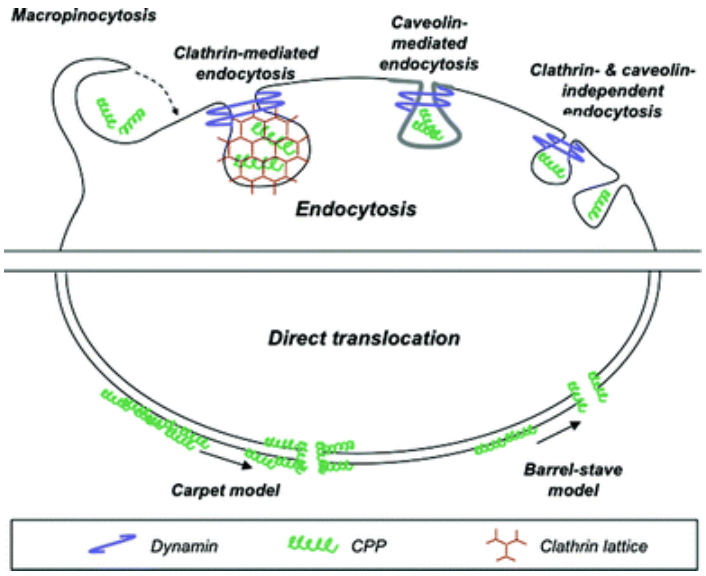

Figure 6. Possible mechanisms of uptake across the plasma membrane (adapted from Stewart *et al.* (*47*)).

Like any other methodology, CPP-assisted delivery also has some limitations. These peptides could induce immunogenicity and toxicity by affecting fundamental cellular functions (*59-61*). Also attention needs to be paid at the technical level for proper evaluation of delivery. Fixation of cells has been reported to induce artifactual intracellular redistribution of CPPs (*62, 63*). In addition, careful detection is needed to separate the surface bound cargo from the internalized one (*63*).

1.2 Aims of the study

Owing to its high spatial resolution, MRI is an optimal method for imaging complex biological processes. There have been reports on conjugation of exogenous MR contrast agents with translocation peptides and observation of intracellular contrast changes in labeled cells (*64-67*). For the purpose of molecular imaging, the first and so far the only study was reported by Heckl and co-workers in 2003 (*68*). Using MRI and fluorescence, they observed a specific accumulation of a c-myc specific PNA in vitro as well as in vivo. However, no further application of the same or any new study has been reported. As a modified acyclic Gd-based chelator was used in this report, its stability at the low pH environment like lysosomes in the cell is uncertain.

Improved MRI based intracellular agents for molecular imaging could be designed by introducing more stable macrocyclic CAs and more efficient CPPs. The aim of the present project was to develop intracellular MR contrast agents targeted to image specific mRNA. As was necessitated by the results obtained, novel agents for membrane translocation were also developed.

The central hypothesis of the projects was that mammalian cell lines mimic in vivo conditions, physiologically as well as biochemically. Assays developed using these cell lines could serve as a primary screen for the identifying an optimal molecule before testing in vivo.

1.2.1 Evaluation of mRNA-targeting intracellular MR Contrast Agents

Molecular imaging of cells and cellular processes can be achieved by tagging intracellular targets such as receptors, enzymes or mRNA. In the first part of the thesis we began with the screening of the optimal derivative of HIV-1 Tat peptide for intracellular delivery of MRI CAs. Seeking to visualize the presence of specific mRNAs by MR imaging, we evaluated peptide nucleic acids (PNA) conjugated with Gd-based MR contrast agents

using cell-penetrating peptides for intracellular delivery. An anti-sense to the mRNA of DsRed2 protein was used as a proof-of-principle. The conjugates were produced by continuous solid phase synthesis followed by chelation with Gd. To begin with, in vitro cell-free assays were established to verify the specificity of the PNA towards target. The cellular uptake of these intracellular targeted CAs was confirmed by fluorescence microscopy and spectroscopy. Studies were performed in target-deficient as well as target-containing cell lines. Cells labeled with these targeted CAs were also imaged by MRI to observe the difference contrast enhancement. Finally, the biodistribution of the CA was confirmed in C57BL/6 mice.

The accomplishments from this part of the project have been compiled in the following two publications:

- W. Su, **R. Mishra**, J. Pfeuffer, K.H. Wiesmüller, K. Ugurbil and J. Engelmann: Synthesis and Cellular Uptake of a MR Contrast Agent Coupled to an Antisense Peptide Nucleic Acid - Cell Penetrating Peptide Conjugate. *Contrast Media & Molecular Imaging*, *2*, 42-49 (2007).
- **R. Mishra**, W. Su, R. Pohmann, M. G. Sauer, J. Pfeuffer, K. Ugurbil and J. Engelmann: Cell Penetrating Peptides and Peptide Nucleic Acid Coupled MRI Contrast Agents: Evaluation of Cellular Delivery and Target Binding. *Bioconjugate Chemistry*, 20, 1860-1868 (2009).

1.2.2 Development of a novel cysteine-rich Cytosolic Localizing Peptide CyLoP-1

The shortcomings of the first project initiated the development of novel CPPs that not only penetrate the plasma membrane but also release the cargo into the cytosol for better interaction with targets located in the cytoplasm. In the second part of the thesis, numerous derivatives of a putative nuclear localization sequence from the snake toxin Crotamine were evaluated. Based on fluorescence spectroscopy and microscopy, cellular delivery and distribution of these peptides was tested. These extensive structure-activity-relationship studies led to the identification of a novel cysteine-rich CPP that distinctly localized in the cytosol. Referred to as CyLoP-1, the factors responsible for the distribution in the cytoplasm were analysed by observing uptake under different conditions and in various cell types and investigating the effect of CyLoP-1 on cells.

The accomplishments from the second part of the project have been compiled in the following two manuscripts:

- **R. Mishra**, D. Jha, K. Ugurbil and J. Engelmann: Novel Cysteine Rich Cell Penetrating Peptide CyLoP-1: Understanding the delivery in cytosol. (In preparation).
- D. Jha, **R. Mishra**, K. Ugurbil, M. E. Maier, K. H. Wiesmüller and J. Engelmann: Development of a Novel Cysteine Rich Cell Penetrating Peptide: Efficient Uptake and Access to Cytosol. (In preparation).

Chapter 2: Evaluation of cellular delivery and target binding of mRNA targeting intracellular MR Contrast Agents

2.1 Introduction

Remarkable progress in the understanding of cellular processes, both at the molecular and genetic level, has been made by the development of molecular-biological assays. Despite this, a myriad of questions about biological processes under normal as well as diseased conditions remain. Of late, the new field of molecular imaging has evolved with the intent to translate knowledge gained from *in vitro* systems into studies of complete biological systems. Molecular imaging aims at non-invasive visualization of biological processes amid the complex networks and interactions in the intact individual (*2-4*). Imaging modalities being extensively used for this purpose are positron emission tomography (PET), single-photon emission computed tomography (SPECT), optical imaging using fluorescence or bioluminescence, and magnetic resonance imaging (MRI) (*5, 69*).

MRI is a powerful tool in clinical diagnostics as well as for understanding developmental and biological processes. It visualizes the differences in tissues and organs, as well as between normal and pathological states as a function of water concentration and relaxation times, T_1 and T_2, in a given volume element (*9*). The main advantages of MRI over other imaging techniques are its high spatial and temporal resolution, the absence of harmful ionizing radiation and the ability to non-invasively scan entire organisms in one, two or three dimensions. The intrinsic contrast of MR images can be augmented by the use of contrast agents (CAs). Chelated paramagnetic metal ions, in particular gadolinium, have been primarily used as T_1-based CAs to increase the contrast in MR images (*16*). An assortment of gadolinium-based CAs is commercially available and these agents are frequently employed for clinical diagnosis. Though, their utility is based on enhancement of anatomical information due to differential biodistribution in the body (*70, 71*). For example, in the brain, these agents do not cross the blood brain barrier (BBB) except when the BBB is broken because of pathology; as such, they lack specificity. Advancing from these agents towards extracellular targeting by conjugation of CAs to certain proteins and especially to monoclonal antibodies or antibody fragments has been explored. Most of the investigations were related to the development of tumor-specific agents (*18-20, 72, 73*).

However, numerous intracellular imaging targets are available and these can be tagged to provide molecular information. Regardless of the low number of targets at DNA level, molecules at RNA (over-expressed) or protein level could serve as potential targets (*3*).

Moreover, since the completion of human genome sequence, there has been considerable research interest in assessing gene expression through non-invasive molecular imaging approaches. Considering that an oligodeoxynucleotide (ODN) with more than 12 bases could target a unique sequence in the whole human genome (*74*), ODNs are good templates for the development of new targeted MR imaging probes with high specificity.

Natural ODNs cannot be directly used for molecular imaging because they are rapidly degraded *in vivo* by endo- and exonucleases (*25*). Furthermore, ODNs can cause degradation of the target mRNA by RNAse H. A number of novel oligonucleotide analogues, designed for improved stability, target binding, and antisense activity, have been synthesized and evaluated *in vitro* and *in vivo* (*75-77*). Modifications include morpholino, phosphorothioate, phosphoroamidate, methylphosphonate, 2'- or 3'- modifications, 2'- 4' bridges, and complete replacement of the backbone with an amide backbone (peptide nucleic acid or PNA). PNA is a DNA mimic containing a pseudopeptide backbone that makes it extremely stable in biological fluids (*78*). Despite the radical difference in the chemical composition of the backbone, PNA not only retains but also improves the hybridization characteristics of DNA and RNA (*79*). In most cases, PNA oligomers with mixed base sequences form duplexes (by Watson-Crick base-pairing) with complementary DNA and RNA with higher thermal stability than corresponding DNA-DNA or DNA-RNA complexes and without sacrificing sequence specificity. These qualities make PNA a leading agent among 'third generation' antisense and antigene agents. Recent work has shown that PNA can be used as molecular hybridization probes (*80*), nuclear imaging tracers (*81*), and to control gene expression and splicing (*82*).

Direct imaging of mRNA can provide information on cellular gene expression patterns and may have the potential to detect molecular changes in disease states at relatively early stages, providing opportunities for pre-emptive therapeutic interventions (*22*). To be useful as a probe, an antisense PNA must target a unique mRNA sequence in the objective cells. In order to ensure good detection sensitivity and selectivity for MR imaging, the targeted mRNA should be highly abundant in cells. Therefore, as a proof of principle we chose the mRNA of DsRed2, a variant of the red fluorescent dsRed protein as target. The gene for dsRed protein, originating from a coral of the Discosoma genus (*83*), is widely used as a transfection marker in molecular biology. Thus, there are increasing numbers of transgenic

cell lines expressing the dsRed and its more stable and better soluble variant DsRed2 protein, which can be used later as models for *in vivo* studies.

However, using antisense PNA as a molecular imaging probe has a major obstacle in that they are not able to penetrate biological membranes. In 2003, Heckl, *et al* (*68*) reported the first results on an intracellular MR contrast agent, composed of a gadolinium complex, a *c-myc*-specific PNA sequence and a trans-membrane carrier peptide, showing the potential of peptide-based delivery to penetrate through the cell membrane. Whether improvements on this strategy can be achieved using different carrier peptides and/or contrast agent moieties remains an important question. Researchers have resorted to several other cargo delivery techniques such as using cationic lipids and liposomes (*84*), nanoparticles (*85*), and direct conjugation with monoclonal antibodies (*86*) or peptides (*87*), etc. to overcome the obstacle of plasma membrane. However, cell-penetrating peptides (CPPs) emerged as an extremely efficient way to overcome this most challenging delivery barrier. They are a class of short peptides that have been reported to import a wide range of cell-membrane impermeable cargos into cells (*88-91*). CPP-oligonucleotide conjugates, unlike oligonucleotide complexes with cationic lipids or polymers, are of relatively modest molecular size. Thus, they are more likely to evade uptake by the phagocytes of the reticuloendothelial system and to attain a widespread biodistribution subsequent to *in vivo* administration. Amongst the large variety of CPPs available, Tat peptide (derived from HIV-1 Tat protein) is the most intensively studied and has high delivery ability for vast variety of cargos (*92*). Thus far, there is no consensus on the mechanism of uptake of CPPs and the maintenance of functionality of cargos after delivery. Variance is also reflected by differences in reported labeling techniques, non-standardized protocols regarding uptake evaluation, and discrepancies caused by the use of different cellular model systems (*93-95*).

Keeping these issues in mind, we began our pursuit for evaluating the most appropriate CPP, selected from three derivatives of the well-established CPP HIV-1 Tat peptide, to deliver CA into cells. The cargo attached to the CPP was a gadolinium-loaded chelator, 1,4,7,10-tetraazacyclododecane-N,N′,N″,N‴-tetraacetic acid (Gd-DOTA), for MR imaging, and fluorescein isothiocyanate (FITC) for optical imaging (Fig. 7).

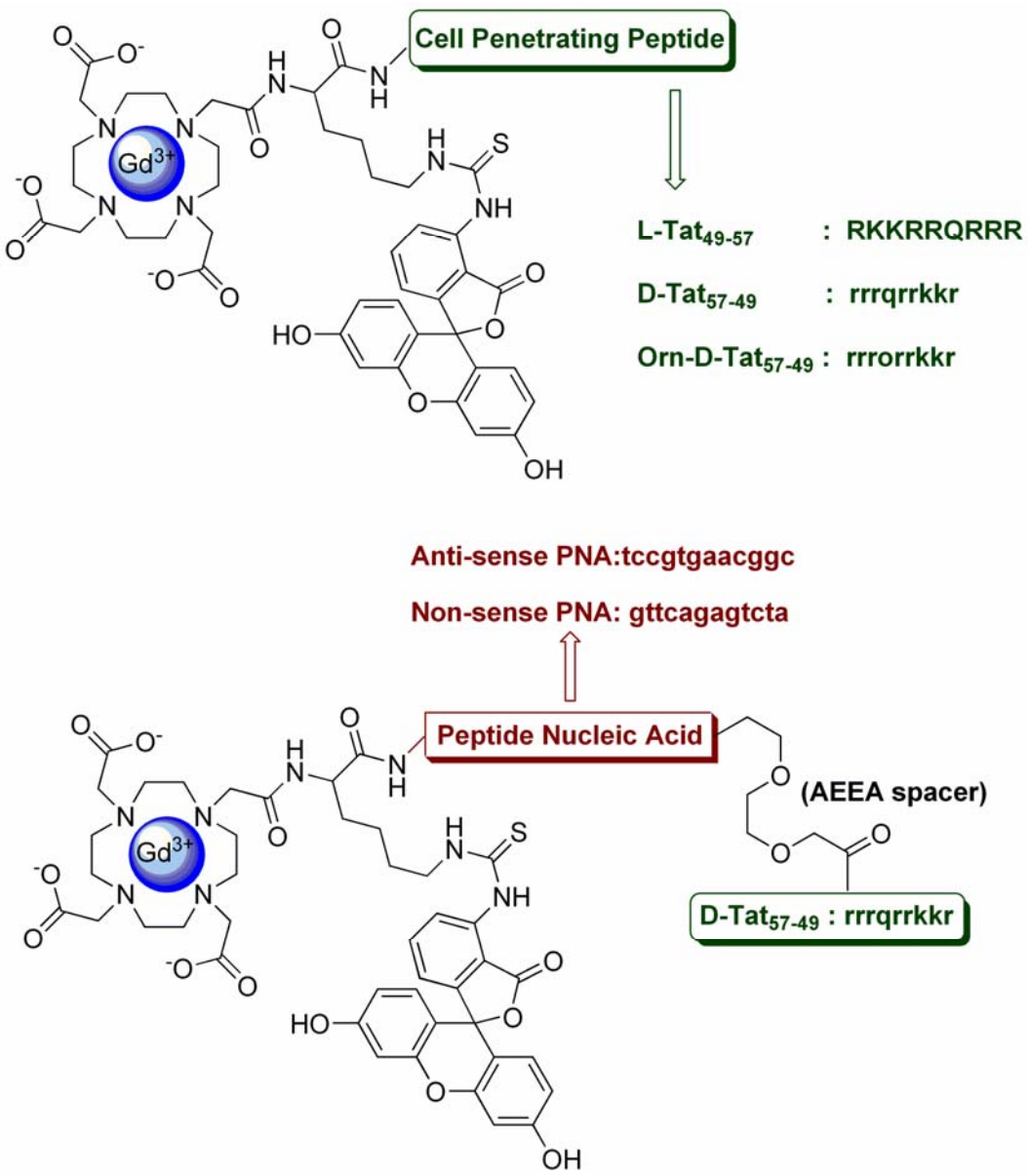

Figure 7. Schematic structures of CPP and PNA conjugated Gd(DOTA) based intracellular contrast agents. All amino acids are represented in a single letter code where R: arginine, K: lysine, Q: glutamine and O: ornithine. D-amino acids are represented in lower case. The PNA building blocks are represented as a: adenine, t: thymine, g: guanine and c: cytosine.

Using the selected CPP, a targeting PNA (either targeting DsRed2 mRNA or a non-sense sequence) was introduced into the above-mentioned conjugate (Fig. 7). The objective was to develop and synthesize PNA targeting intracellular MR contrast agents. Initial cell biological assays were made on normal NIH 3T3 mouse fibroblasts to test the internalization of these compounds into cells and their biocompatibility using MR and fluorescent optical imaging

techniques. Since the DsRed2 protein was used as a model system, the proof-of-principle was examined in a transgenic DsRed2-expressing cell line (*96*). The aim was to assess the intracellular delivery and distribution of these larger molecules in the presence or absence of target mRNA in the cells. The ability of the agents to bind with targets in a cell-free *in vitro* system, as well as by labeling cells, was also evaluated. In the end, the biodistribution of the CA containing the anti-sense PNA will also be briefly presented here using fluorescence for detection.

2.2 Materials and methods

2.2.1 Chemical synthesis

All CPP conjugates and contrast agents were obtained by in-house synthesis performed by colleagues in the Chemistry section of the Chemical Biology Group, High-Field Magnetic Resonance Center, Max Planck Institute for Biological Cybernetics. In brief, the following steps were followed to synthesize Gd(DOTA) conjugates with CPPs (Scheme 1) and PNA (Scheme 2).

2.2.1.1 Peptide synthesis

All the CPPs used in this work were chemically synthesized by solid-phase peptide synthesis with Fmoc/*t*Bu-strategy on a Heidolph Synthesis 1 synthesizer (Germany) using polystyrene-based Wang resin as solid support.

2.2.1.2 PNA synthesis

Synthesis of anti-dsRed-PNA (tcc gtg aac ggc) and nonsense PNA (gtt cag agt cta) were performed in a manual reaction synthesizer. Fmoc/Bhoc chemistry was used to couple PNA building blocks through an AEEA spacer to D-$Tat_{(57-49)}$ by a continuous solid phase synthesis scheme.

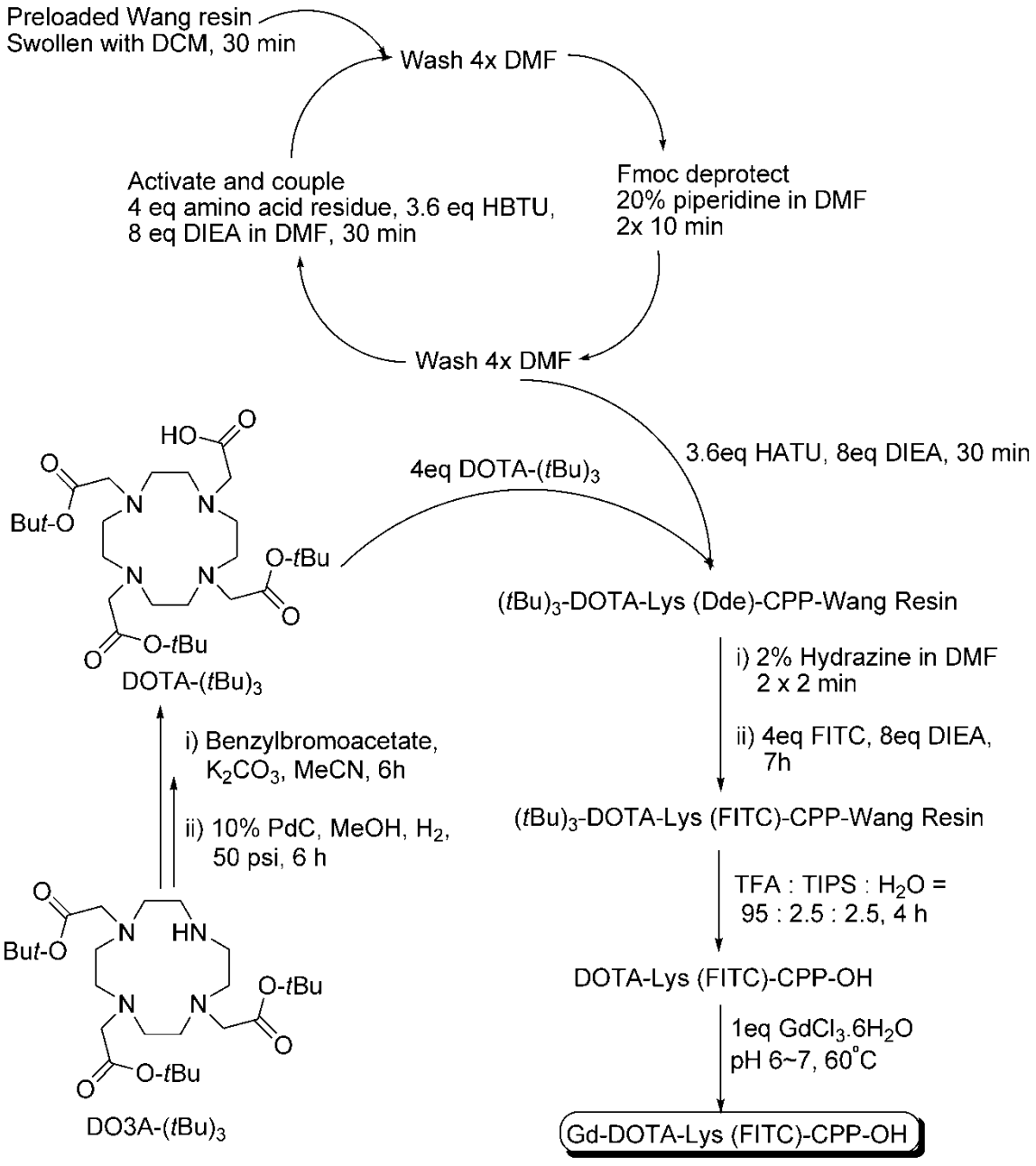

Scheme 1. Synthesis of CPP conjugated MR contrast agents by continuous solid-phase synthesis scheme.

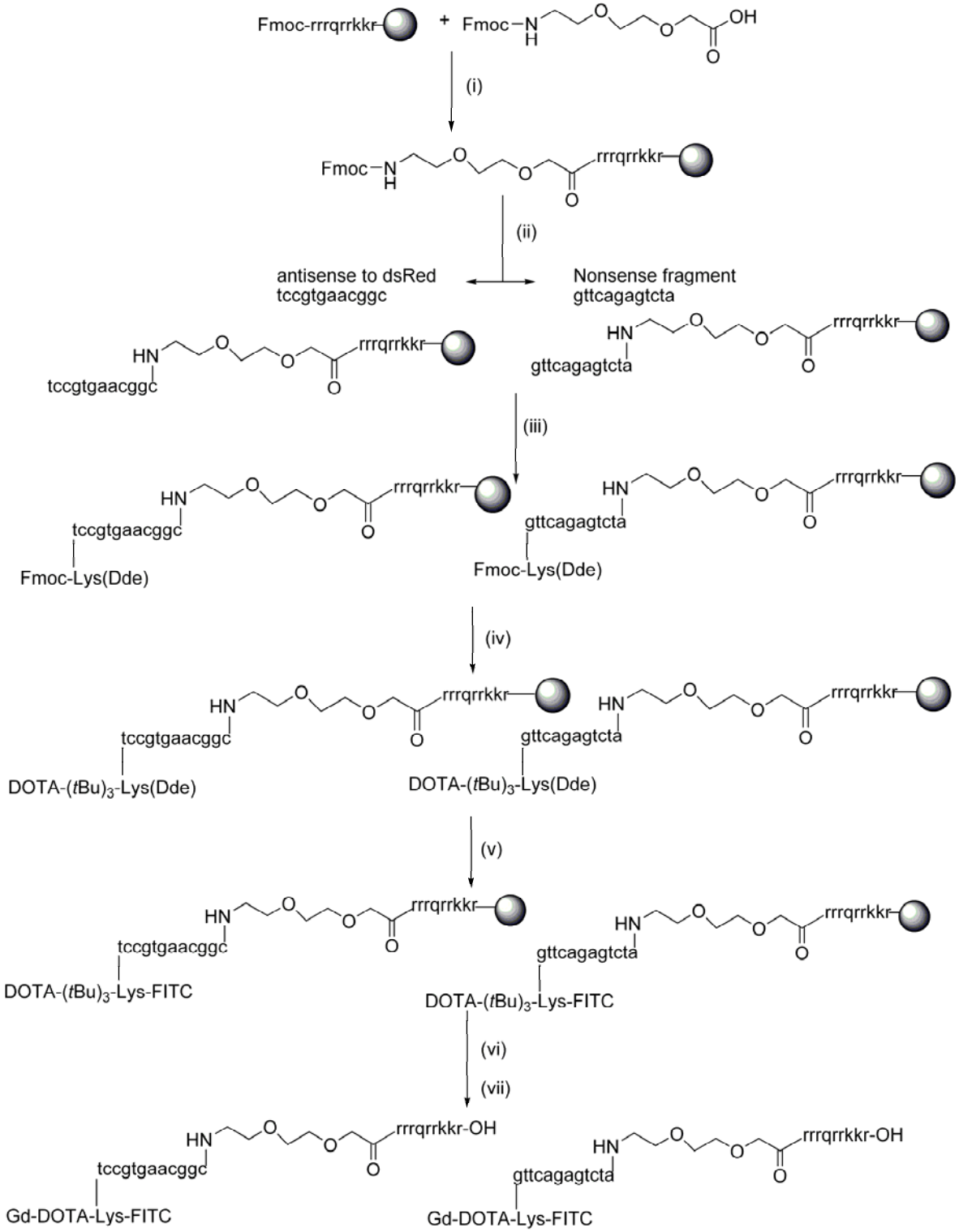

Scheme 2. Synthetic scheme followed for making PNA conjugated MR contrast agent. Reagents and conditions: (i) Fmoc-AEEA-OH, HATU, DIEA, DMF; (ii) Fmoc/Bhoc protected monomers,

HATU, DIEA, DMF; (iii) Fmoc-Lys(Dde)-OH, HATU, DIEA, DMF; (iv) DOTA-$(tBu)_3$-OH, HATU, DIEA, DMF, 12 h; (v) FITC, DIEA, DMF, 7 h; (vi) TFA: TIS: H_2O (95:2.5:2.5), 4 h; (vii) $GdCl_3.6H_2O$, 60°C, 12 h.

2.2.1.3 Conjugation of DOTA and labeling with FITC

On completion of the PNA sequence, a Fmoc and Dde protected Lys residue was conjugated. DOTA tris(*tert*-butyl) ester was synthesized in-house (*97*) and coupled to the Lys on its α-NH_2 group after deprotection of Fmoc. Next FITC was conjugated with the ε-NH_2 group of the Lys.

2.2.1.4 Chelation with gadolinium

The conjugates were cleaved off the resin and loaded with gadolinium using $GdCl_3.6H_2O$ under mild conditions for 12 h. The pH was periodically checked and adjusted between 6.0-7.0 using a solution of Na_2CO_3 and HCl as needed.

2.2.1.5 Purification and characterization

Gd-DOTA-conjugated CPPs and PNAs were analyzed and purified using analytical and semipreparative RP-HPLC on a Varian PrepStar Instrument (Australia) equipped with PrepStar SD-1 pump heads. The purification was performed both before and after gadolinium loading. The reaction mixture was dialyzed (Float-A-Lyzer, cellulose ester membranes, MWCO: 2,000; Spectrum Laboratories, Inc.) to remove other impurities and finally the solution was lyophilized till used. Characterization was performed by ESI-MS on Agilent SL 1100 Series LC/MSD Trap system (Agilent, Germany).

2.2.2 Concentration estimation

Peptide conjugates were dissolved in MilliQ water to obtain a 10 mM solution by weight. For the determination of the real concentration, these stock solutions were diluted 1:100 in Dulbecco's Modified Eagle's Medium (DMEM; Biochrom AG, Germany). The absorbance of the solutions was measured in a multiplate reader (BMG Labtech, Germany) at 485 nm with ratiometric correction of turbidity at 690 nm. The concentrations of the stock solutions were calculated after background correction assuming $\varepsilon_{carboxyfluorescein\ 485\ nm}$=81,000 l/(mol·cm) and all further dilutions were done according to this calculated concentration.

2.2.3 Cell culture

NIH 3T3 cells were obtained from DSMZ, Germany, CCL-11 fibrosarcoma cells from ATCC, USA, and the DsRed2 protein-expressing fibrosarcoma CCL-11 cell line (DsRed

cells) was a kind gift of Dr. Marna Ericsson, University of Minnesota, USA. NIH 3T3 mouse fibroblasts were cultured as a monolayer at 37°C with 10% CO_2 in DMEM supplemented with 10% fetal bovine serum (FBS), 4 mM L-glutamine, 100 µg/mL streptomycin and 100 U/mL penicillin (all purchased from Biochrom AG, Germany). Cultures of DsRed cells and the parent cell line CCL-11 were maintained at 37°C with 5% CO_2 in NCTC 135 medium (Sigma, Germany) supplemented with 10% heat-inactivated fetal horse serum, 2.2 g/L sodium bicarbonate and pH adjusted to 7.2. All cells were passaged by trypsinization with trypsin/EDTA 0.05/0.02% (w/v) in phosphate-buffered saline (PBS; Biochrom AG, Germany) every second to third day.

2.2.4 In vitro binding assay

2.2.4.1 Cell-free FITC-based immunoassay

The *in vitro* proof of specific binding of anti-dsred CA was obtained in a cell-free FITC immunoassay with slight modifications (*98*). A synthetic 45-mer single-stranded deoxynucleotide sequence (5'-CTC GAA CTC GTG GCC GTT CAC GGA GCC CTC CAT GCG CAC CTT GAA GCG CAT GAA CTC CTT GAT-3') containing the complementary target site of anti-dsred CA was obtained commercially (Eurofins MWG, Germany). The target ODN sequence extended by a 12-mer C linker was immobilized on DNA binding plates (Corning, Germany) in DNA binding buffer (50 mM sodium phosphate, 1 mM EDTA, pH 8.5) at 4°C for 24 h. After washing off excess ODN with PBS, the plates were incubated with blocking buffer (DNA binding buffer containing 10% FBS and 3% bovine serum albumin (BSA)) for 2 h at 37°C. Following a PBS wash, incubation with 16 nM of either anti-dsred CA or non-sense CA in 10 mM sodium phosphate, pH 6.5 was performed. For hybridization, the binding temperature was maintained at 60°C for 1 h and then slowly decreased to 37°C for another 1 h. The plates were left overnight at room temperature. The following day, plates were washed 3 times for 5 min each with wash buffer (PBS containing 0.01% Tween). Incubation with an anti-FITC-horseradish peroxidase (HRP)-conjugated antibody (Invitrogen, Germany) was carried out. Subsequent to thorough PBS washing to remove unbound antibody, the signal was developed with tetramethyl benzidine for 30 min at room temperature and absorbance was measured at 650 nm in multiplate reader (BMG Labtech, Germany). Experiments were run at least three times for each CA with two replicates. Statistical analysis was performed by Student's *t*-test. P values < 0.05 were considered significant.

2.2.4.2 Gel retardation assay

The specificity of interaction between the anti-sense PNA and target sequence after pre-gel hybridization was verified by gel retardation assay (*99*). The aforementioned 45-mer single-stranded deoxynucleotide sequence selected from the DsRed2 cDNA was obtained commercially (Eurofins MWG, Germany). This sequence contained a stretch of bases complementary to the anti-sense sequence used in the anti-sense CA. The anti-sense CA or non-sense CA (10 pmol) were incubated with the synthetic 45-mer single-stranded deoxynucleotide (12.5 pmol) in hybridization buffer (12.5 mM Tris buffer, pH 8 containing 2.5 mM sodium chloride, 0.5 mM magnesium chloride and 0.05 mM dithiothritol (DTT)). This pre-loading hybridization was performed at 60°C for 1 h followed by a gradual reduction to room temperature. The samples were then run on 8% native acrylamide gel and subjected to electrophoresis in running buffer (200 mM Tris-acetate buffer, pH 8.3, 1 mM EDTA). Silver staining was used to detect the mobility of the DNA on the gel.

2.2.5 Cellular uptake assay

Internalization experiments on cells were performed in 96 well microplates. At 70-80% confluency, cells were incubated with different concentrations of peptide-coupled CAs in complete culture medium for additional 18 h at routine culture conditions. After incubation, the labeling CA were removed and cells were incubated with Bisbenzimid 33342 (Hoechst 33342), a nuclear stain, in order to estimate the cell number. Extracellular fluorescence was quenched by incubation with cold trypan blue (0.05% (w/v) in PBS) for 3 min followed by repeated washes with HBSS (*100*). Cell-related FITC fluorescence (Ex 485 nm/Em 530 nm) and cell number (Ex 346 nm/ Em 460 nm) were evaluated in a multiplate reader. Experiments were run at least three times for each CA with six replicates. Statistical analysis was performed by ANOVA with Tukey's post test. P values < 0.05 were considered significant.

2.2.6 Microscopy

The cells in plates processed for fluorescence spectroscopic measurement, as mentioned above, were used for complementary fluorescence microscopy. Microscopy was performed without fixation of cells using a Zeiss Axiovert 200 M microscope (Germany) with an LD Plan NeoFluor 40X objective. For high resolution microscopy, 5×10^5 cells/mL were cultured on channel slides (Ibidi, Germany) for 24 h. Then cells were incubated with CA in culture medium for another 18 h under normal culture conditions. These cells were subjected to nuclear staining and trypan blue quenching followed by extensive washing with HBSS.

Images were made using a Zeiss Plan APOCHROMAT 63X/1.4 oil DIC objective. OptiGrid (Improvision, England), a structured light device, was used for acquiring images of confocal quality and Volocity Acquisition and Visualization software (Improvision, England) was used for high speed image capture and high resolution rendering of data sets as images or movies. The imaging conditions were kept constant for the observation of all the different samples. Cellular localization and distribution of the CA was observed by irradiating with blue light (Ex 470/40 nm) and observing at Em 525/50 nm. Apart from FITC fluorescence, the nuclear labeling by Hoechst was observed by Ex 365/15 nm and Em 460/50 nm and trypan blue fluorescence viewed by Ex 535/50 and Em 645/75 nm. Also phase contrast images with differential interference contrast (DIC) microscopy of the same area were made to observe if the cells maintain their normal morphology in the presence of CAs.

2.2.7 MR measurement

2.2.7.1 Relaxivity measurement of contrast agents in solution

Different concentrations (5 μM, 10 μM, 15 μM, 20 μM, 30 μM, 40 μM) of Gd(DOTA) conjugates were prepared in aqueous solution for relaxivity measurement of 1 ml aliquots in 1.5 mL Eppendorf tubes. The protocol was further standardized for high throughput measurement in 96well plates requiring only 175 μl of sample.

The measurement of the relaxation rates R_1 and R_2 (longitudinal and transverse relaxation) of Gd-complexes were performed at 7T (300 MHz) on a vertical 7T/60 cm MRI Biospec system (Bruker Biospin, Germany) or 3T (123 MHz) human MR scanner (MAGNETOM Tim Trio, Siemens Healthcare, Germany).

2.2.7.2 In vitro MR measurement in cells

For MR imaging of cells, exponentially growing cells were labeled with different concentrations of CAs in 175 cm^2 tissue culture flasks for 18 h. After repeated washes with HBSS, cells were trypsinized, centrifuged and re-suspended in 1.5 mL Eppendorf tubes at 2×10^7 cells for DsRed and CCL-11 in 500 μL complete medium. Cells were allowed to settle before MR measurements. Tubes with medium only and cells without CA were used as controls.

MR imaging of the cell pellets at room temperature (~21 ˚C) was performed on a 3 T (123 MHz) human MR scanner (MAGNETOM Tim Trio, Siemens Healthcare, Germany),

using a 12-channel RF Head coil and slice selective measurements from a slice with a thickness of 1 mm positioned through the cell pellet.

All MR measurements were performed by Dr. Rolf Pohmann, High-Field Magnetic Resonance Center, Max Planck Institute for Biological Cybernetics using the following parameters. T_1 was measured using an inversion-recovery sequence, with an adiabatic inversion pulse followed by a turbo-spin-echo readout. Between 10 and 15 images were taken, with the time between inversion and readout varying from 23 ms to 3000 ms. With a repetition time of 10 s, 15 echoes were acquired per scan and averaged six times. For T_2, a homewritten spin-echo sequence was used with echo times varying from 19 ms to 1000 ms in about 10 steps and a repetition time of 8 s. Diffusion sensitivity was reduced by minimizing the crusher gradients surrounding the refocusing pulse. All experiments scanned 256^2 voxels in a field-of-view of 110 mm in both directions resulting in a voxel volume of $0.43 \times 0.43 \times 1$ mm^3.

Data analysis was performed by fitting to relaxation curves with self-written routines under MATLAB 7.1 R14 (The Mathworks Inc., United States). The series of T_1 and T_2 relaxation data were fitted to the following equations:

a) T_1 series with varying $t = T_I$: $S = S_0 (1 - \exp(-t / T_1) + S(T_I = 0) \exp(-t / T_1)$.

b) T_2 series with varying $t = TE$: $S = S_0 \exp(-t / T_2)$.

Nonlinear least-squares fitting of three parameters S_0, $S_{(TI = 0)}$, and T_1/T_2 was done for manually selected regions-of-interest with the Trust-Region Reflective Newton algorithm implemented in MATLAB. The quality of the fit was controlled by visual inspection and by calculating the mean errors and residuals.

2.2.8 Biodistribution study

C57BL/6 mice were used to study the *in vivo* distribution of anti-dsred CA. The CA was injected intravenously via the tail vein at a dose of 10 µmol/kg in 100 µL saline. An equivalent volume of saline was injected into the control animal. After 20 min, animals were sacrificed and biodistribution assessed. Tissues harvested included lungs, liver, spleen, kidney, heart, bladder, and brain. All tissues were rinsed with PBS to remove blood or hair and a slice of arbitrary thickness from each tissue was placed on a glass slide for microscopic observation. Microscopy was performed using a Zeiss EC Plan-NEOFLUOR 20x/0.5 objective. Fluorescence and bright field images of the tissues were obtained and observed for CA related FITC fluorescence.

2.3 Results

2.3.1 Evaluation of optimal CPP

The Gd-DOTA-Lys(FITC) conjugates of L-Tat$_{(49-57)}$ (L-Tat CA), D-Tat$_{(57-49)}$ (D-Tat$_{inv}$ CA) and Orn-D-Tat$_{(57-49)}$ (substitution of the glutamine residue with ornithine) (Orn-D-Tat$_{inv}$ CA) were synthesized in-house (*101*) (Fig. 1). Peptide segments were synthesized by an on-line solid-phase synthesis scheme. Using an additional lysine as linker, DOTA tris(*tert*-butyl) ester was coupled on its α-NH_2 group and FITC on the ε-NH_2 group. The final gadolinium-loaded compounds were used to label cells. Fluorescence spectroscopy was applied to assess cellular uptake by FITC fluorescence and toxicity by nuclear DNA content estimation after staining with Hoechst 33342.

Of the three sequences tested, Orn-D-Tat$_{(57-49)}$ was the most efficient in delivering the conjugates across the plasma membrane (Fig. 8). However, its uptake was accompanied by a very high toxicity, thus limiting its exploitation. Our results did not reveal noteworthy difference in the uptake of conjugates with L-Tat$_{(49-57)}$ or D-Tat$_{(57-49)}$ both of which had negligible toxicity (although D-Tat$_{(57-49)}$ has been reported to be a more efficient transporter for other cargos (*102*)). The D-form of the amino acids has been reported to show higher metabolic stability and almost no enzymatic degradation. Thus, we chose D-Tat$_{(57-49)}$ as the CPP for experiments on further coupling of PNA sequences together with Gd-DOTA and FITC to obtain bimodal targeting agents.

The results of MR measurement of CPP conjugated Gd chelates gave similar T_1 relaxivity (r_1) values for L-Tat CA (7.1 mM^{-1} s^{-1}) and Orn-D-Tat$_{inv}$ CA (7.1 mM^{-1} s^{-1}) while higher relaxivity was measured for D-Tat$_{inv}$ CA (14.2 mM^{-1} s^{-1}). This high relaxivity was consistently reproduced over several batches synthesized and subjected to variety of purification methods to get rid of free Gd. The standard value for DOTA loaded with Gd is reported to be between 3 - 4 mM^{-1} s^{-1} while of Gd-DTPA-$(Arg)_8$ is 6.8 mM^{-1} s^{-1} at 3T (*66*).

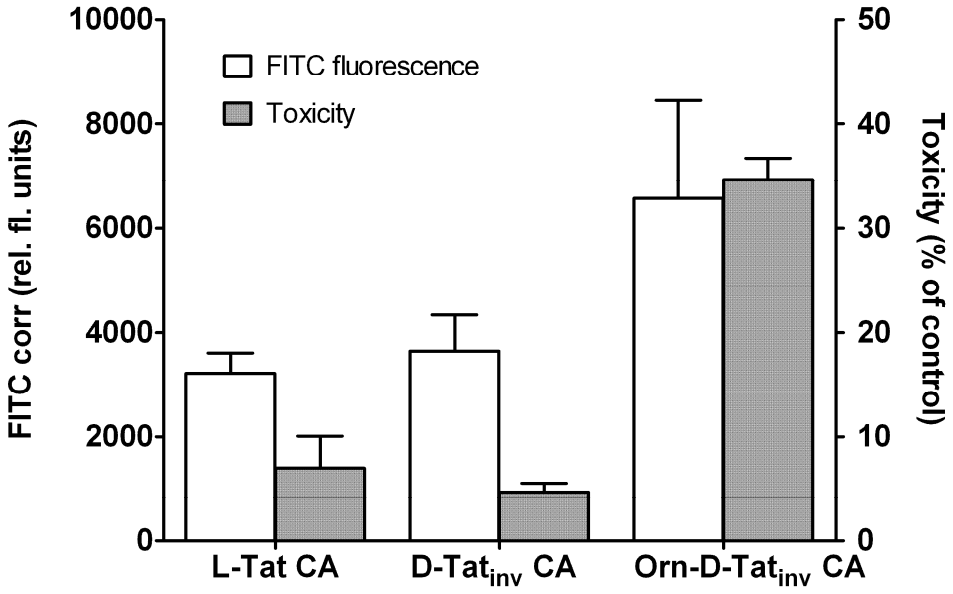

Figure 8. CA-related fluorescence measured by fluorescence spectroscopy in NIH 3T3 embryonic mouse fibroblast cells. Cells were incubated with contrast agents at a concentration of 20 μM in complete medium for 18 h. External fluorescence was quenched with trypan blue and subsequent washes with HBSS. Values are means ± SEM, n=3 with six replicates each.

2.3.2 Design and synthesis of mRNA-targeted CA

PNA was selected to target unique mRNA sequences. These polyamide nucleic acids are reported to be resistant to enzymatic cleavage in biological fluids and hybridize with DNA or RNA with high specificity and affinity (*38*). As per the base pairing rule, these PNAs could bind sequences in cellular mRNA and, therefore, serve as high affinity probes for molecular imaging. Although most mRNAs are expressed at low copy numbers under normal conditions (50-1000 per cell at any particular time point), these numbers increase many-fold in certain situations like disease or stress (*3*). The use of PNA for imaging specific mRNA could potentially serve for early detection of anomalies by monitoring molecular processes. Because PNAs have poor cellular uptake, they need to be coupled to delivery agents such as CPPs in order to pass through the biological membrane and interact with the intracellular target (*103*).

The intention of our study was to design a multi-modal probe by the use of a facile building block approach. The blocks could easily be altered according to the target requirement without significant modification in the synthetic scheme. The molecule eventually designed contained MR and optical imaging moieties linked to PNA for targeting

and CPP for intracellular transport. In order to establish a proof-of-principle, mRNA from a variant of the red fluorescent protein, DsRed2, was chosen as the target. Through a BLAST database search, a 12mer anti-sense sequence (tcc gtg aac ggc, anti-dsred) specific to the DsRed2 mRNA was identified (*104*). Another sequence (gtt cag agt cta) that did not correspond to any known mammalian gene was selected as the non-sense control sequence (*104*).

Two PNA-containing conjugates, anti-dsred CA and non-sense CA were synthesized using the same synthetic scheme as reported in detail before (*104*) (Fig. 1). The chelation of gadolinium in the macrocyclic chelator was confirmed by relaxivity measurements of CA in aqueous solutions. The relaxivity values for both the CAs (2.8 ± 0.3 $mM^{-1}s^{-1}$ for anti-sense CA and 4.3 ± 0.2 $mM^{-1}s^{-1}$ for non-sense CA) were corresponding with values for compounds with one DOTA complexed gadolinium.

2.3.3 In vitro proof for binding specificity of anti-sense CA

The hybridization properties of PNA are crucial for specific antisense targeting. It is established that oligonucleotides of 12 or more bases are adequate for targeting unique genomic sequences (*74*). The targeting specificity of anti-dsred CA in comparison to non-sense CA was determined *in vitro* using a synthetic single-stranded ODN sequence (45-mer) as described in Experimental Procedures. Significant specific binding of the anti-sense CA to the synthetic target was observed (Fig. 9a). The non-sense counterpart almost completely failed to bind, such that the hybridization signal obtained can be mainly ascribed to specific binding. Thus, *in vitro* studies clearly demonstrated the applicability of the selected anti-sense PNA sequence for mRNA targeting. Gel retardation studies further verified the specific binding affinity of the anti-sense CA compared to the non-sense CA (Fig. 9b). A retarded mobility only of the synthetic single-stranded DNA hybridized with the anti-sense PNA was observed, while DNA incubated with non-sense PNA showed no change in mobility in comparison to unhybridized DNA.

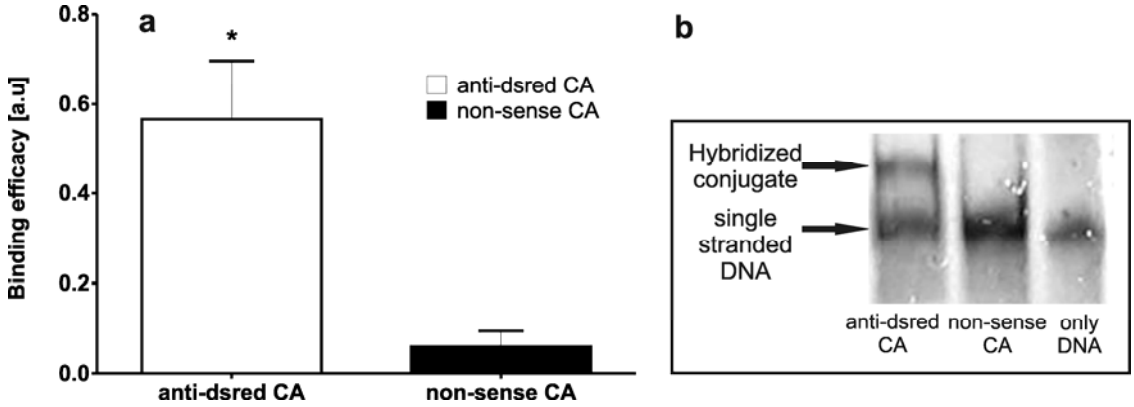

Figure 9. *In vitro* binding efficacy of anti-dsred and non-sense CA using (a) FITC based immunoassay and (b) gel retardation assay. For the immunoassay synthetic single-stranded target DNA was immobilized on DNA binding plates and hybridization was performed with anti-dsred and non-sense CA, followed by extensive washing to eliminate non-specific binding. Detection was performed by anti-FITC-HRP-conjugated antibody. Gel retardation of the mobility of target ODN was detected by silver staining after hybridization with anti-sense CA.

2.3.4 In vitro fluorescence studies in 3T3 cells

To determine whether these synthesized PNA-peptide conjugates are internalized into immortalized cells and to evaluate the distribution of the compounds in sub-cellular compartments, fluorescence spectroscopy and fluorescence microscopic studies were performed with both contrast agents on 3T3 mouse embryonic fibroblasts.

The results of fluorescence spectroscopy (Fig.10a) showed that both contrast agents could enter efficiently into 3T3 cells and in a concentration dependent manner from 0.5 μM to 5.0 μM. But at concentrations higher than 5.0 μM, the cytotoxicity of these compounds increased dramatically (data not shown). Therefore, further experiments were performed at concentrations below 5.0 μM. No significant differences between the two compounds were observable, as expected for a cell line without any target mRNA.

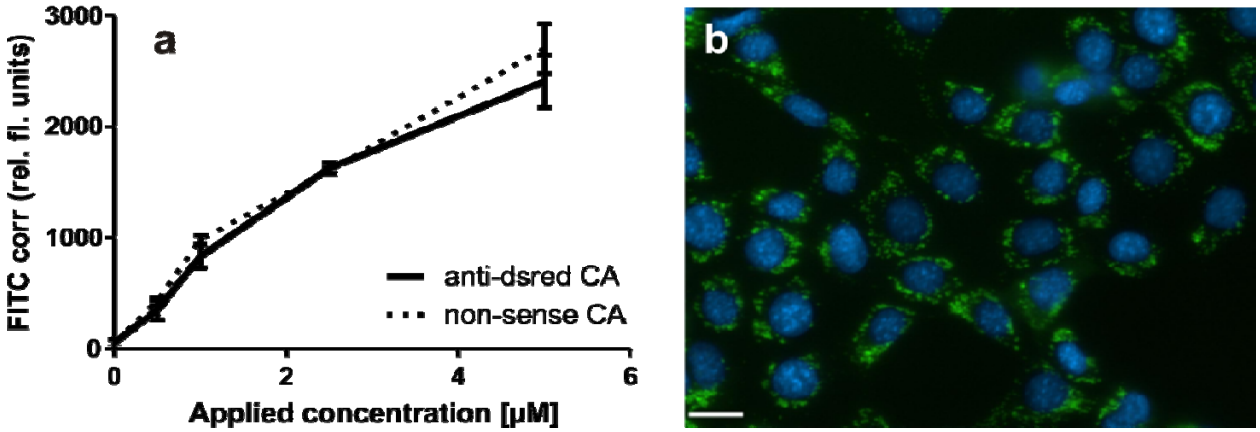

Figure 10. Cell internalization of anti-dsred and non-sense CA into 3T3 cells evaluated by (a) fluorescence spectroscopy and (b) microscopy. Cells were incubated with contrast agents at various concentrations in complete medium for 18 h. External fluorescence was quenched with trypan blue and subsequent washes with HBSS ; values are means ± SEM, n=3-10 with six replicates each, bar represents 20 µm.

Fluorescence microscopy imaging (Fig. 10b) demonstrated that the anti-dsred CA (green) could enter cells and was located predominantly in vesicles around the nucleus (blue) whereas no uptake into the nucleus was observed.

2.3.5 In vitro MR studies in 3T3 cells

Cellular uptake of the synthesized contrast agents were also confirmed by *in vitro* MR studies at 300 MHz. After loading with anti-dsred CA, the relaxation rate $R_{1,cell}$ inside 3T3 cells (Fig. 11a) increased linearly with the applied (extracellular) labeling concentration of contrast agent (from 0.1 µM to 1.0 µM). The apparent "intracellular" relaxation rates were plotted against the extracellularly applied concentration. Nevertheless, the measured intracellular relaxation rate increased significantly after loading with 0.5 µM and 1 µM anti-dsred CA. Contrast enhancement in T_1-weighted MR images of cells was also observable at these low concentrations; an example is shown for a single experiment in Figure 11b. The results of the MR measurements are summarized in Table 3, also illustrating that already at 0.5 µM applied concentration, a statistically significant increase of the intracellular relaxation rate $R_{1,cell}$ and thus a contrast enhancement was detectable.

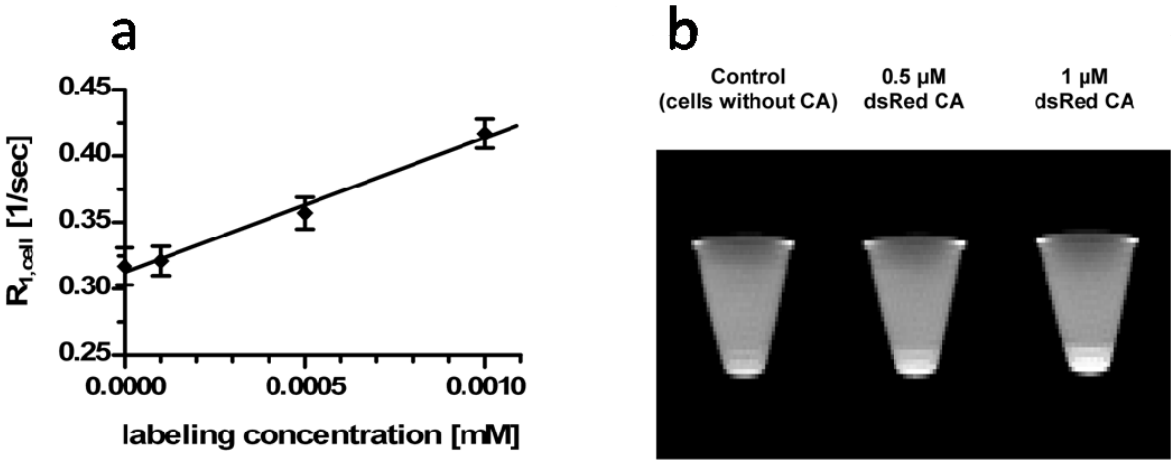

Figure 11. Contrast enhancement properties of anti-dsred CA in 3T3 cells. (a) Relaxation rate $R_{1,cell}$ and (b) T_1 weighted MR images of 3T3 cells after loading with anti-dsred CA. After treated with anti-dsred CA for 18 h, cells were trypsinized, centrifuged and re-suspended in 1.5 mL Eppendorf tubes at 1 x 10^7 cells/500 µL in complete DMEM for MR studies. The measured relaxation rates were plotted vs. the extracellularly applied labeling concentration. The sagittal images were obtained with a field of view 14 x 6.9 cm^2, matrix 256 x 256, slice thickness 2 mm, SW 100 kHz, TE 9.2 ms, TR 1500 ms, 26 averages for T1 weighted images.

Labeling concentration [µM]	0.5	1.0	2.5
$R_{1,cell}$ [% of control]	112 ± 0.5**	132 ± 3.7**	144 ± 1.9**
n	3	3	2

Table 3. Intracellular relaxation rates $R_{1,cell}$ in 3T3 cells after loading with anti-dsred CA for 18 h. Values are means ± SEM; **: $p<0.01$ statistically different as compared to control (100 ± 0.6 %), ANOVA with Dunnett´s post test; n: number of experiments, each with two replicates.

The results from both fluorescence and MR studies directed towards further studies on transgenic cell lines to prove the specific accumulation by targeting the mRNA.

2.3.6 Cellular uptake and internalization studies in target-containing cells

CPPs have been used for the delivery of a vast variety of biomolecules. The ability of D-$Tat_{(57-49)}$ to transport our covalently-conjugated PNAs along with the imaging moieties was next investigated in target containing cells. Murine fibrosarcoma cells transfected with the

DsRed2 gene (*96*), referred to as DsRed cells, and their parent cell line CCL-11 were used for internalization assessment by fluorescence spectroscopy and microscopy.

The anti-sense CA as well as the non-sense CA labeled DsRed cells very efficiently (Fig. 12). Both CAs showed a concentration-dependent transfer into cells up to a labeling concentration of 5 μM. Saturation in internalization was observed at labeling concentrations >2.5 μM and a further dose increase was accompanied by increased toxicity but only a marginal improvement in cellular delivery. Thus, for subsequent studies a labeling concentration of 2.5 μM of the PNA-containing CA was used. A comparable uptake profile for both CAs was observed in the non-target containing CCL-11 cells (data not shown).

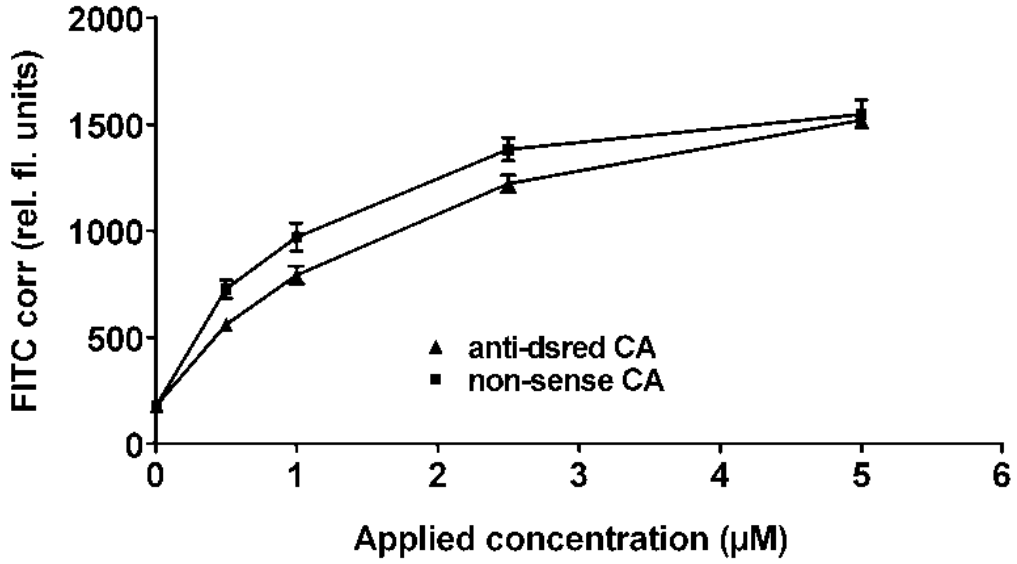

Figure 12. Internalization of anti-dsred and non-sense CA in DsRed mouse fibrosarcoma cells. Fluorescence spectroscopy was performed on cells incubated with 2.5 μM of either anti-dsred or non-sense CA for 18 h. External fluorescence was quenched with trypan blue and subsequent washes with HBSS; Values are means ± SEM, n=3 with six replicates each.

Additionally, observations of DsRed and CCL-11 cells by fluorescence microscopy revealed similar uptake and distribution for both the PNA-containing CAs (Fig. 13). These agents were distributed in the peri-nuclear area as bright punctuate dots in both cell lines. This indicates that despite the difference in the base composition of the two PNA sequences, both anti-sense and non-sense CA have similar cellular internalization efficacy and properties.

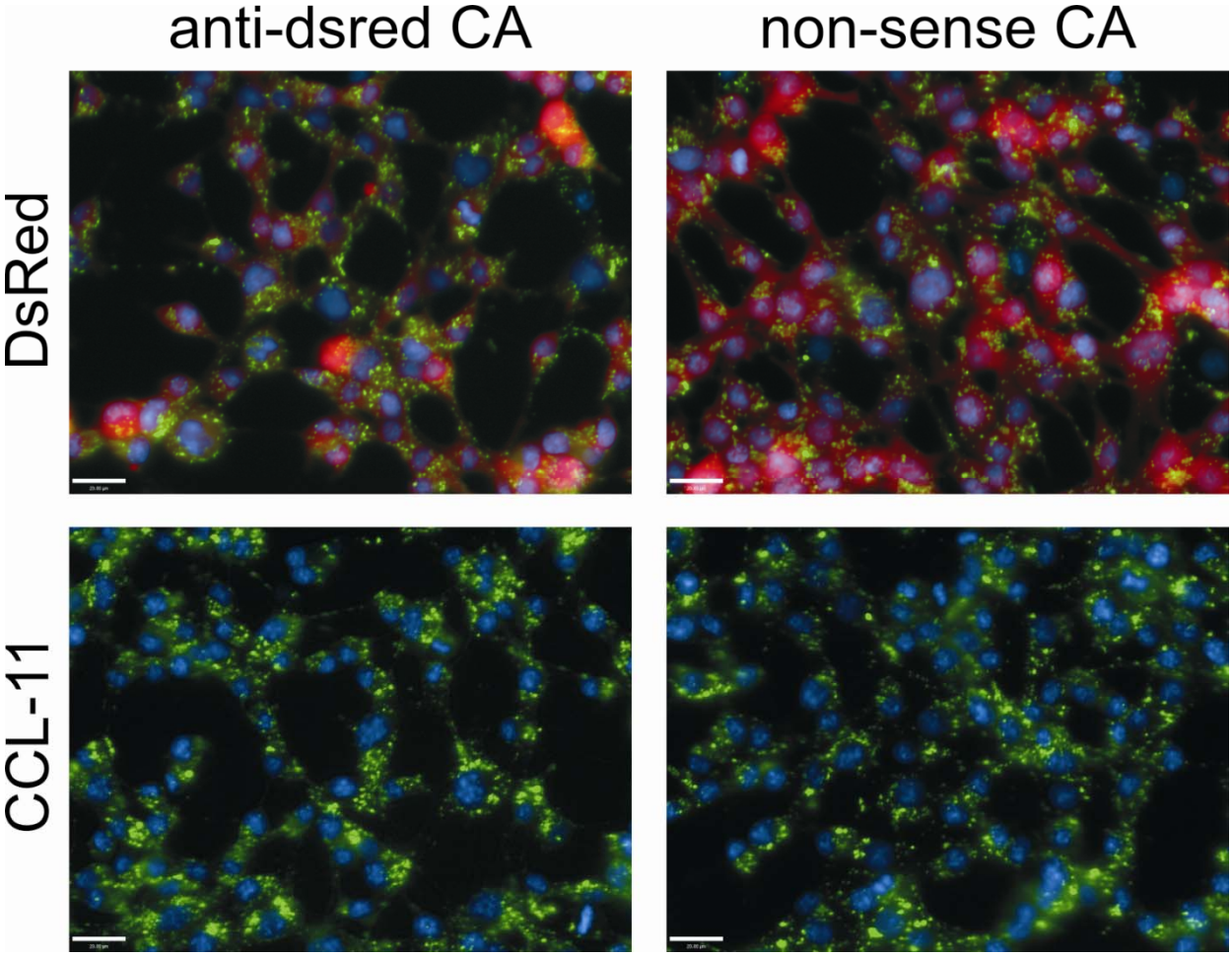

Figure 13. Intracellular distribution of anti-dsred and non-sense CA in DsRed and CCL-11 mouse fibrosarcoma cells. Fluorescence microscopy was performed on cells incubated with 2.5 μM of either anti-dsred or non-sense CA for 18 h. External fluorescence was quenched with trypan blue and subsequent washes with HBSS. The bar represents 20μm.

2.3.7 Enhancement of MR contrast in target-containing cells

The possibility to utilize these PNA-containing conjugates as MR contrast-enhancing agents in target-containing cells was assessed. Cells producing target mRNA as well as non-target expressing cells were labeled with 2.5 μM of either the anti-sense CA or non-sense CA.

In agreement with our earlier observations, both conjugates showed significant contrast enhancement in cells (*104*). The T_1 relaxation times in DsRed cells were substantially altered by the non-sense as well as anti-sense CA at concentrations as low as 2.5 μM (Fig. 14). Remarkably, this labeling concentration was 20-1000 times lower than the amount of CPP linked Gd-based chelators used for delivery into cells (*20, 64, 66, 68, 105*). T_1-weighted

images of CCL-11 cells showed similar contrast changes at these low concentrations. The extended incubation times used for CA delivery into cells could be the reason why this low concentration is sufficient for significant contrast enhancement.

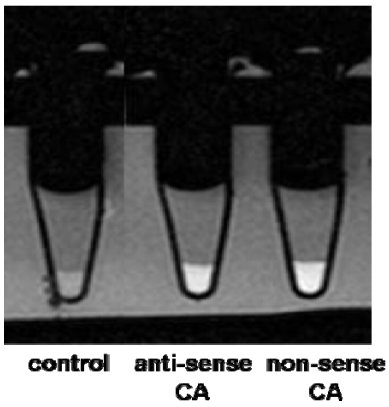

Figure 14. T_1-weighted MR images of DsRed cells after loading with 2.5 μM of anti-dsred and non-sense CA for 18 h. After treatment with anti-dsred CA for 18 h, cells were trypsinized, centrifuged and re-suspended in 1.5ml Eppendorf tubes at 2 x 10^7 cells/500 μl in complete medium for MR studies. Control: cells incubated with culture medium without CA.

The target-containing DsRed cells demonstrated a slightly increased uptake of the anti-sense CA compared to the parent CCL-11 cells (Fig. 15). However, no specific accumulation of the anti-sense CA in comparison to the non-sense CA could be detected in DsRed cells. A decreased rotational correlation time and thus a greater τ_r effect was expected upon binding of anti-sense CA with DsRed2 mRNA (*106*). However, no such effect was observed even in the target-containing cells. These findings suggest that although the CPP-PNA CAs efficiently permeate cells, their interaction with the target mRNA appears limited.

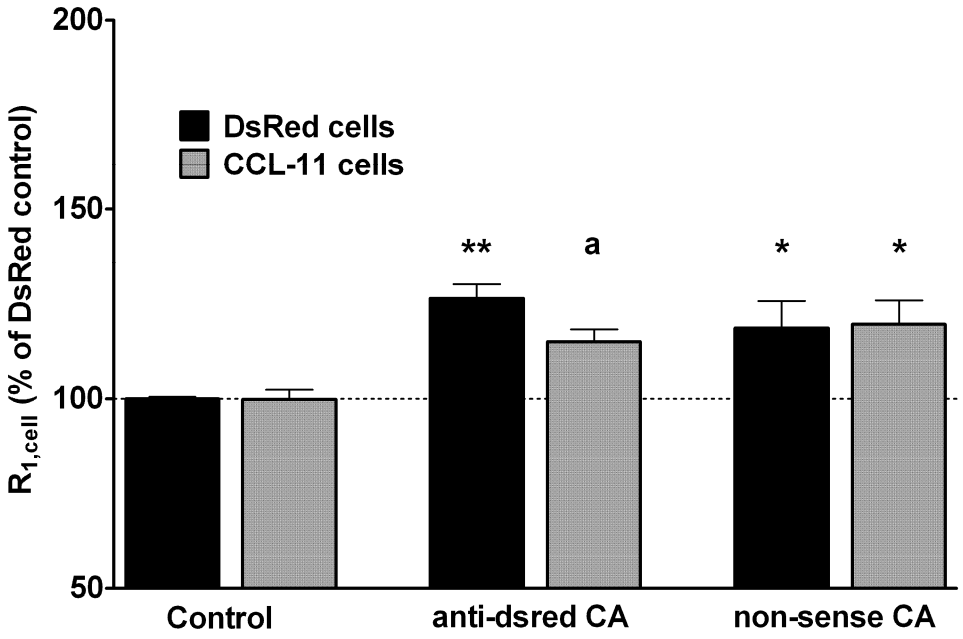

Figure 15. Cellular relaxation rate $R_{1,cell}$ in DsRed and CCL-11 cells after labeling with anti-dsred or non-sense CA. After treatment with DsRed CA for 18 h, cells were trypsinized, centrifuged and re-suspended in 1.5ml Eppendorf tubes at 2 x 10^7 cells/500 µl in complete medium for MR studies. The measured relaxation rates were plotted vs. the applied extracellular labeling concentration. Control: cells incubated with culture medium without CA. Values are means ± SEM, n=3 with two replicates each. *: $p<0.05$, **: $p<0.01$ statistically significantly different to control; a: $p<0.05$ statistically significantly different between contrast agents, ANOVA with Tukey's post test.

2.3.8 Fluorescence microscopy studies

High resolution microscopy was performed to further elucidate the intracellular distribution of the FITC-containing CPP-PNA conjugates. DsRed cells were cultured in channel slides and labeled with anti-sense CA. After removal of surface-bound fluorescence by trypan blue and nuclear staining with Hoechst, cells were examined under the microscope. 3D images were reconstructed from the 2D slice images thus obtained (*107*).

Examination of DsRed cells labeled with anti-sense CA in 3D clearly revealed encapsulation of green fluorescent CA in intracellular vesicles around the nucleus (Fig. 16). Although the target mRNA cannot be visualized by microscopy, it is expected to be distributed mainly throughout the cytosol, as is the case with the red fluorescent DsRed2 protein itself. On the other hand, the CA seemed to be entering cells by endocytosis and subsequently entrapped in endosomal/lysosomal vesicles with little or no release into the cytosol.

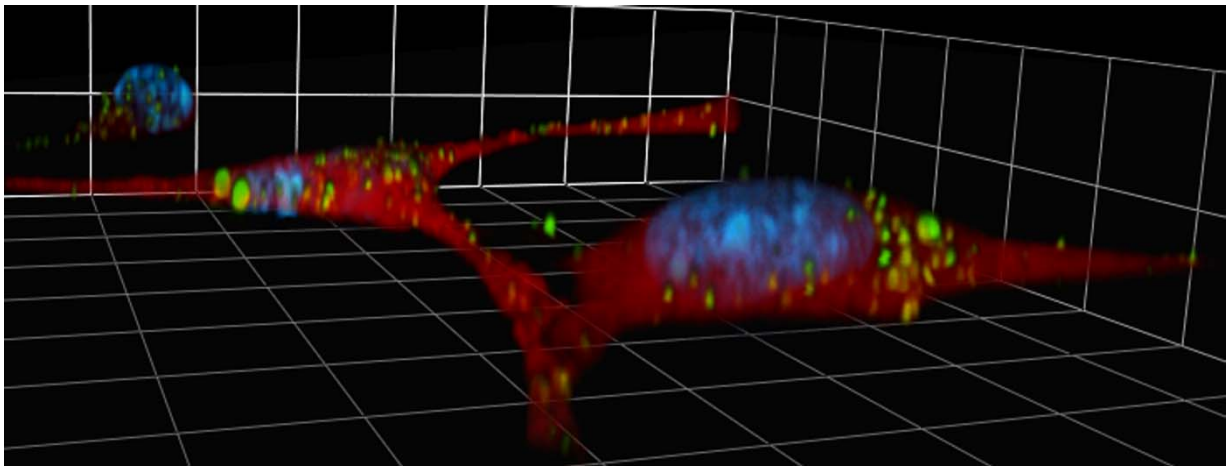

Figure 16. Endosomal localization of anti-dsred CA in DsRed cells. Cells were incubated with anti-dsred CA and cell nuclei were counterstained by Hoechst 33342. External fluorescence was quenched by trypan blue and subsequently washed with HBSS; DsRed CA: green (FITC fluorescence); nuclei: blue (Hoechst 33342). The 3D image was rendered from obtained 2D slices. A single unit of the grid represents 13.3 µm.

An interesting observation was that subsequent to quenching with trypan blue no traces of green fluorescence binding to the cellular membrane were noticed. Trypan blue interacts with the aromatic groups on FITC and therefore the fluorophore in the extracellular environment as well as the FITC in cells with compromised cell membrane integrity becomes quenched. This justifies the use of this stain to efficiently eliminate extracellular and membrane-bound fluorescence. Microscopic examination also indicates that, because of the quenching step in our washing protocol, only the internalized probe signal is quantified by fluorescence spectroscopy.

2.3.9 Biodistribution properties

Coupling of PNA with Gd-DOTA-CPP(FITC) more than doubles the size of the conjugate. Thus, it was important to investigate the mobility of this large molecule *in vivo.* Fluorescence studies performed 20 mins after i.v. injection showed that within minutes the compound entered various organs via the bloodstream, and was by no means limited to the injection site (Table 4).

Tissue	Fluorescence Intensity
Liver	+++
Urinary bladder	+++
Kidney	++
Spleen	++
Lungs	+
Heart	+/-
Brain	-
Blood	-

Table 4. Biodistribution of the anti-sense CA in various tissues represented qualitatively. Tissues from C57/BL6 mice were extracted 20 min after CA administration and tissue slices were assessed for anti-sense CA-related green fluorescence. Tissues from animals injected with saline alone served as control.

The fluorescence observed in the liver and bladder was very high and the exposure time for fluorescence images was reduced almost 3.5 times in comparison to the rest of the tissues (Fig. 17). The lipophilic nature of the PNA-containing CA explains the affinity of the conjugate for liver tissues. Kidney and spleen were moderately labeled whereas heart and lungs were only faintly fluorescent. Absolutely no fluorescence of FITC from the CA was detected in the brain, thus indicating a lack of penetration of the blood brain barrier. Although these biodistribution studies are preliminary, they clearly indicate that the bulky PNA-containing anti-sense CA spontaneously disperses in the organism after injection and also rapidly enters the excretory system.

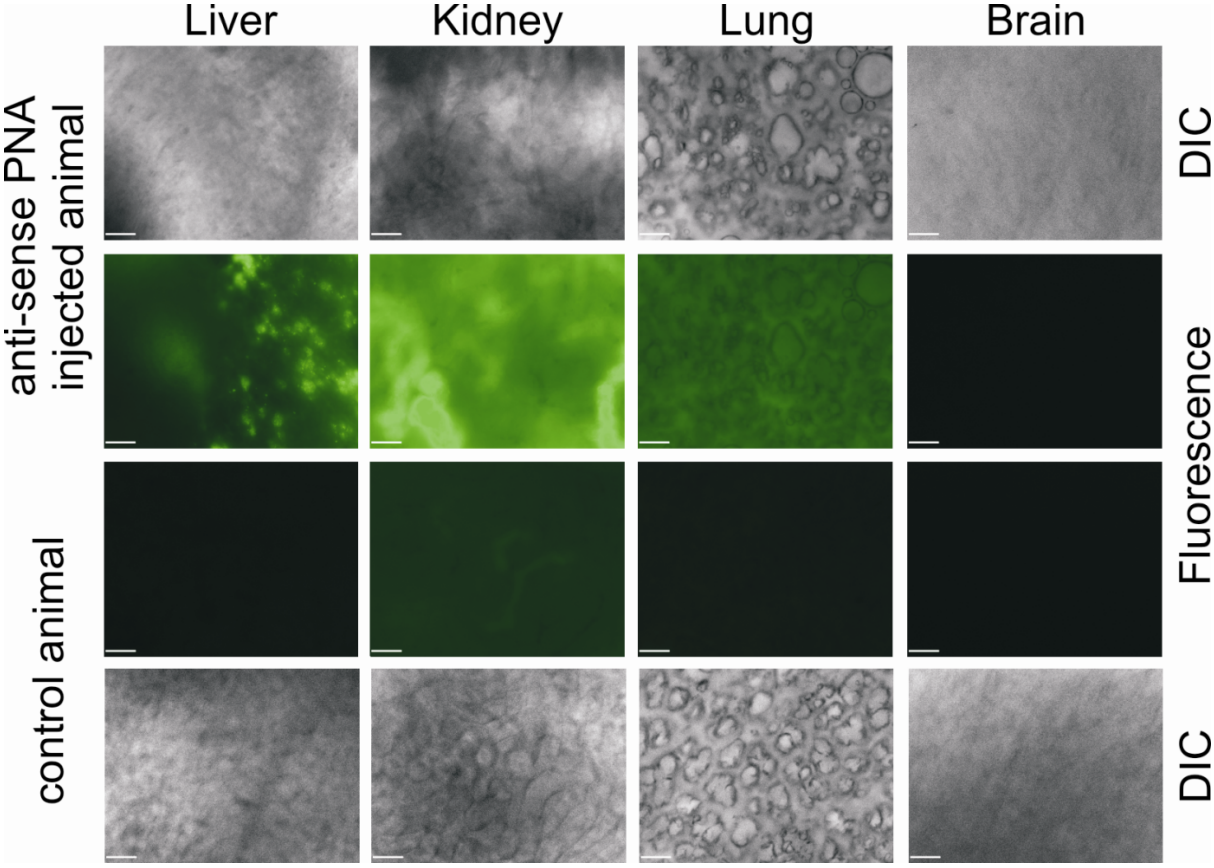

Figure 17. Distribution of anti-dsred CA in different tissues after *in vivo* labeling. Tissues were extracted 20 min after intravenous administration of anti-dsred CA to C57/BL6 mice. Fluorescence and bright field images of the tissues were obtained. For fluorescence images of liver an exposure time of 175 ms was used while for all other tissues it was adjusted to 600 ms. The bar represents 160 µm.

2.4 Discussion

Among the increasing number of transduction peptides that are being characterized, HIV-1 Tat and polyarginines represent two of the particularly well-studied. Over the years more efficient sequences have been derived by modifications of Tat CPP (*56, 101*). Furthermore, a higher toxicity of polyarginines in comparison to Tat has been suggested (*108*). Therefore, we started with the evaluation of the efficiency of three HIV-1 Tat derivatives to translocate MR CAs together with FITC into cells. Thus far, there are only a few publications about the use of HIV-1 Tat to transport CAs for MRI (*64, 65*). Large amounts of CA need to be transported into cells to obtain maximum MR contrast enhancement because of the low sensitivity of MRI. Therefore, we chose long incubation times and labeling protocols comprising of incubation in the presence of serum supplemented medium and an incubation temperature of 37°C. A routine laboratory embryonic mouse fibroblasts cell line NIH 3T3 was selected for comparison of uptake efficiency.

Our results accounted highest uptake accompanied with high cell death for Orn-D-Tat_{inv} CA, thus limiting its further exploitation. Although D-$Tat_{(57-49)}$ has been accounted for more efficient delivery of variety of cargos (*102*), in our hands we obtained a comparable delivery with the L-Tat CA. This difference could be attributed to the influence of the Gd-loaded chelate on the molecular charge or three-dimensional conformation of the conjugate. On the other hand, it is well-established that D-isomers of amino acids are resistant to enzymatic cleavage and remain longer in the circulation (*102*). Thus, D-$Tat_{(57-49)}$ was chosen as the CPP for experiments on further coupling of PNA sequences together with Gd-DOTA and FITC to obtain bimodal targeting agents.

Based on this evaluation, our goal was to design a multi-modal probe by the use of a facile building block approach. The blocks could easily be altered according to the target requirement without significant modification in the synthetic scheme. The final molecule designed consisted of MR and optical imaging parts linked to a PNA essential for targeting and a CPP for intracellular delivery. Antisense PNA conjugated with different cell penetrating peptides (such as PTD-4 or poly-lysine) and radiometal complexes (such as ^{111}In, ^{90}Y or ^{64}Cu) has been reported as nuclear imaging probes (PET and SPECT) (*81, 109*). But the utilization of such conjugates as contrast agents for MR imaging is very limited, probably because the accumulation of the PNA imaging probes in the targeting cells could barely reach a detectable level. Heckl et al. developed a MR contrast agent combining a Gd^{3+}-complex with antisense PNA targeting the c-*myc* mRNA and Antennapedia peptide (*68*). Using this contrast agent, an increase in MR signal intensity and prolonged retention in tumor cells highly expressing this gene was observed *in vitro* and *in vivo*.

The cell-free *in vitro* binding studies clearly depicted a considerable specificity in the interaction between the anti-sense PNA and the complementary ODN sequence. In contrast, the non-sense CA showed no binding to the target sequence. Attempts were made to establish a similar specificity of the intracellularly taken up CAs using fluorescence *in situ* hybridization (FISH). To our surprise, no detectable fluorescence signal was identified in cells labeled with anti-dsred CA.

Our anti-dsred and non-sense CAs are very efficiently taken up by target containing (DsRed) as well as non-target containing (3T3, CCL-11) cell. Thus, the feasibility of using D-$Tat_{(57-49)}$ as a transport vector for large-sized cargos has again been demonstrated. In fact, efficiency similar to that of the D-Tat_{inv} CA was observed when an almost 10 times lower

labeling concentration of the PNA-containing CAs was used. Despite the large increase in molecular weight, the PNAs increase the hydrophobic nature of the cargo. We hypothesize that the CPP-PNA CAs might interact better with the cell membrane and hence enhance uptake. Also, the applied concentration of contrast agent (0.5 mM) in Heckl's study (*68*) was 1000x higher compared to the lowest concentration of anti-dsred CA in our experiments showing a significant increase in relaxation $R_{1,cell}$ within the cells. The difference is likely attributable to the different cell penetrating peptides and the Gd^{3+} moiety used. Thus, the synthesized anti-dsred CA has an excellent potential to be used as targeted contrast agent for MR imaging in cells expressing the DsRed2 gene. Although, the high hydrophobicity of the conjugates containing PNA reduced their solubility in water, therefore, the PNA-containing conjugates could be used only at low micro-molar concentrations for labeling cells.

The target containing cells labeled with anti-dsred and non-sense CAs were subjected to MR studies as well as high resolution microscopy. No considerable interaction between the targeting PNA with mRNA was observed by any examination. MR studies did depict a significant increase in cellular relaxation rates of DsRed cells labeled with anti-dsred CA compared to cells without any target. However, the non-sense CA also showed a significant contrast enhancement in comparison to the control cells. This could mainly be due to the endosomal entrapment of most of the targeting CA in spite of having entered into cells, thus segregating and hindering binding with target mRNA. As more information is obtained about the mechanism of cellular delivery by CPPs, it is becoming evident, as also reported by other groups, that endocytosis is the main route of trans-membrane movement (*110-112*). However, there is a lack of definitive evidence on the maintenance of functionality of the CPP-associated cargo once it is conveyed into cells. Some studies indicate successful PNA interaction with the target after being delivered by membrane-transducing peptides (*113-115*). Other studies indicate limited PNA binding with the target due to entrapment of PNA conjugates in endosomes (*116, 117*).

Another possible reason could be the non-specific interaction of the non-sense sequence in the rich pool of biomolecules inside the cell. These non-specific interactions could be the cause of cellular relaxation rate enhancement of both the CAs in cells deficient of target sequence. Thus, other non-sense sequences need to be tested to verify this.

The small amount anti-dsred CA that might be reaching the target could be out of the detection limit of MR. Thus, more methods like PET could be used for improving the

sensitivity. This could be easily performed by replacement of Gd with a radiometal and testing with target containing or deficient cells.

For future application, additional modifications are needed for developing CPPs with better penetration properties, especially directed into the cytoplasmic compartment. Endosomal localization of the probes is expected to be a hindrance to specific binding to the targeted mRNA located in the cytoplasm. This is, in fact, a general problem facing many, if not all, MR contrast agents synthesized to date for the purpose of intracellular reporting. Endosomal uptake, however, is likely to represent only "inefficiency", as endosomes retain a majority of the CA while only a minute part does ultimately show up in the cytoplasm. Leakage from endosomes or a direct uptake into the cytoplasm is a possibility and towards achieving this goal we are currently working on developing novel CPPs. Release from endosomes depending on their acidification is reported for some fluorescein coupled CPP (*57*) but is also cell type dependent. In this study Fischer et al. depicted an enhanced degradation of the CPP followed by a rapid exit of its fragments from the cytosol for the HIV-Tat peptide (consisting of the native L-form aminoacids) coupled to fluorescein resulting in a low cytosolic fluorescence. Since for our study, we used the D-form of the amino acids for synthesizing CPPs, an increase of their stability towards proteases would prevent the cytosolic release of our CA. Thus, it will be interesting to look for novel CPPs that possess high delivery efficiency with the native form of amino acids and also evade the entrapment into the endosomes.

Chapter 3: Development of a novel cysteine-rich Cytosolic Localizing Peptide CyLoP-1 and understanding its delivery into the cytosol

3.1 Introduction

Cell delivery vectors (CDVs) possess the innate ability to permeate through biological membranes and also efficiently translocate meagerly penetrating macromolecules inside cells (*118*). Often referred as cell penetrating peptides (CPPs) or peptide transduction domains (PTDs), CDVs are generally short cationic peptides that could either be derived from natural proteins like HIV1-Tat (*119, 120*) and penetratin (*90, 121*) or have a synthetic origin like polyarginine (*51*) and transportan (*52*). These peptides have been reported to deliver cargoes ranging from small molecules like fluorophores to large sized plasmid DNA and liposomes (*122, 123*). However, the activity for the imported cargo was maintained in some cases (*49, 103, 124, 125*) while many accounted failures (*62, 116, 126-130*). The lack of functionality was reasoned by the mechanism of internalization of CDVs which is not only complex but also extensively debated. Interestingly, most of the recent studies indicated that majority of CDVs entered the cells by one or the other endocytotic pathways (*58, 110, 112, 131*), thus, limiting the target molecule into the endosomal compartment. This necessitates the release of endocytosed material, before lysosomal enzymes and low pH degrade them.

An alteration of intracellular distribution pattern as a result of the induction of alternative non-endocytic routes of uptake was observed by Brock and coworkers upon application of high concentrations of HIV1-Tat and nona-arginine (*58*). More often liberation of cargo has been investigated using the combination of CDVs with lysosomotropic agents like chloroquine (*132, 133*), addition of calcium (*134*) or introduction of influenza virus HA2 hemagglutinin subunit (*132, 135*). Futaki *et al.* also reported the use of pyrenebutyrate as a counteranion with poly-arginines for rapid and direct cytosolic delivery (*136, 137*). Nevertheless, most of these chemicals effectively transport into the cytosol only in the absence of serum which is a very non-natural condition for *in vivo* applications. In addition, these chemicals are effective at concentrations that either induce toxicity or cause stress on cells, thus, initiating several other degenerative pathways (*138, 139*).

An ideal approach for cellular delivery would assist in enhanced uptake of the molecule of interest either by direct permeation of the cellular membrane or be followed by discharge and localization in intracellular compartment of interest. In nature, there are quite a few examples of peptides and proteins from bacterial or plant toxins and venoms from snakes, spiders, jellyfish and sting rays (*140-142*). They induce their detrimental effects by directly

overcoming the barriers of plasma membrane and/or deliver their active domain inside cells. Based on the structural properties of these toxins, new classes of CPPs having the optimum delivery, localization and efficiency are being engineered (*143, 144*).

The cell-penetrating properties of crotamine, a toxin from the venom of a South American rattlesnake, were recently reported by Kerkis *et al.* (*145*). The unique feature of this 42 amino acid polypeptide is its ability to mark actively proliferating cells and to bind chromosomes and centrioles. We selected one of the proposed sequences ($Crot_{27-39}$) that could be apparently guiding the nuclear localization of this polypeptide. Herein we present an extensive structure and functionality evaluation that was performed on the sequence involving the synthesis of different peptides using systematic substitution and/or deletion of amino acid residues as well as epimerizations (Table 5) and testing for their uptake efficiency. This investigation lead to the identification of a novel peptide, CyLoP-1, distinguishingly localizing into the cytosol (*146*). This short cationic peptide with three cysteine residues offers abundant possibility for exploitation as a delivery tool for intracellular targeting.

A further detailed characterization of the intracellular delivery ability of CyLoP-1 was carried out. The purpose of this study was the characterization of the biochemical properties and intracellular delivery of CyLoP-1 to achieve a better understanding of the unique uptake behavior of this peptide. The factors responsible for the distribution within the cytoplasm were examined by observing serum stability, uptake under different conditions and in various cell types as well as investigating the effect of CyLoP-1 on the cellular metabolism.

3.2 Materials and Methods

3.2.1 Materials

All chemicals for synthesis were purchased at purest HPLC and peptide synthesis grade from commercial sources. 3T3 embryonic mouse fibroblasts and C6 rat glioma cells were obtained from DSMZ, Germany, PANC-1 human carcinoma cells were procured from ATCC, USA, N18 mouse neuroblastoma cells were a kind gift of Prof. Bernd Hamprecht (University of Tuebingen, Germany) and SHIN3 human ovarian cancer cell line was kindly gifted by Prof. Silvio Aime (University of Torino, Italy). Dulbecco's Modified Eagle's Medium (DMEM), Iscove's Modified Dulbecco's Medium (IMDM), Hank's buffered saline (HBSS), phosphate buffered saline (PBS), fetal bovine serum (FBS), granulocyte

macrophage colony-stimulating factor (GM-CSF), interleukin-4 (IL-4) were obtained from Biochrom AG (Germany). Bisbenzimid 33342 (Hoechst 33342), 2,3-bis(2-methoxy-4-nitro-5-sulfophenyl)-2H-tetrazolium-5-carboxanilide inner salt (XTT), monobrombimane (MBBr), N-ethylmaleimide (NEM), propidium iodide (PI), Nonidet P-40, trypan blue were procured from Sigma Aldrich (Germany).

3.2.2 Peptide synthesis

N-terminally labeled fluorescein isothiocyanate conjugated peptides were synthesized using an automated peptide synthesizer (peptides&elephants, Germany) by continuous solid phase Fmoc/*t*Bu chemistry. All samples were purified by semi-preparative RP-HPLC (Varian PrepStar Instrument, Australia) equipped with PrepStar SD-1 pump heads. Mass spectrometry (ESI-MS) was used for further characterization. The purified products were lyophilized, divided into aliquots and stored at -20°C till used.

3.2.3 Cell Culture

3T3 embryonic mouse fibroblasts, SHIN 3 human ovarian cancer cells, C6 rat glioma cells and PANC-1 human pancreatic carcinoma cells were cultured as monolayers in DMEM supplemented with 10% FBS, 4 mM L-glutamine, 100 µg/ml streptomycin and 100 U/ml penicillin at 37°C with 10% CO_2. Cells were trypsinized and passaged every second to third day.

N18 mouse neuroblastoma cells were cultured in an antibiotic free DMEM supplemented with 10% FBS and 4 mM L-glutamine at 37°C with 5% CO_2. Cells were sub-cultivated by trypsinization two times a week. In order to induce differentiation of neuroblastomas, slow step-wise serum deprivation was used till FBS content was reduced to 1.25% in medium.

Hematopoietic stem cells (HSCs) were isolated from C57/BL6 mouse bone marrow and cultured in IMDM supplemented with 10% FBS, 1% GM-CSF, 1% IL-4 and antibiotics. The cells were cultured for 7 days with change of medium on day 3 and day 5. On the 7^{th} day, cells were scraped from plates and re-seeded in µ-dish (Ibidi, Germany) for another 24 h.

3.2.4 Evaluation of peptide uptake by fluorescence spectroscopy

The uptake efficiency was assessed using 3T3 fibroblasts grown to 70-80% confluency in 96well microplates. The cells were incubated with different peptides at identical concentration or single peptide over a range of concentrations in supplemented DMEM for

additional 18 h at 37°C with 10% CO_2. In order to estimate the cell number, the cellular nuclei were stained by incubating cells with Hoechst 33342 for another 30 min. All traces of peptide-related extracellular fluorescence were quenched by incubating with cold trypan blue in PBS for 3 min followed by repeated washes with HBSS (*100, 147*). In a multiplate reader (BMG Labtech, Germany), the cell-related FITC fluorescence (Ex 485nm/Em 530nm) and cell number (Hoechst fluorescence, Ex 346nm/ Em 460nm) were measured. Intracellular FITC fluorescence intensity was corrected for cell number and the result, multiplied by 1000, expressed as "corrected fluorescence units" (corr. f.u.).

Time course studies were made by maintaining the labeling concentration of peptides constant and incubating cells for various periods of time.

To study the effect of low temperature on cellular uptake and distribution, 3T3 cells were pre-chilled for 30 min at 4ºC. These cells were then incubated with FITC labeled peptide for additional 4h at 4ºC.

Experiments were run at least three times for each peptide with six replicates. Statistical analysis was performed by Student´s t-test or ANOVA with Bonferroni's post test for multiple comparisons. P values < 0.05 were considered significant.

3.2.5 Analysis of cellular localization by live cell imaging

The cells from the 96well plates for spectroscopy imaged without fixation using a Zeiss Axiovert 200 M microscope (Zeiss, Germany) with a LD Plan NeoFluor 40X objective. Imaging of N18 neuroblastoma was performed in single channel slides (Ibidi, Germany) and stem cells isolated from mouse bone marrow in µ-dish (Ibidi, Germany). The imaging conditions were kept constant for the observation of different samples. Cellular localization and distribution of the peptide was observed by irradiating with blue light (470/40 nm) and observing at 525/50 nm. The bright punctate and encapsulated appearing FITC fluorescence was categorized as vesicular uptake while diffused fluorescence appeared to be distributed in the entire cell. Manual observations of at least three independent experiments were compiled to conclude if the peptide shows diffused, vesicular or both types of uptake. Apart from FITC fluorescence, the nuclear labeling by Hoechst 33342 was observed at 460/50 nm and trypan blue fluorescence viewed at 645/75 nm. Also phase contrast images of the same area were made to observe if the cells maintained their normal morphology in the presence of peptides.

The uptake of peptide was also assessed by labeling different cells (SHIN3, N18 and HSCs) for 18 h at a concentration of 2.5 μM followed by washing and microscopic observation as explained before.

3.2.6 Cytotoxicity assay

Toxicity of the peptides was investigated by a XTT based colorimetric cellular viability assay. 3T3 cells were grown to subconfluency in 96-well plates. The cells were incubated with various concentrations of peptides for 4 or 18 h under normal growth conditions and cell viability was subsequently measured by the XTT assay. After treatment, cells were incubated for 30 min with a freshly prepared solution of XTT (0.25 mM) with PMS (0.5 μM). The absorption of the water-soluble colored formazan derivative formed by the conversion of XTT was measured at 450 nm with reference wavelength at 690 nm in the multiplate reader. The DNA content of the cells was also quantified by Hoechst labeling of the same cells and a correlation to the cell number was made measuring the fluorescence at Ex 346nm/ Em 460nm.

3.2.7 Propidium iodide membrane integrity assay

3T3 cells were seeded 24 h before treatment in 96well plates at 6×10^3 cells/well. Cells were treated for different durations by incubating with medium containing 5 or 2.5 μM of peptide conjugates (CyLoP-1 and penetratin). After incubation, the peptide-containing solution was removed and PI in HBSS was added to cells. After another 20 min the fluorescence of this labeling was measured at Ex 530 nm/Em 645 nm. Also microscopic observations were made to look for cells with compromised plasma membranes labeled with PI. As PI stains only DNA of non-vital cells, the surfactant Nonidet P-40 was added afterwards for 20 min to lyse all vital cells. Their fluorescence was measured again to determine the total cell number per well.

3.2.8 Analyzing interaction of peptide with glutathione

The glutathione content of cells was measured by a slightly modified assay using MBBr as described elsewhere (*148*). Briefly, 3T3 cells were grown in 96well plates for 24 h followed by treatment with various concentrations of peptide conjugates (CyLoP-1 and penetratin) for 1, 4 or 18 h. Subsequent to incubation and removal of treatment medium, cells were washed with HBSS. Then, MBBr in HBSS was added to the plate and after 30 min incubation in dark the fluorescence intensity of MBBr-glutathione was measured at an

excitation wavelength (Ex) of 360 nm and an emission wavelength (Em) of 460 nm. MBBr readings were corrected by total cell number values determined by PI staining. Background staining of the protein sulfhydryl groups was determined in cultures after depletion of glutathione with NEM.

3.2.9 Serum stability

FITC labeled CyLoP-1 and L- and D-form of Tat and octaarginine were incubated in serum-free or serum-containing medium for 30 min. The peptides were then analyzed by a nondenaturing gel electrophoresis. The bands were imaged for FITC fluorescence. Also coomassie brilliant blue staining of the peptides in the gel was conducted.

3.3 Results

3.3.1 Generation of a more effective CPP by Structure-Activity-Relationship studies

The starting sequence tridecapeptide $Crot_{27-39}$ (peptide 1, KMDCRWRWKCCKK) included three cysteine residues, tryptophans, aspartic acid, methionine along with six basic amino acids (arginine and lysine). The positively charged amino acids were kept unaltered considering the requirement of cationic residues for membrane adherence (*51*). Cysteine residues in peptides are known to modify the biological activity of the peptide by their ability to form intra- and intermolecular bridges and hence promote oligomerization (*149*). However cysteine, methionine and tryptophan moieties in peptides also cause side reactions such as racemization, oxidation and alkylation (*150-153*). Therefore, studies were carried out to evaluate the functional significance of these residues. SAR studies were performed to achieve a sequence optimized for cell penetrating properties, as well as production and shelf life. The importance of each of the amino acids of $Crot_{27-39}$ for the cellular internalization was assessed leading to the optimal peptide, CyLoP-1, with unique properties (Table 5).

Table 5. Sequences of 38 synthesized peptides, the calculated and observed molecular mass $(M+H)^+$, intracellular fluorescence intensity and percentage of CyLoP-1 of the conjugates. (K(FITC) was coupled to all peptides at the N-terminus), and intracellular fluorescence intensity (corr. f.u.) values in NIH 3T3 cells after a labeling period of 18h at 2.5 µM. D-amino acids are represented in lower case. In some cases molecular ion is calculated from the divalent ion.

Peptide	Sequence	Molecular Weight		Intracellular fluorescence intensity [corr. f.u.]		% of CyLoP-1
		Expected $(M+H)^+$	Observed $(M+H)^+$	Mean	SEM	
1	KMDCRWRWKCCKK $Crot_{27-39}$	2288.7	2288.6	3176	271	78
2	MDCRWRWKCCKK	2160.5	2162.0	3344	374	83
3	DCRWRWKCCKK	2029.3	2029.9	1909	272	47
4	CRWRWKCCKK (CyLoP-1)	1914.3	1914.9	4050	322	100
5	RWRWKCCKK	1809.1	1811.3	1511	256	37
6	KMDCRWRWKCKK	2185.6	2186.4	1516	181	79
7	KMDCRWRWKKK	2082.4	2084.7	1202	218	30
8	KMDRWRWKKK	1979.3	1979.6	100	50	2
9	KDCRWRWKCCKK	2157.5	2159.2	1043	137	26
10	KCRWRWKCCKK	2042.4	2043.0	1583	246	39
11	KRWRWKCCKK	1939.3	1940.8	1226	120	30
12	MDCRWRWKXCKK	2142.5	2142.0	1937	335	48
13	DCRWRWKXCKK	2011.3	2013.0	1741	427	43
14	DCRWRWKCXKK	2011.3	2011.6	943	313	23
15	CRWRWKXCKK	1896.2	1897.0	2044	408	50
16	CRWRWKCXKK	1896.2	1896.6	1347	171	33
17	RWRWKXCKK	1793.1	1793.1	1211	529	30
18	MDCRWRWKXXKK	2124.5	2124.8	1256	187	31
19	DCRWRWKXXKK	1993.3	1993.8	872	554	22
20	CRWRWKXXKK	1878.2	1880.0	1390	199	34
21	RWRWKXXKK	1775.0	1776.2	405	109	10
22	CRWRWKCSKK	1898.2	1899.0	2172	597	54
23	SRWRWKCCKK	1898.2	1898.6	1867	367	46
24	SRWRWKCSKK	1882.1	1881.9	572	94	14

Peptide	Sequence	Molecular Weight		Intracellular fluorescence intensity [corr. f.u.]		% of CyLoP-1
		Expected $(M+H)^+$	Observed $(M+H)^+$	Mean	SEM	
25	SRWRWKSCKK	1882.1	1882.4	475	77	12
26	CRWRWKSSKK	1882.1	1882.0	415	109	10
27	SRWRWKSSKK	1866.1	1866.0	193	89	5
28	CRFRWKCCKK	1875.2	1875.0	2656	320	66
29	CRWRFKCCKK	1875.2	1875.8	2476	382	61
30	CRFRFKCCKK	1836.2	1836.8	2569	197	63
31	crwrwkcckk	1914.3	1914.8	2109	503	52
32	KCCKWRWRCK	1914.3	1914.9	1713	148	42
33	kcckwrwrck	1914.3	1914.9	1449	295	36
34	CrWRWKCCKK	1914.3	1914.1	1529	163	38
35	CRwRWKCCKK	1914.3	1913.9	1229	40	30
36	CRWrWKCCKK	1914.3	1915.0	1304	345	32
37	CRWRwKCCKK	1914.3	1914.0	1412	456	35
38	CrwrwKCCKK	1914.3	1915.0	1488	360	37

3.3.2 CyLoP-1 shows efficient cellular internalization

Cellular uptake efficiency of CyLoP-1 conjugated to lysine-FITC was investigated by fluorescence spectroscopy. A concentration of 2.5 μM was chosen for labeling 3T3 cells as at this concentration the peptide had good solubility in supplemented culture medium and demonstrated no cytotoxicity. A time course of uptake was evaluated and compared with standard CPPs namely penetratin and d-Tat (HIV-1 $Tat_{(47-59)}$) sequence with d-form of amino acids) also coupled to lysine-FITC. CyLoP-1 exhibited a time dependent increase of uptake even after 24 h of treatment (Fig. 18). Although, both penetratin and d-Tat also labeled cells very rapidly, they displayed a constant increase in the first 12 h which was followed by a decrease after longer incubation.

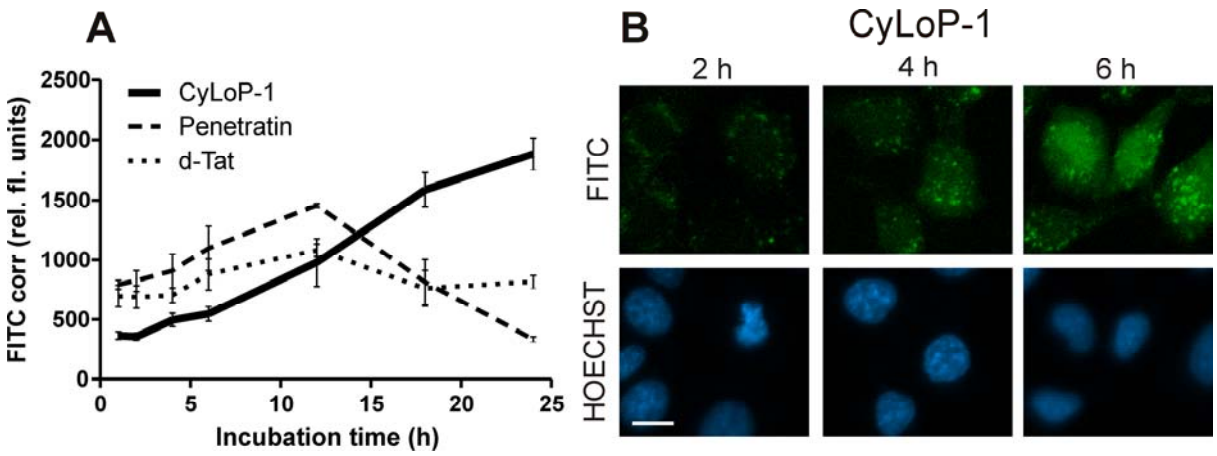

Figure 18. Time dependent uptake of CyLoP-1 in 3T3 cells. Cells were incubated for various time points with 2.5 µM of the different peptides in complete medium at 37 °C. After nuclear staining and trypan blue quenching A) fluorescence spectroscopy and B) microscopy were performed to assess the internalization. Spectroscopy values are mean ± SEM, n = 3-6 with six replicates each. The bar represents 20 µm.

On increased labeling doses, a concentration dependent increase in uptake efficiency was observed (Fig. 19 A). The maximum applicable amount was 5 µM as at higher concentrations a precipitation was observed (Fig. 19 B). CyLoP-1 was soluble up to milli-molar concentrations in pure water but in supplemented medium its solubility was limited. Nevertheless, these low micro-molar concentrations are sufficient for long term labeling of cells.

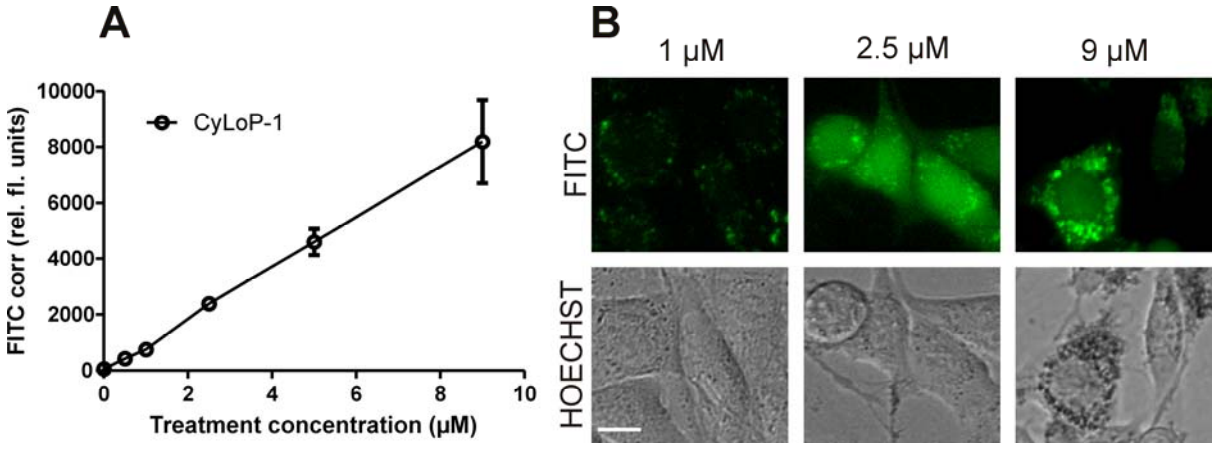

Figure 19. Concentration dependent uptake of CyLoP-1 in 3T3 cells. Cells were incubated for 18 h with 2.5 µM of CyLoP-1 in complete medium at 37 °C. After nuclear staining and trypan blue quenching A) fluorescence spectroscopy and B) microscopy were performed to assess the uptake. Spectroscopy values are mean ± SEM, n = 3 with six replicates each. The bar represents 20 µm.

To avoid any over-estimation of uptake efficiency by surface-bound extracellular fluorescence, a quenching step with trypan blue was incorporated (*100, 147*). Cells treated with CyLoP-1 up to 5 µM of labeling concentration appeared to have normal morphology and density with almost no signs of membrane permeation by trypan blue. In addition, the long term detrimental effects at different peptide concentrations and various time points was evaluated by XTT and Hoechst staining (Fig. 20). We observed that on measuring XTT, the high labeling dose of 9 µM also did not indicate any toxicity in 3T3 cells even when treated for long term. On the other hand, the evaluation of DNA content by Hoechst displayed about 30% reduction in cell number at 9 µM while lower concentrations were non-toxic. When the results of both assays were combined to normalize XTT values by the number of cells (XTTcorr. = XTT/Hoe×1000), an increase by 50% was observed at the highest concentration.

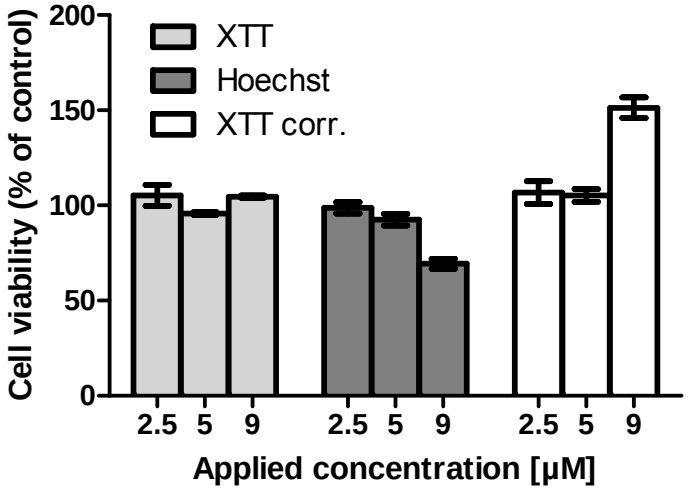

Figure 20. Cytotoxicity induced after long term application of high concentrations of CyLoP-1 on 3T3 cells. Cells were incubated with different concentrations of the peptide in complete medium at 37 °C. After HBSS wash, XTT assay was performed followed by DNA content estimation with Hoechst. The values from these two assays were combined for correction of XTT for cell number and the result after multiplication by 1000 was represented as XTT corrected (XTT corr.), values are mean ± SEM, n = 3 with six replicates each.

3.3.3 Serum is essential for the solubility of CyLoP-1

With the aim of evaluating the effect of serum on uptake efficiency, internalization assays were performed in the absence of serum or in the presence of various serum concentrations. The complete removal of serum from medium resulted in up to 50% reduction in the uptake of CyLoP-1 (Fig. 21).

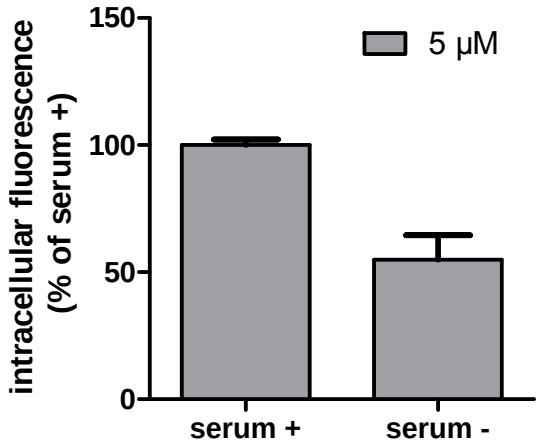

Figure 21. Effect of serum in incubation medium on uptake of CyLoP-1 in 3T3 cells. Cells were incubated for 4 h with 5 µM of CyLoP-1 in serum containing (serum +) or serum deficient (serum -) medium at 37 °C. After nuclear staining and trypan blue quenching, fluorescence spectroscopic evaluation of internalization was performed, values are mean ± SEM, n = 6.

Microscopic observations depicted the formation of a precipitate in serum-free medium even at a concentration of 2.5 µM which disappeared on addition of 1.25% FBS to the medium for treatment. The precipitation limited the uptake of CyLoP-1 and FITC fluorescence was largely detected bound to the membrane (Fig. 22). The increase of serum content in medium directly correlated with a rise in cellular uptake and cytosolic distribution of fluorophore.

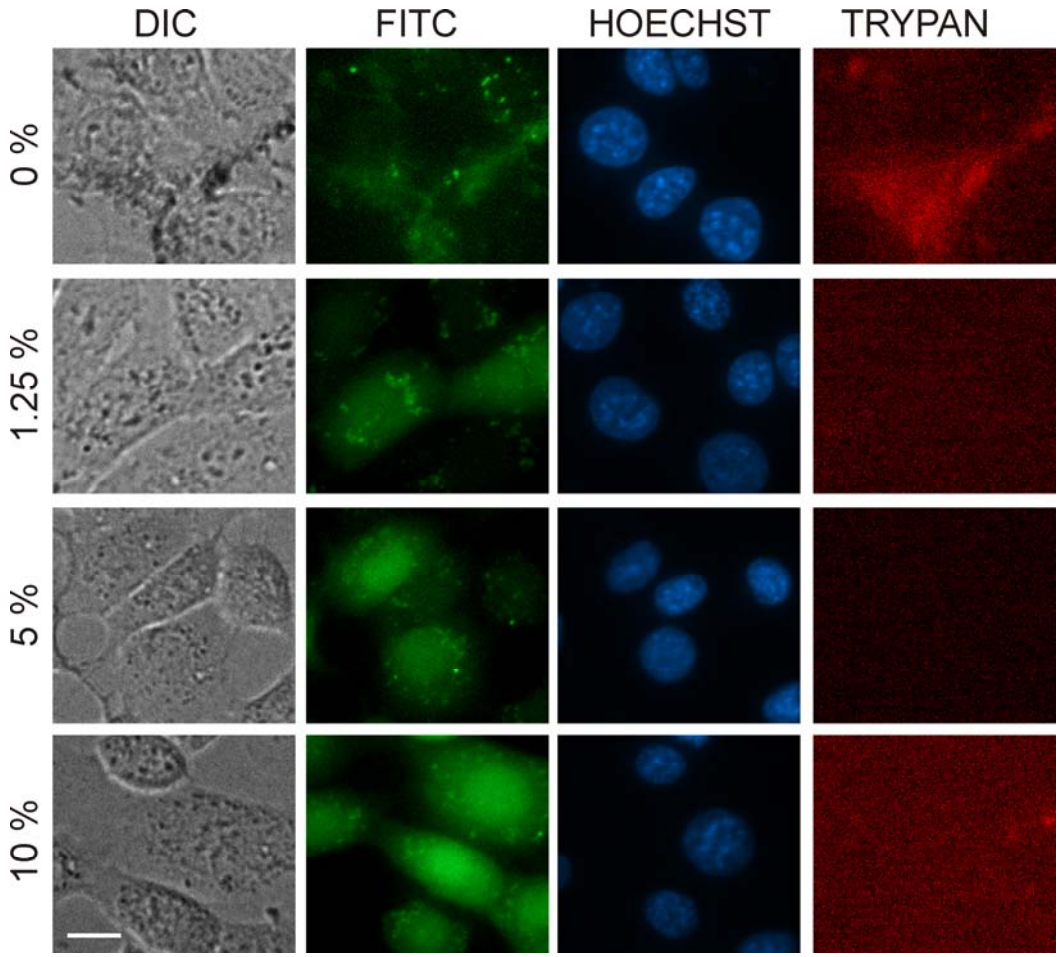

Figure 22. Presence of serum in incubation medium enhances the uptake and cytosolic localization of CyLoP-1 in 3T3 cells. Cells were incubated for 4 h with 5 μM of CyLoP-1 in serum-containing (serum +) or serum-deficient (serum -) medium at 37 °C. After nuclear staining and trypan blue quenching fluorescence spectroscopic evaluation of internalization was performed, values are mean ± SEM, n = 6. The bar represents 20 μm.

The stability of CyLoP-1 was tested in the presence of serum to ensure that the internalization of fluorophore resulted by assistance of complete peptide and not through any by-products formed by extracellular degradation. CyLoP-1 was dissolved in serum supplemented medium and incubated under culture conditions for 18 h. On running this peptide solution through a polyacrylamide gel followed by coommassie brilliant blue staining, a band corresponding to the intact peptide was detected (Fig. 23). Comparison was made with the same peptide incubated in serum-free medium.

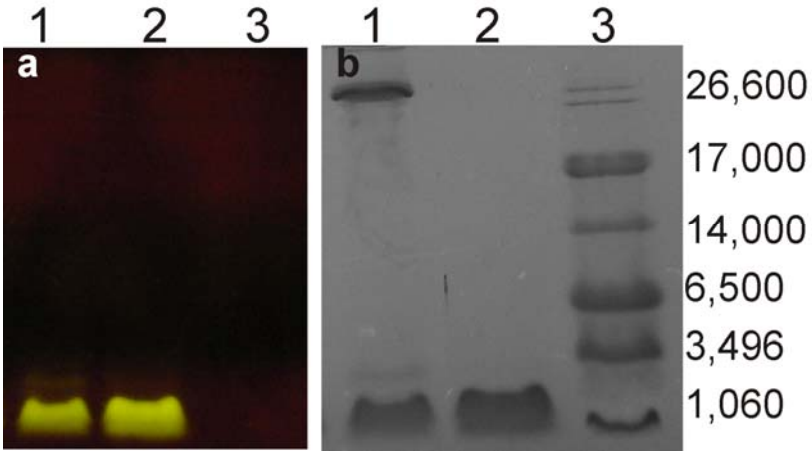

Figure 23. Stability of CyLoP-1 in serum containing medium after long term incubation. CyLoP-1 was incubated in serum containing (lane 1) or serum-free (lane 2) medium for 18 h followed by a run on denaturing gel. Ultra-low molecular weight marker (lane 3) was run to verify the molecular weights of the bands. The stability of the peptide was verified by FITC fluorescence (a) and after coommassie blue staining (b).

To corroborate these results, the cellular internalization of lysine and cysteine-lysine, both conjugated to FITC, was quantified after 18 h incubation. No traces of the fluorescence were found inside cells, thus confirming the inability of small conjugates to enter into cells (Fig. 24).

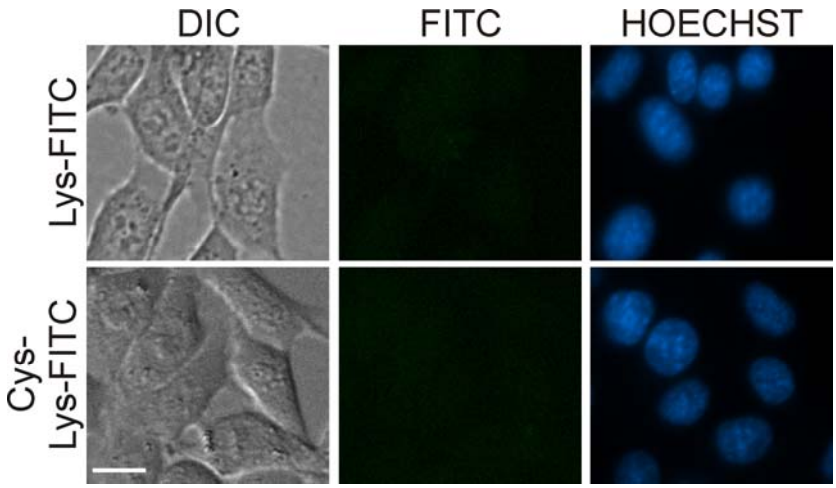

Figure 24. Possible fluorophore-linked degradation products of CyLoP-1 do not penetrate into cells. 3T3 cells were labeled with FITC linked lysine (Lys-FITC) and cysteine-lysine (Cys-Lys-FITC) for 18 h with 2.5 µM of CyLoP-1 in serum containing medium at 37 °C. After nuclear staining and trypan blue quenching fluorescence microscopy was performed. The bar represents 20 µm.

3.3.4 Cytosolic distribution of CyLoP-1

CyLoP-1 labeled cells were assessed for cellular distribution by fluorescence imaging of living cells. A particularly cytosolic localization along with some vesicular uptake distinguished CyLoP-1 from penetratin, d-Tat (Fig. 25). A faint diffuse green fluorescence was observed in the early hours of incubation while longer incubation times displayed bright diffuse cytosolic localization at 2.5 µM of labeling concentration. Moreover, this time could be shortened by application of higher peptide concentration. Fig. 25 A appropriately demonstrates the intense cytosolic and dotted vesicular distribution patterns of CyLoP-1 after 4 h of treatment with 5 µM concentration in interphase 3T3 cells after synchronization of culture. For synchronization, fresh mitotic cells were collected by gently tapping loosely adhering dividing cells from the culture flask and transferring for further culture in a new flask.

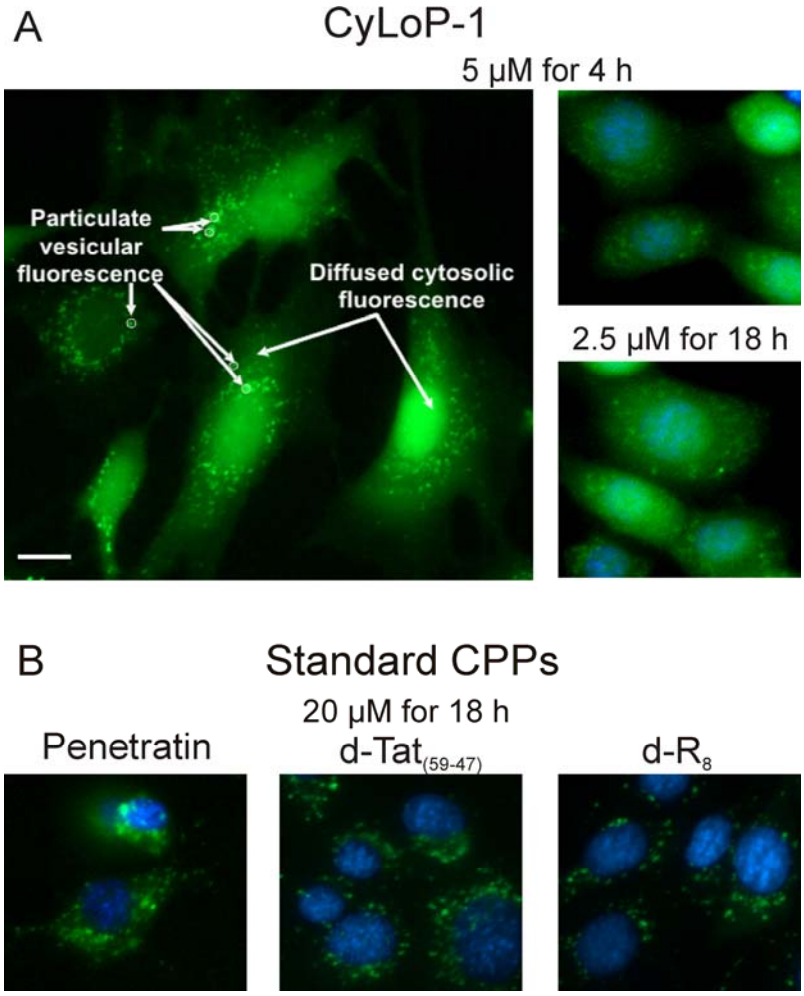

Figure 25. Intracellular distribution of various CPPs in 3T3 cells. A.) CyLoP-1 shows vesicular and diffuse cytosolic distribution on application of 5 µM concentration for 4 h in synchronized 3T3 cells (left), 3T3 cells in routine culture (top right) and on application of 2.5 µM for 18 h (bottom right). In comparison the standard CPPs, penetratin (left), d-Tat$_{(59-47)}$ (middle) and d-octaarginine (right) displayed mainly a vesicular

distribution when 20 µM of CPP was applied for 18h on 3T3 cells in culture. All labeling was performed in serum supplemented medium. Before microscopy, cells were stained with Hoechst 33342, quenched with trypan blue and extensively washed with HBSS. The bar represents 20 µm.

The intracellular distribution of CyLoP-1 was evaluated at different temperatures to determine the energy dependence of uptake of this peptide. Interestingly, at low incubation temperature the diffused cytosolic fluorescence was maintained but a strongly reduced vesicular distribution was observed (Fig. 26). Fluorescence spectroscopic measurements showed a significant reduction in the amount of peptide delivered into cells. Nevertheless, a complete inhibition of uptake could not be detected at low temperature.

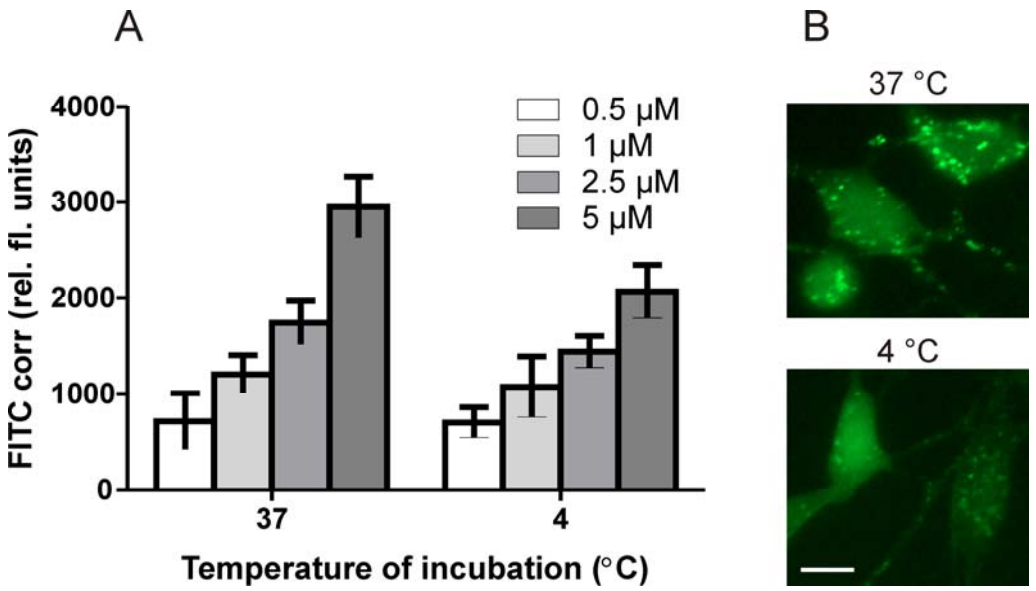

Figure 26. Cytosloic distribution of CyLoP-1 is maintained at low labeling temperature. 3T3 cells were labeled with different concentrations of CyLoP-1 for 4 h at 37 °C or 4 °C. Subsequent to nuclear labeling and trypan blue quenching A.) fluorescence spectroscopy and B.) fluorescence microscopy were performed. The bar represents 20 µm.

3.3.5 CyLoP-1 interacts with cellular membrane and integrity of membrane is maintained

To facilitate the transfer of cargo into cells, delivery vectors need to circumvent the phospholipid bilayer. Experiments were performed to evaluate the interaction of CyLoP-1 with the plasma membrane in the initial uptake phase. Pre-chilled 3T3 fibroblasts were incubated with 5 µM of CyLoP-1 at 4ºC for 2 h. After incubation, labeling peptide was removed from cells without the step of trypan blue quenching. The same cells were further incubated in fresh peptide-free supplemented medium at 37ºC for another 2 h.

Microscopic observations after the removal of CyLoP-1 from cells depicted membrane bound distribution of most of the fluorescence (Fig. 27) indicating the role of the membrane-peptide interaction before internalization. Furthermore, this membrane-bound peptide permeated inside the cells on subsequent incubation at 37°C and displayed vesicular along with minor diffuse fluorescence.

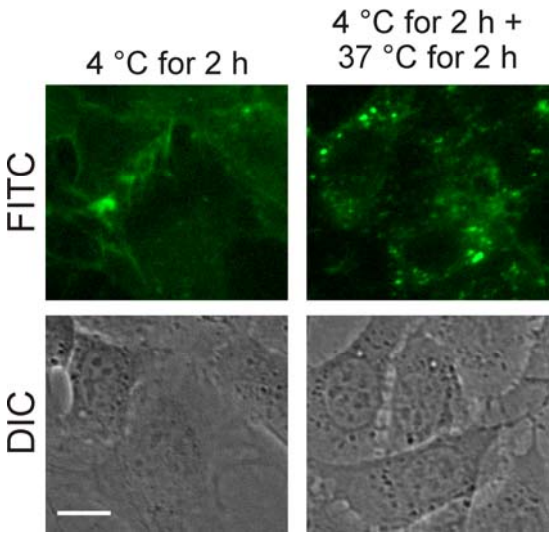

Figure 27. Interaction of CyLoP-1 with cellular membrane at 4 °C followed by internalization of bound peptide on further incubation at 37 °C. 3T3 cells were labeled with 5 μM of CyLoP-1 for 2 h at 4 °C. Microscopy was performed after removal of peptide-containing solution and one HBSS wash. The same cells were further incubated at 37 °C in peptide-free medium for an additional 2 h. After rigorous washing, the cells were observed under the microscope. No trypan blue quenching was performed for this evaluation. The bar represents 20 μm.

The integrity of the plasma membrane was checked by PI to rule out that the intracellular diffuse localization was due to disruption of the lipid bilayer. After treatment with 2.5 or 7.5 μM of CyLoP-1 for different time points, 3T3 cells were labeled with PI solution. In parallel, penetratin was tested at same concentrations and time durations. PI enters cells with leaky membranes and labels their DNA. Both peptides displayed an absence of nuclear staining by PI when evaluated by spectroscopic measurements (data not shown) as well as by microscopy (Fig. 28). The leftmost panel displays PI labeling of a dead cell after treatment with 7.5 μM of CyLoP-1. Almost 98% of the cell population comprised of healthy cells after CyLoP-1 or penetratin labeling and did not exhibit permeation of PI stain into cells.

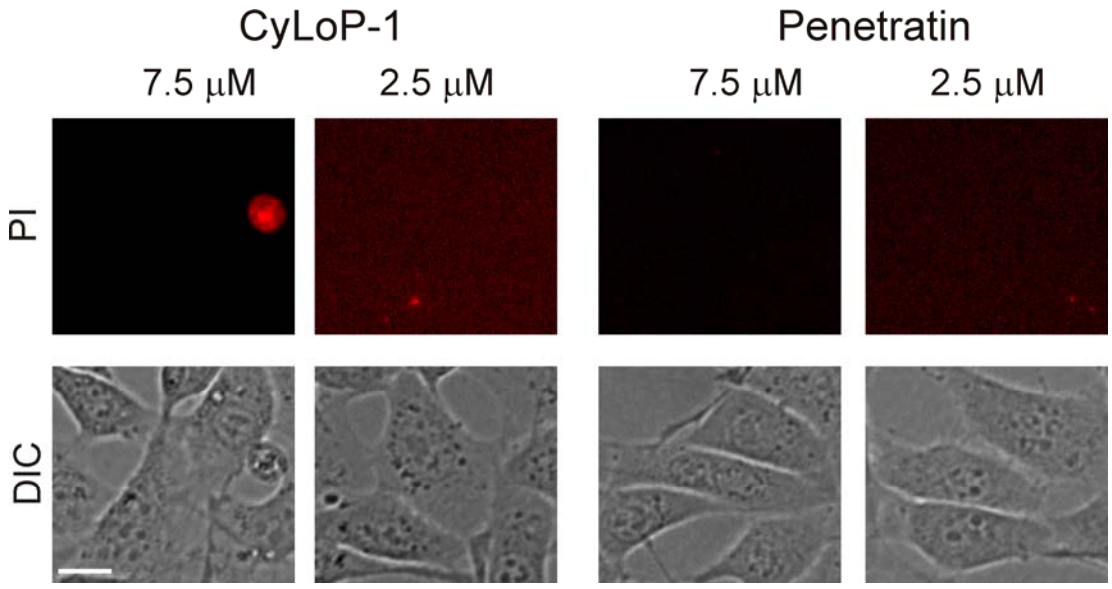

Figure 28. Integrity of the plasma membrane assessed by PI staining after incubation of cells with CyLoP-1 or penetratin. 3T3 cells were labeled with different concentrations of CyLoP-1 or penetratin for 18h. Microscopy was performed after removal of peptide-containing solution, one time HBSS wash and staining of cells with PI to evaluate membrane integrity. The bar represents 20 μm.

3.3.6 Effect of stereochemical modifications on uptake

The CPP-based delivery approach is potentially hampered by the instability of the vector to endogenous peptidases (*56*). The possible solutions to this hurdle could be the use of the D-form instead of the naturally occurring L- amino acids, use of beta-peptides (*154*) or peptoids (*56*) to enhance vector stability. We studied further analogues of CyLoP-1 to evaluate the influence of the stereochemistry of the peptide backbone (enantiomeric purity of CyLoP-1 was about 95% as shown by GC-MS analysis on chiral phase) as well as the sequence alignment. Incorporation of D-amino acids and reversal of the sequence (inverse isomers) of the peptide is shown to increase the transmembrane delivery in the case of the Tat peptide (*56*). Therefore, the D-isomer [peptide 31] and L-inverse as well as D-inverse isomers of CyLoP-1 [peptide 32, peptide 33] were synthesized. Unexpectedly, these analogues showed reduced uptake by about 50% (Figure 29 A). In addition to the reduction in uptake, a decrease in diffuse cytoplasmic distribution was observed as compared to CyLoP-1 (Figure 29 B). These results demonstrate that stereochemistry has a clear effect on cellular uptake of CyLoP-1. Unlike known CPPs, CyLoP-1 proved to be most efficient in its natural L-amino acid form.

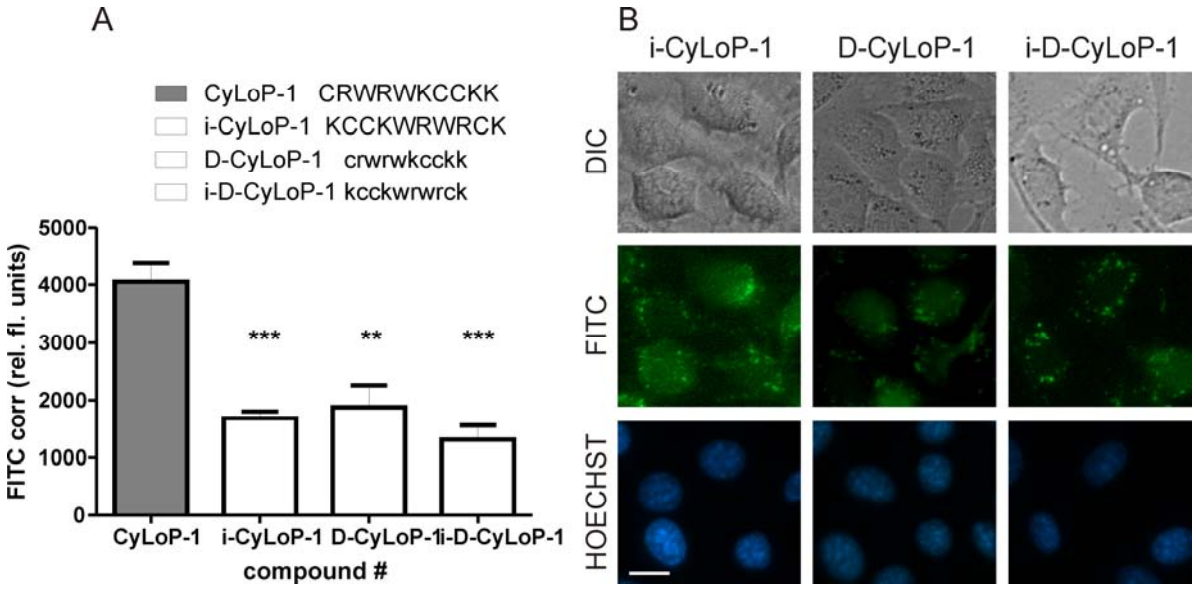

Figure 29. Stereochemistry and sequence of CyLoP-1 affect its transport into cells and intracellular distribution. 3T3 cells were treated with 2.5 µM of different peptides for 18h in serum supplemented medium. A.) Cellular uptake was assessed by fluorescence spectroscopy after nuclear labeling and trypan quenching. B.) The same cells were subjected to fluorescence microscopy to evaluate intracellular distribution. The bar represents 20 µm.

3.3.7 Effect of substitution of cysteines

Next to truncated peptides, variety of peptides were synthesized by substitution of cysteines with α-amino-*n*-butyric acid (*155*) to study the combined effect of cysteine deletion and/or substitution [peptides 12-21]. This resulted in an immensely reduced cellular uptake to a level of 10% when compared to CyLoP-1 (Table 5).

The significance of cysteines for internalization in peptide 1 (KMDCRWRWKCCKK) and peptide 4 (CyLoP-1, CRWRWKCCKK) was determined by substituting cysteine residues with Abu or serine (*156*). Substitution of one to three cysteine(s) by serine(s) in CyLoP-1 [peptides 22-27] revealed a positively correlated decrease in the uptake efficiency with the number of cysteines being replaced. Total exchange led to a nearly complete loss of activity (Figure 30). Similar results were obtained for Abu-substituted peptides. Furthermore, deleting single cysteine residues one by one [peptides 6-8] led to a decrease of uptake as well. Therefore, the number of cysteines in CyLoP-1 is vital for internalization and especially diffused cytosolic distribution. Replacement or deletion negatively affected uptake indicating that cysteines are substantial and could be involved in the mechanism of membrane penetration.

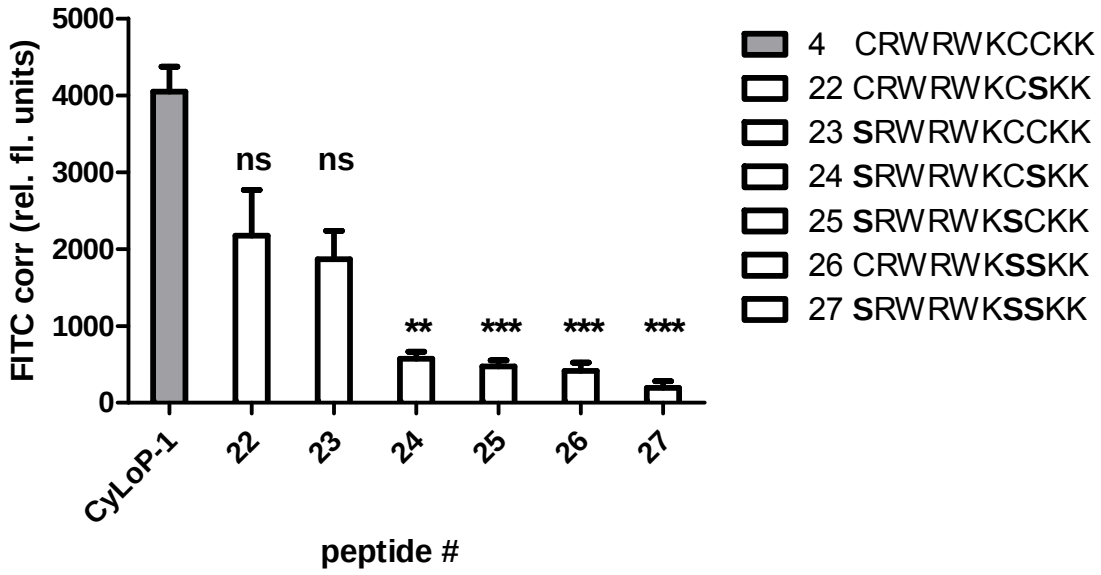

Figure 30. Cysteines are important for stereochemistry and affect its transport into cells and intracellular distribution. 3T3 cells were treated with 2.5 μM of different peptides for 18h in serum-supplemented medium. After treatment, cells were labeled with Hoechst 33342 followed by trypan quenching and rigorous HBSS washing. Cellular uptake was assessed by fluorescence spectroscopy, values are mean ± SEM, n = 3-6 each with six replicates.

Tryptophan has been shown by others to participate in membrane permeation. They are reported to destabilize the membrane once the peptide is adhered to the surface. To examine these effects in CyLoP-1, replacement of either one or both tryptophans was investigated [peptides 28-30]. A decreased uptake (Table 5) and almost complete loss of diffusion was observed. Lowering of cytosolic distribution and uptake by substitution of tryptophan with phenylalanine (*157*) also signifies the substantial role played by the tryptophan residues. Results suggests the not only the presence but also the number of tryptophans are inevitable to maintain the required hydrophobicity and well functioning of CyLoP-1.

3.3.8 Interaction of the cysteine-rich peptide with glutathione

Apart from the cationic amino acids, CyLoP-1 contains three cysteine residues. To assess if these cysteines interact with the intracellular glutathione, cells were treated with various CyLoP-1 concentrations for 1, 4 and 18 h. A cysteine-deficient CPP, penetratin, was tested at similar concentrations and time points. No decrease in glutathione levels was observed at any of the tested concentrations (Fig. 31). Instead at all time points, a minor increase (5-10 %)

from the control values was obtained for CyLoP-1. As expected, penetratin also exhibited no interaction with intracellular glutathione.

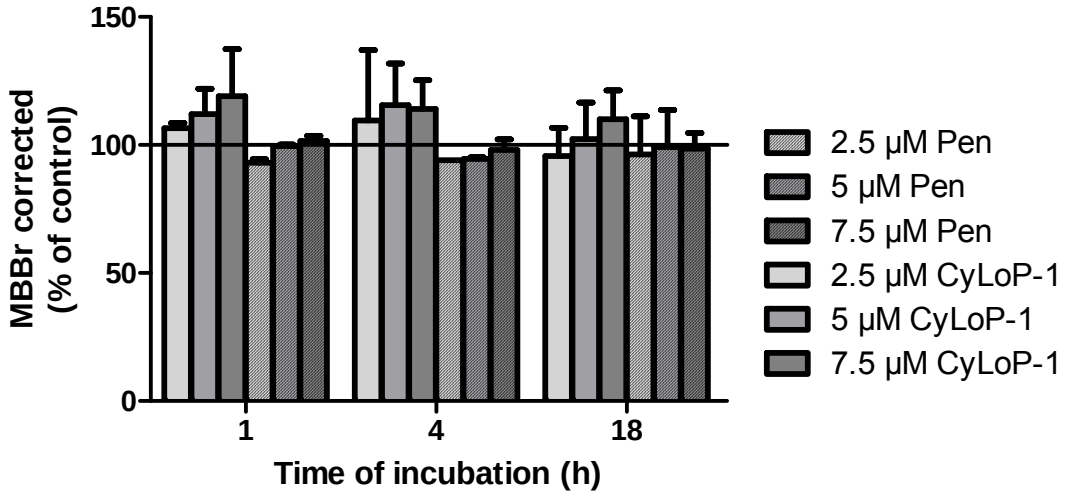

Figure 31. Interaction of CyLoP-1 with cellular glutathione compared to penetratin. 3T3 cells were labeled with different concentrations of CyLoP-1 or penetratin for various time points. The content of cellular glutathione was evaluated by MBBr assay followed by PI staining to estimate the cell number.

3.3.9 CyLoP-1 delivers into various cell types

To exclude that the distinguished cytosolic localization of CyLoP-1 is specific only for 3T3 cells, cellular uptake was tested in other cell types. The chosen cell lines were from different origins, obtained from different tissues and other species. The human cervical cancer cell line, SHIN 3, displayed an intense diffuse fluorescence while the vesicles spread in the perinuclear region upon long term treatment with 2.5 µM of CyLoP-1 (Fig. 32). A similar diffuse uptake was observed in human pancreatic carcinoma cells, PANC-1, along with fluorescent vesiclular distribution in a restricted perinuclear region. This difference in the vesicular distribution was explained by the area occupied by the nucleus of different cell types. The fluorescent vesicles distributed in the cells according to the location of nucleus and availability of free cytoplasm. Differentiated mouse neuroblastoma N18 cells also showed a modest uptake of the peptide (Fig. 32). Cytsolic fluorescence was observed mainly in the cell bodies while the processes contained some fluorescent vesicles. However, C6 rat gliomas took up the peptide better and demonstrated bright diffuse fluorescence. Alike 3T3, all cell lines showed a heterogeneous distribution of diffuse fluorescence from CyLoP-1. The diffuse uptake was not detected in all cells, although vesicular uptake was seen in all.

Apart from these established cell lines, CyLoP-1 was proficiently taken up in primary cells derived from mouse bone marrow. In HSCs, the fluorescence was spread in the cytoplasm and also filled large vacuoles and small vesicles (Fig. 32).

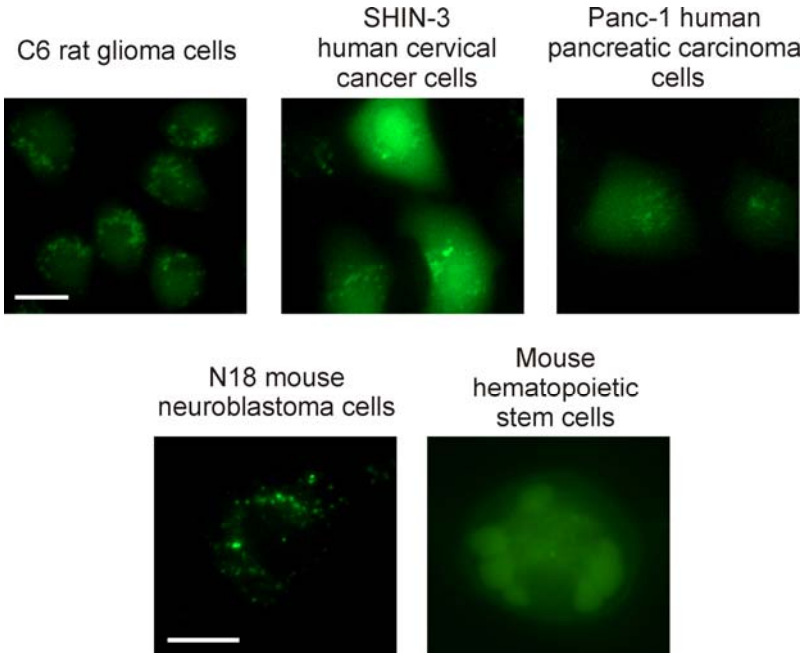

Figure 25. Intracellular localization of CyLoP-1 in various cell types. CyLoP-1 was applied to various cell types at the common concentration of 2.5 µM for 18 h. The labeling was performed in serum supplemented medium. Before microscopy, cells were stained with Hoechst 33342, quenched with trypan blue and extensively washed with HBSS. C6, SHIN-3 and Panc-1 were imaged at 40x magnification and N18 and HSCs at 63x. The bar represents 20 µm.

3.4 Discussion

Crotamine, a very basic toxin present in the venom of some species of the South American rattlesnake, was first identified by Goncalves and co-workers in early 1950's (*158*). Since then this protein has been thoroughly investigated and characterized. However, in 2004 Kerkis *et al*. identified a novel feature of crotamine where this protein was shown to successfully cross cellular membranes (*145*). Due to the chromosomal and centriole labeling properties of this toxin, it has a potential for use as a marker of actively proliferating cells and for the identification of cell stages. Focusing on the two ends of this 42 amino acids protein, Radis-Baptista and co-workers illustrated a shortened sequence combining residues 1-9 and 38-42, that also localized in cellular nuclei after membrane translocation (*159*).

Our primary interest was to develop a vector that could permeate the lipid bilayer and enter into the cytoplasm. In structure activity studies starting from one of the presumed NLS

sequence of crotamine ($Crot_{27-39}$, KMDCRWRWKCCKK), a novel cysteine-rich peptide, namely CyLoP-1 (CRWRWKCCKK) was identified (*146*). The results of the present study demonstrate that CyLoP-1 is an efficient CPP with the ability to label cells at low micro-molar concentrations. Unlike the complete toxin crotamine and the minimalist sequence studied by Radis-Baptista, CyLoP-1 did not show any karyophilic trait. In fact, the peculiar characteristic of our shortened sequence was the intense localization in the cytosol along with some vesicular uptake. Dispersed cytoplasmic fluorescence was observed after labeling cells for 4h with 5 μM of CyLoP-1 while lower concentrations needed elongated duration of incubation. The cytosolic distribution of CPPs in living cells is not very common and of late most of the conventional delivery peptides have been accounted for uptake by endocytosis (*58, 110, 112, 131*). The distribution into the cytosolic compartment has been reported for only some delivery vectors, worth mentioning are the cytoplasmic transduction peptide (*160*), $S4_{13}$ peptide (*161*), Rath peptide (*162*) and GALA peptide (*163*). Nevertheless, for all these CPPs and many more the distribution in the cytoplasm has been accounted for after fixation or following delivery assisted with other transport agents like Lipofectamine.

CyLoP-1 not just efficiently labeled 3T3 cells but was also delivered into the cytoplasm of a variety of other cell types. The cytoplasmic localization of this peptide was not restricted to 3T3 cells. A similar distribution was observed in immortalized cell lines, tumour cells as well as in primary cells. Also the tissue of origin or the species of cell lines did not affect the intracellular distribution of CyLoP-1. This indicates the applicability of our peptide for delivery into a variety of cell types. However, the cells with large nucleus and limited cytosplasmic space like the cell bodies of differentiated neuroblastoma cells showed reduced cytosolic distribution.

The uptake was compared to the internalization of well characterized CPPs, namely d-Tat i.e. HIV-1 $Tat_{(49-57)}$ with d-form of amino acids and penetratin. A striking difference was observed between the time course of CyLoP-1 and the other two standard CPPs in 3T3 cells. Our peptide showed the ability to transport into cells for prolonged durations, thus, potentially maximizing the amount of cargo delivered across the membrane. The cell-free stability studies supported the stability of the peptide in supplemented medium for these long hours. Furthermore, in our hands d-Tat and penetratin depicted mainly a vesicular distribution without any nuclear labeling. This could be justified due to the use of serum-supplemented medium for all uptake experiments. A cytosolic distribution of these standard CPPs has been

displayed by other groups, where studies at other time-points and concentrations were conducted in serum free conditions (*58, 164*).

CyLoP-1 is a delivery vector obtained by shortening of a proposed nuclear localizing sequence (NLS) from the larger protein crotamine. In the minimization process, the main feature maintained was the ability to translocate cellular membranes and enter into cells. However, the uptake efficiency of CyLoP-1 decreased compared to the intact protein. Crotamine was reported to proficiently label cells at a concentration of 1 µM while CyLoP-1 showed only a faintly detectable fluorescence at the same low dose. A concentration of 2.5 µM was optimal for long-term labeling and 5 µM for short term. Refuting the suggestion for the sequence being a putative NLS, neither the original (Cro_{27-38}) nor the shortened peptide depicted nuclear penetration and labeling. At all applicable concentrations and incubation times, CyLoP-1 showed vesicles distributed in the perinuclear area and diffuse fluorescence showed no overlapping with Hoechst labeling of nuclei. In addition, no centriole or chromosomal labeling by CyLoP-1 was observed at various cell stages.

Negligible cytotoxicity was detected for CyLoP-1 up to 5 µM of labeling concentrations while higher concentrations showed increased toxicity. In addition, CyLoP-1 was not soluble at higher concentrations and showed precipitation. The results from the XTT assay as well as nuclear labeling by Hoechst were combined for a proper interpretation of toxicity. The XTT (like the MTT) assay, commonly used to determine cell viability, is detecting the cellular activity of reducing enzymes and is, thus, a measure of metabolic activity (*165, 166*). However, under certain conditions, cells can exhibit changed metabolic activity independent of the number of cells (*167*). For the incubation with 9 µM of CyLoP-1 an enhanced metabolic activity could be observed (Fig. 20) if the cell number normalized value was used. Here, the XTT value alone was indicating that there seemed to be any significant cytotoxic action of the conjugate at this concentration, whereas the Hoechst assay displayed a 30% reduction in the number of cells. Accordingly, an estimation of DNA or protein content and its correlation to the metabolic activity need to be done for appropriate assessment of induced toxicity. As a photometric assay based on the absorbance of the dye, an interference of remaining precipitate of CyLoP-1 on cells should also be taken into account which was observed at 9 µM.

The incorporation of a quenching step with trypan blue in washing before evaluation of cellular delivery served as a supplement for toxicity verification. The dead cells could be

clearly identified as stained blue by this dye in bright-field microscopy. Besides, fluorescence microscopy detected low amounts of the trypan blue entering into partially compromised cells. Thus, trypan blue treatment avoided misinterpretation of uptake by quenching of extra-cellular FITC fluorescence as well as allows toxicity elucidation by its red fluorescence (*168*).

To consider the peptide for potential *in vivo* applications, an important factor that needs to be taken care of is the effect of serum. It has been reported that arginine-rich peptides transduce cell membranes directly when the uptake is performed in the absence of serum or in buffers like PBS (*164*). In contrast, the intracellular diffuse fluorescence was reduced when serum-supplemented medium was used. Interestingly, CyLoP-1 has a completely different behaviour regarding serum. This novel peptide has a good solubility in water but it requires serum for solubility in medium. Under serum-free conditions an insoluble precipitate was observed in solution that settled on cell surfaces. The precipitate stuck to external cell membranes and considerably low cellular delivery was obtained. A concentration of 10% serum in medium was sufficient for attaining a solubility of 5 μM of CyLoP-1. This obligation complicated the mechanistic investigation of uptake (as most chemical inhibitors are effective in serum-free conditions) but provides the opportunity to utilize CyLoP-1 for *in vivo* application. The interaction with serum proteins could perhaps elongate the half-life of this CDV as well.

The internalization of CyLoP-1 might not exclusively involve endocytosis, as incubation of cells at low temperature did not completely abolish its uptake. A reduction of the fluorescence signal was observed after labeling cells at 4 ºC compared to 37 ºC. Fluorescence microscopy revealed that the vesicular transport considerably decreased at low temperature. On the other hand, the diffuse transport into the cytosolic compartment was maintained under the same labeling conditions. Due to the energy dependence, endocytosis could be the main pathway for vesicle-entrapped uptake of CyLoP-1. The diffuse distribution in the cytoplasm could be attributed to an alternate temperature-insensitive entry route. To understand this, the effect of the presence of various drugs like chloroquine, wortmannin, methyl-β-cyclodextrin, sodium azide, etc. that selectively inhibited selective pathways of cellular uptake processes was investigated. No interpretable conclusions could be drawn as all these analyses required the use of serum-free medium but serum was essential for solubility and delivery of CyLoP-1 (data not shown). Another source of the diffuse fluorescence could be a re-distribution of the

endocytically taken up peptide after retrograde transport. It has been shown for crotamine that its cytotoxic effects involve lysosomal leakage which leads to a series of events resulting in cell death (*169*).

Some peptides and proteins have been accounted for permeating cells by forming pores or disrupting the cell membrane (*95, 143, 170*). The membrane lytic activity of CyLoP-1 was evaluated and no indications of the rupture of the phospholipid bilayer were detected. Although, we did perceive that the peptide tends to initially bind cellular membranes and then permeate them. The membrane binding has been reported for other arginine rich CPPs (*171-174*) as well as for the complete toxin crotamine (*175*). Plasma membrane-associated moieties, mainly heparin sulphate proteoglycans and glycosaminoglycans (*53*), interact with the guanidinium groups of arginines and assist the cationic peptides to bind in high amounts to the outer cell membrane. Thus local peptide concentrations are enhanced stimulating uptake of these peptides. As CyLoP-1 is also rich in arginines, a similar interaction with cell-surface carbohydrates and proteins is likely. The SAR studies also highlighted the importance of tryptophan in the uptake and distribution of CyLoP-1. The involvement of tryptophan in membrane permeation has been reported for penetratin.

Apart from arginines and lysines, a unique residue not very common in other CDVs but present in CyLoP-1 is cysteine. Due to problems linked with synthesis and short shelf-life of cysteine-containing peptides, we studied modifications of CyLoP-1 by removal or substitution of this sulphur-containing amino acid (*146*). Significant reductions in cellular delivery along with the removal of cytoplasmic localization of FITC lead to the maintenance of cysteines in CyLoP-1 (data not shown). Also the three disulfide bridges in crotamine have been hypothesized to be responsible for the unique penetration ability (*145*).

The importance of the cysteine residues in CyLoP-1 for uptake and cytosolic distribution made us look for potential intracellular targets which might interact with these groups. Aside of proteins the most prominent cysteine-containing molecule inside cells is the tripeptide glutathione (γ-glutamylcysteinylglycine), an important intracellular reducing agent that participates in various decisive intracellular pathways (*176-178*) e.g. oxidative protection keeping the intracellular environment in a reduced state. Glutathione is directly involved in metabolic and transport functions, thus, amongst others causing the detoxification and inactivation of allogenic substances by conjugation (e.g. via mercapturic acid efflux pathway or direct excretion). To address if the amount of CyLoP-1 delivered into cells might have an

influence on these metabolic pathways, we assessed the effect on the glutathione content after labeling with various concentrations. No reduction was detected in the amount of glutathione even after long term incubations with CyLoP-1, thus verifying that at these concentrations this CPP did not significantly interact with glutathione and did not disturb the protective function of this tripeptide. Similar observation was made for the cysteine-free standard CPP penetratin. The small but not significant increase in glutathione content observed for CyLoP-1 might be due to a direct interaction between the peptide's cysteine groups and the reagent MBBr.

In conclusion, CyLoP-1 is presented as a cysteine-rich CDV derived from crotamine that particularly delivers into the cytosolic compartment of cells. We hypothesize the involvement of two different mechanisms for the uptake of CyLoP-1: 1.) an endocytosis based mechanism that leads to the vesicular delivery of peptide, 2.) a supplementary direct membrane translocation by CyLoP-1 or a re-distribution after retrograde transport of endocytotically taken up peptide. Further detailed investigations at biophysical characterizatios are needed to confirm the exact uptake mechanism(s). Low threshold concentrations required for cellular labeling and transport maintained in the presence of serum recommend the application of CyLoP-1 for *in vivo* applications. This economically sustainable short deca-peptide could be utilized for intracellular delivery of biomolecules like therapeutics or imaging moieties directed to interact with targets located in the cytoplasm. Although with the current investigations it is premature to comment on the intracellular stability of CyLoP-1 and the cargo attached, yet delivery of desired cargo into cells and their release into cytosol is conceivable. Thus, with this peptide we present a novel delivery tool that efficiently evades entrapment into endosomal compartments.

Summary

Noninvasive imaging techniques like MRI possess the prospective to observe molecular-genetic and cellular processes. But the exogenously administered molecular imaging agents are unable to reach their molecular and cellular targets as the lipid bilayer of the cell poses a formidable natural barrier. However, a unique class of peptides known as cell penetrating peptides or CPPs has the ability to traverse this barrier and convey cargo molecules attached to it across the cell membrane. Thus the combination of CPPs with MR/optical agents would permit the evaluation of cellular processes through the interaction of imaging probes with intracellular targets like proteins, mRNA or DNA.

In the first part of the thesis, two mRNA targeting MR based contrast agents were designed using the most efficiently transporting derivative of HIV-1 Tat. *In vitro* cell free studies depicted their ability to selectively bind to complementary oligonucleotide sequence. The agents also showed a significant MR contrast enhancement in labeled cells. However, no specific enrichment was observed in transgenic target containing cells. Some reasons hypothesized to reason the lack of specificity of these agents were the high non-specific binding of the non-sense sequence or the low sensitivity of MRI. But the primary cause could be the entrapment of most of the compound in vesicles, thus, hindering their interaction with specific mRNA.

The second part of the thesis was based on the search for a CPP that could efficiently deliver cargos into the cytosol permitting there interaction with cytosolic targets like mRNA, proteins, etc. Extensive Structure Activity Relationship (SAR) studies were carried out on a putative nuclear localization sequence derived from the main toxin in snake venom. CyLoP-1 was identified as a cysteine rich CPP with distinguished cytosolic diffusion as well as endosomal uptake at low concentrations. Further characterization of the biochemical properties and understanding of the unique intracellular localization of CyLoP-1 was performed. Our results indicate the involvement of two possible mechanisms. One is the endocytosis as reported for several other CPPs and the other could either be a direct delivery across membrane or a re-distribution after retrograde transport. Nevertheless, CyLoP-1 has potential for exploitation as a novel tool for cytosolic delivery of cargos.

References

1. Pfeifer, A., and Verma, I. M. (2001) Gene therapy: promises and problems, *Annu Rev Genomics Hum Genet 2*, 177-211.
2. Willmann, J. K., van Bruggen, N., Dinkelborg, L. M., and Gambhir, S. S. (2008) Molecular imaging in drug development, *Nat Rev Drug Discov 7*, 591-607.
3. Weissleder, R., and Mahmood, U. (2001) Molecular imaging, *Radiology 219*, 316-333.
4. Doubrovin, M., Serganova, I., Mayer-Kuckuk, P., Ponomarev, V., and Blasberg, R. G. (2004) Multimodality in vivo molecular-genetic imaging, *Bioconjug Chem 15*, 1376-1388.
5. Massoud, T. F., and Gambhir, S. S. (2003) Molecular imaging in living subjects: seeing fundamental biological processes in a new light, *Genes Dev 17*, 545-580.
6. Josephson, L., Kircher, M. F., Mahmood, U., Tang, Y., and Weissleder, R. (2002) Near-infrared fluorescent nanoparticles as combined MR/optical imaging probes, *Bioconjug Chem 13*, 554-560.
7. Townsend, D. W. (2001) A combined PET/CT scanner: the choices, *J Nucl Med 42*, 533-534.
8. Jacobs, R. E., and Cherry, S. R. (2001) Complementary emerging techniques: high-resolution PET and MRI, *Curr Opin Neurobiol 11*, 621-629.
9. Merbach, A. E., and Toth, E. (2001) *The Chemistry of Contrast Agents in Medical Magnetic Resonance Imaging*, John Wiley and Sons, New York.
10. Burtea, C., Laurent, S., Vander Elst, L., and Muller, R. N. (2008) Contrast agents: magnetic resonance, *Handb Exp Pharmacol*, 135-165.
11. Koenig, S. H., and Brown, R. D., 3rd. (1987) Relaxometry of magnetic resonance imaging contrast agents, *Magn Reson Annu*, 263-286.
12. Caravan, P., Ellison, J. J., McMurry, T. J., and Lauffer, R. B. (1999) Gadolinium(III) Chelates as MRI Contrast Agents: Structure, Dynamics, and Applications, *Chem Rev 99*, 2293-2352.
13. Sherry, A. D., Cacheris, W. P., and Kuan, K. T. (1988) Stability constants for Gd3+ binding to model DTPA-conjugates and DTPA-proteins: implications for their use as magnetic resonance contrast agents, *Magn Reson Med 8*, 180-190.

14. Weissleder, R., Elizondo, G., Wittenberg, J., Rabito, C. A., Bengele, H. H., and Josephson, L. (1990) Ultrasmall superparamagnetic iron oxide: characterization of a new class of contrast agents for MR imaging, *Radiology 175*, 489-493.
15. Yoo, B., and Pagel, M. D. (2008) An overview of responsive MRI contrast agents for molecular imaging, *Front Biosci 13*, 1733-1752.
16. Aime, S., Cabella, C., Colombatto, S., Geninatti Crich, S., Gianolio, E., and Maggioni, F. (2002) Insights into the use of paramagnetic Gd(III) complexes in MR-molecular imaging investigations, *J Magn Reson Imaging 16*, 394-406.
17. Jasanoff, A. (2007) MRI contrast agents for functional molecular imaging of brain activity, *Curr Opin Neurobiol 17*, 593-600.
18. Artemov, D., Mori, N., Ravi, R., and Bhujwalla, Z. M. (2003) Magnetic resonance molecular imaging of the HER-2/neu receptor, *Cancer Res 63*, 2723-2727.
19. Artemov, D., Mori, N., Okollie, B., and Bhujwalla, Z. M. (2003) MR molecular imaging of the Her-2/neu receptor in breast cancer cells using targeted iron oxide nanoparticles, *Magn Reson Med 49*, 403-408.
20. Lee, J., Burdette, J. E., MacRenaris, K. W., Mustafi, D., Woodruff, T. K., and Meade, T. J. (2007) Rational design, synthesis, and biological evaluation of progesterone-modified MRI contrast agents, *Chem Biol 14*, 824-834.
21. Sharma, V., Luker, G. D., and Piwnica-Worms, D. (2002) Molecular imaging of gene expression and protein function in vivo with PET and SPECT, *J Magn Reson Imaging 16*, 336-351.
22. Lewis, M. R., and Jia, F. (2003) Antisense imaging: and miles to go before we sleep?, *J Cell Biochem 90*, 464-472.
23. Marwick, C. (1998) First "antisense" drug will treat CMV retinitis, *JAMA 280*, 871.
24. Dewanjee, M. K., Ghafouripour, A. K., Kapadvanjwala, M., Dewanjee, S., Serafini, A. N., Lopez, D. M., and Sfakianakis, G. N. (1994) Noninvasive imaging of c-myc oncogene messenger RNA with indium-111-antisense probes in a mammary tumor-bearing mouse model, *J Nucl Med 35*, 1054-1063.
25. Tavitian, B., Terrazzino, S., Kuhnast, B., Marzabal, S., Stettler, O., Dolle, F., Deverre, J. R., Jobert, A., Hinnen, F., Bendriem, B., Crouzel, C., and Di Giamberardino, L. (1998) In vivo imaging of oligonucleotides with positron emission tomography, *Nat Med 4*, 467-471.

26. Lewis, M. R., Jia, F., Gallazzi, F., Wang, Y., Zhang, J., Shenoy, N., Lever, S. Z., and Hannink, M. (2002) Radiometal-labeled peptide-PNA conjugates for targeting bcl-2 expression: preparation, characterization, and in vitro mRNA binding, *Bioconjug Chem 13*, 1176-1180.

27. Liu, C. B., Liu, G. Z., Liu, N., Zhang, Y. M., He, J., Rusckowski, M., and Hnatowich, D. J. (2003) Radiolabeling morpholinos with 90Y, 111In, 188Re and 99mTc, *Nucl Med Biol 30*, 207-214.

28. Hnatowich, D. J. (2000) Antisense imaging: where are we now?, *Cancer Biother Radiopharm 15*, 447-457.

29. Zhang, Y. M., Rusckowski, M., Liu, N., Liu, C., and Hnatowich, D. J. (2001) Cationic liposomes enhance cellular/nuclear localization of 99mTc-antisense oligonucleotides in target tumor cells, *Cancer Biother Radiopharm 16*, 411-419.

30. Nakamura, K., Kubo, A., and Hnatowich, D. J. (2005) Antisense targeting of p-glycoprotein expression in tissue culture, *J Nucl Med 46*, 509-513.

31. Zhang, Y. M., Wang, Y., Liu, N., Zhu, Z. H., Rusckowski, M., and Hnatowich, D. J. (2001) In vitro investigations of tumor targeting with (99m)Tc-labeled antisense DNA, *J Nucl Med 42*, 1660-1669.

32. Hnatowich, D. J., and Nakamura, K. (2004) Antisense targeting in cell culture with radiolabeled DNAs--a brief review of recent progress, *Ann Nucl Med 18*, 363-368.

33. Miller, P. S. (1996) Development of antisense and antigene oligonucleotide analogs, *Prog Nucleic Acid Res Mol Biol 52*, 261-291.

34. Egholm, M., Buchardt, O., Christensen, L., Behrens, C., Freier, S. M., Driver, D. A., Berg, R. H., Kim, S. K., Norden, B., and Nielsen, P. E. (1993) PNA hybridizes to complementary oligonucleotides obeying the Watson-Crick hydrogen-bonding rules, *Nature 365*, 566-568.

35. Summerton, J., and Weller, D. (1997) Morpholino antisense oligomers: design, preparation, and properties, *Antisense Nucleic Acid Drug Dev 7*, 187-195.

36. Efimov, V. A., Buryakova, A. A., and Chakhmakhcheva, O. G. (1999) Synthesis of polyacrylamides N-substituted with PNA-like oligonucleotide mimics for molecular diagnostic applications, *Nucleic Acids Res 27*, 4416-4426.

37. Lubini, P., Zurcher, W., and Egli, M. (1994) Stabilizing effects of the RNA 2'-substituent: crystal structure of an oligodeoxynucleotide duplex containing 2'-O-methylated adenosines, *Chem Biol 1*, 39-45.

38. Shakeel, S., Karim, S. and Ali, A. (2006) Peptide Nucleic Acids (PNA) - a review, *Journal of Chemical Technology and Biotechnology 81*, 892-899.
39. Hyrup, B., and Nielsen, P. E. (1996) Peptide nucleic acids (PNA): synthesis, properties and potential applications, *Bioorg Med Chem 4*, 5-23.
40. Demidov, V. V., Potaman, V. N., Frank-Kamenetskii, M. D., Egholm, M., Buchard, O., Sonnichsen, S. H., and Nielsen, P. E. (1994) Stability of peptide nucleic acids in human serum and cellular extracts, *Biochem Pharmacol 48*, 1310-1313.
41. Berg, J. M., Tymoczko, J. L., Stryer, L., and Clarke, N. D. (2002) *Biochemistry*, Fifth ed., W. H. Freeman and Company, New York.
42. Stephens, D. J., and Pepperkok, R. (2001) The many ways to cross the plasma membrane, *Proc Natl Acad Sci U S A 98*, 4295-4298.
43. Gao, X., Kim, K. S., and Liu, D. (2007) Nonviral gene delivery: what we know and what is next, *AAPS J 9*, E92-104.
44. Anderson, J. L., and Hope, T. J. (2005) Intracellular trafficking of retroviral vectors: obstacles and advances, *Gene Ther 12*, 1667-1678.
45. Sells, M. A., Li, J., and Chernoff, J. (1995) Delivery of protein into cells using polycationic liposomes, *Biotechniques 19*, 72-76, 78.
46. Foerg, C., and Merkle, H. P. (2008) On the biomedical promise of cell penetrating peptides: limits versus prospects, *J Pharm Sci 97*, 144-162.
47. Stewart, K. M., Horton, K. L., and Kelley, S. O. (2008) Cell-penetrating peptides as delivery vehicles for biology and medicine, *Org Biomol Chem 6*, 2242-2255.
48. Torchilin, V. P., Levchenko, T. S., Rammohan, R., Volodina, N., Papahadjopoulos-Sternberg, B., and D'Souza, G. G. (2003) Cell transfection in vitro and in vivo with nontoxic TAT peptide-liposome-DNA complexes, *Proc Natl Acad Sci U S A 100*, 1972-1977.
49. Schwarze, S. R., Ho, A., Vocero-Akbani, A., and Dowdy, S. F. (1999) In vivo protein transduction: delivery of a biologically active protein into the mouse, *Science 285*, 1569-1572.
50. Derossi, D., Joliot, A. H., Chassaing, G., and Prochiantz, A. (1994) The third helix of the Antennapedia homeodomain translocates through biological membranes, *J Biol Chem 269*, 10444-10450.
51. Futaki, S., Suzuki, T., Ohashi, W., Yagami, T., Tanaka, S., Ueda, K., and Sugiura, Y. (2001) Arginine-rich peptides. An abundant source of membrane-permeable peptides

having potential as carriers for intracellular protein delivery, *J Biol Chem 276*, 5836-5840.

52. Pooga, M., Hallbrink, M., Zorko, M., and Langel, U. (1998) Cell penetration by transportan, *FASEB J 12*, 67-77.
53. Fuchs, S. M., and Raines, R. T. (2006) Internalization of cationic peptides: the road less (or more?) traveled, *Cell Mol Life Sci 63*, 1819-1822.
54. Derossi, D., Calvet, S., Trembleau, A., Brunissen, A., Chassaing, G., and Prochiantz, A. (1996) Cell internalization of the third helix of the Antennapedia homeodomain is receptor-independent, *J Biol Chem 271*, 18188-18193.
55. Brugidou, J., Legrand, C., Mery, J., and Rabie, A. (1995) The retro-inverso form of a homeobox-derived short peptide is rapidly internalised by cultured neurones: a new basis for an efficient intracellular delivery system, *Biochem Biophys Res Commun 214*, 685-693.
56. Wender, P. A., Mitchell, D. J., Pattabiraman, K., Pelkey, E. T., Steinman, L., and Rothbard, J. B. (2000) The design, synthesis, and evaluation of molecules that enable or enhance cellular uptake: peptoid molecular transporters, *Proc Natl Acad Sci U S A 97*, 13003-13008.
57. Fischer, R., Kohler, K., Fotin-Mleczek, M., and Brock, R. (2004) A stepwise dissection of the intracellular fate of cationic cell-penetrating peptides, *J Biol Chem 279*, 12625-12635.
58. Duchardt, F., Fotin-Mleczek, M., Schwarz, H., Fischer, R., and Brock, R. (2007) A comprehensive model for the cellular uptake of cationic cell-penetrating peptides, *Traffic 8*, 848-866.
59. Shahana, S., Kampf, C., and Roomans, G. M. (2002) Effects of the cationic protein poly-L-arginine on airway epithelial cells in vitro, *Mediators Inflamm 11*, 141-148.
60. Bonavia, R., Bajetto, A., Barbero, S., Albini, A., Noonan, D. M., and Schettini, G. (2001) HIV-1 Tat causes apoptotic death and calcium homeostasis alterations in rat neurons, *Biochem Biophys Res Commun 288*, 301-308.
61. Benjouad, A., Mabrouk, K., Moulard, M., Gluckman, J. C., Rochat, H., Van Rietschoten, J., and Sabatier, J. M. (1993) Cytotoxic effect on lymphocytes of Tat from human immunodeficiency virus (HIV-1), *FEBS Lett 319*, 119-124.
62. Lundberg, M., and Johansson, M. (2001) Is VP22 nuclear homing an artifact?, *Nat Biotechnol 19*, 713-714.

63. Richard, J. P., Melikov, K., Vives, E., Ramos, C., Verbeure, B., Gait, M. J., Chernomordik, L. V., and Lebleu, B. (2003) Cell-penetrating peptides. A reevaluation of the mechanism of cellular uptake, *J Biol Chem 278*, 585-590.

64. Bhorade, R., Weissleder, R., Nakakoshi, T., Moore, A., and Tung, C. H. (2000) Macrocyclic chelators with paramagnetic cations are internalized into mammalian cells via a HIV-tat derived membrane translocation peptide, *Bioconjug Chem 11*, 301-305.

65. Prantner, A. M., Sharma, V., Garbow, J. R., and Piwnica-Worms, D. (2003) Synthesis and characterization of a Gd-DOTA-D-permeation peptide for magnetic resonance relaxation enhancement of intracellular targets, *Mol Imaging 2*, 333-341.

66. Allen, M. J., MacRenaris, K. W., Venkatasubramanian, P. N., and Meade, T. J. (2004) Cellular delivery of MRI contrast agents, *Chem Biol 11*, 301-307.

67. Allen, M. J., and Meade, T. J. (2003) Synthesis and visualization of a membrane-permeable MRI contrast agent, *J Biol Inorg Chem 8*, 746-750.

68. Heckl, S., Pipkorn, R., Waldeck, W., Spring, H., Jenne, J., von der Lieth, C. W., Corban-Wilhelm, H., Debus, J., and Braun, K. (2003) Intracellular visualization of prostate cancer using magnetic resonance imaging, *Cancer Res 63*, 4766-4772.

69. Min, J. J., and Gambhir, S. S. (2004) Gene therapy progress and prospects: noninvasive imaging of gene therapy in living subjects, *Gene Ther 11*, 115-125.

70. Weinmann, H. J., Ebert, W., Misselwitz, B., and Schmitt-Willich, H. (2003) Tissue-specific MR contrast agents, *Eur J Radiol 46*, 33-44.

71. Karabulut, N., and Elmas, N. (2006) Contrast agents used in MR imaging of the liver, *Diagn Interv Radiol 12*, 22-30.

72. Towner, R. A., Smith, N., Doblas, S., Tesiram, Y., Garteiser, P., Saunders, D., Cranford, R., Silasi-Mansat, R., Herlea, O., Ivanciu, L., Wu, D., and Lupu, F. (2008) In vivo detection of c-Met expression in a rat C6 glioma model, *J Cell Mol Med 12*, 174-186.

73. Wang, Z. J., Boddington, S., Wendland, M., Meier, R., Corot, C., and Daldrup-Link, H. (2008) MR imaging of ovarian tumors using folate-receptor-targeted contrast agents, *Pediatr Radiol 38*, 529-537.

74. Woolf, T. M., Melton, D. A., and Jennings, C. G. (1992) Specificity of antisense oligonucleotides in vivo, *Proc Natl Acad Sci U S A 89*, 7305-7309.

75. Sazani, P., Gemignani, F., Kang, S. H., Maier, M. A., Manoharan, M., Persmark, M., Bortner, D., and Kole, R. (2002) Systemically delivered antisense oligomers upregulate gene expression in mouse tissues, *Nat Biotechnol 20*, 1228-1233.

76. Sazani, P., Astriab-Fischer, A., and Kole, R. (2003) Effects of base modifications on antisense properties of 2'-O-methoxyethyl and PNA oligonucleotides, *Antisense Nucleic Acid Drug Dev 13*, 119-128.

77. Younes, C. K., Boisgard, R., and Tavitian, B. (2002) Labelled oligonucleotides as radiopharmaceuticals: pitfalls, problems and perspectives, *Curr Pharm Des 8*, 1451-1466.

78. Nielsen, P. E., Egholm, M., Berg, R. H., and Buchardt, O. (1991) Sequence-selective recognition of DNA by strand displacement with a thymine-substituted polyamide, *Science 254*, 1497-1500.

79. Larsen, H. J., Bentin, T., and Nielsen, P. E. (1999) Antisense properties of peptide nucleic acid, *Biochim Biophys Acta 1489*, 159-166.

80. Paulasova, P., Andreo, B., Diblik, J., Macek, M., and Pellestor, F. (2004) The peptide nucleic acids as probes for chromosomal analysis: application to human oocytes, polar bodies and preimplantation embryos, *Mol Hum Reprod 10*, 467-472.

81. Tian, X., Aruva, M. R., Qin, W., Zhu, W., Sauter, E. R., Thakur, M. L., and Wickstrom, E. (2005) Noninvasive molecular imaging of MYC mRNA expression in human breast cancer xenografts with a [99mTc]peptide-peptide nucleic acid-peptide chimera, *Bioconjug Chem 16*, 70-79.

82. McMahon, B. M., Stewart, J., Fauq, A., Younkin, S., Younkin, L., and Richelson, E. (2002) Using peptide nucleic acids as gene-expression modifiers to reduce beta-amyloid levels, *J Mol Neurosci 19*, 71-76.

83. Baird, G. S., Zacharias, D. A., and Tsien, R. Y. (2000) Biochemistry, mutagenesis, and oligomerization of DsRed, a red fluorescent protein from coral, *Proc Natl Acad Sci U S A 97*, 11984-11989.

84. Mologni, L., Marchesi, E., Nielsen, P. E., and Gambacorti-Passerini, C. (2001) Inhibition of promyelocytic leukemia (PML)/retinoic acid receptor-alpha and PML expression in acute promyelocytic leukemia cells by anti-PML peptide nucleic acid, *Cancer Res 61*, 5468-5473.

85. Coester, C., Kreuter, J., von Briesen, H., and Langer, K. (2000) Preparation of avidin-labelled gelatin nanoparticles as carriers for biotinylated peptide nucleic acid (PNA), *Int J Pharm 196*, 147-149.

86. Shi, N., Boado, R. J., and Pardridge, W. M. (2000) Antisense imaging of gene expression in the brain in vivo, *Proc Natl Acad Sci U S A 97*, 14709-14714.

87. Gait, M. J. (2003) Peptide-mediated cellular delivery of antisense oligonucleotides and their analogues, *Cell Mol Life Sci 60*, 844-853.

88. Lindgren, M., Hallbrink, M., Prochiantz, A., and Langel, U. (2000) Cell-penetrating peptides, *Trends Pharmacol Sci 21*, 99-103.

89. Kersemans, V., Kersemans, K., and Cornelissen, B. (2008) Cell penetrating peptides for in vivo molecular imaging applications, *Curr Pharm Des 14*, 2415-2447.

90. Derossi, D., Chassaing, G., and Prochiantz, A. (1998) Trojan peptides: the penetratin system for intracellular delivery, *Trends Cell Biol 8*, 84-87.

91. Mae, M., and Langel, U. (2006) Cell-penetrating peptides as vectors for peptide, protein and oligonucleotide delivery, *Curr Opin Pharmacol 6*, 509-514.

92. Zhao, M., and Weissleder, R. (2004) Intracellular cargo delivery using tat peptide and derivatives, *Med Res Rev 24*, 1-12.

93. Howl, J., Nicholl, I. D., and Jones, S. (2007) The many futures for cell-penetrating peptides: how soon is now?, *Biochem Soc Trans 35*, 767-769.

94. Zorko, M., and Langel, U. (2005) Cell-penetrating peptides: mechanism and kinetics of cargo delivery, *Adv Drug Deliv Rev 57*, 529-545.

95. El-Andaloussi, S., Jarver, P., Johansson, H. J., and Langel, U. (2007) Cargo-dependent cytotoxicity and delivery efficacy of cell-penetrating peptides: a comparative study, *Biochem J 407*, 285-292.

96. Wacnik, P. W., Baker, C. M., Herron, M. J., Kren, B. T., Blazar, B. R., Wilcox, G. L., Hordinsky, M. K., Beitz, A. J., and Ericson, M. E. (2005) Tumor-induced mechanical hyperalgesia involves CGRP receptors and altered innervation and vascularization of DsRed2 fluorescent hindpaw tumors, *Pain 115*, 95-106.

97. Aarons, R. J., Notta, J. K., Meloni, M. M., Feng, J., Vidyasagar, R., Narvainen, J., Allan, S., Spencer, N., Kauppinen, R. A., Snaith, J. S., and Faulkner, S. (2006) A luminescent probe containing a tuftsin targeting vector coupled to a terbium complex, *Chem Commun (Camb)*, 909-911.

98. Kelly, K. A., Reynolds, F., Weissleder, R., and Josephson, L. (2004) Fluorescein isothiocyanate-hapten immunoassay for determination of peptide-cell interactions, *Anal Biochem 330*, 181-185.

99. Perry-O'Keefe, H., Yao, X. W., Coull, J. M., Fuchs, M., and Egholm, M. (1996) Peptide nucleic acid pre-gel hybridization: an alternative to southern hybridization, *Proc Natl Acad Sci U S A 93*, 14670-14675.

100. Rennert, R., Wespe, C., Beck-Sickinger, A. G., and Neundorf, I. (2006) Developing novel hCT derived cell-penetrating peptides with improved metabolic stability, *Biochim Biophys Acta 1758*, 347-354.

101. Gammon, S. T., Villalobos, V. M., Prior, J. L., Sharma, V., and Piwnica-Worms, D. (2003) Quantitative analysis of permeation peptide complexes labeled with Technetium-99m: chiral and sequence-specific effects on net cell uptake, *Bioconjug Chem 14*, 368-376.

102. Wright, L. R., Rothbard, J. B., and Wender, P. A. (2003) Guanidinium rich peptide transporters and drug delivery, *Curr Protein Pept Sci 4*, 105-124.

103. Oehlke, J., Wallukat, G., Wolf, Y., Ehrlich, A., Wiesner, B., Berger, H., and Bienert, M. (2004) Enhancement of intracellular concentration and biological activity of PNA after conjugation with a cell-penetrating synthetic model peptide, *Eur J Biochem 271*, 3043-3049.

104. Su, W., Mishra, R., Pfeuffer, J., Wiesmuller, K. H., Ugurbil, K., and Engelmann, J. (2007) Synthesis and cellular uptake of a MR contrast agent coupled to an antisense peptide nucleic acid--cell- penetrating peptide conjugate, *Contrast Media Mol Imaging 2*, 42-49.

105. Endres, P. J., Macrenaris, K. W., Vogt, S., and Meade, T. J. (2008) Cell-Permeable MR Contrast Agents with Increased Intracellular Retention, *Bioconjug Chem*.

106. Zech, S. G., Eldredge, H. B., Lowe, M. P., and Caravan, P. (2007) Protein binding to lanthanide(III) complexes can reduce the water exchange rate at the lanthanide, *Inorg Chem 46*, 3576-3584.

107. Neil, M. A., Juskaitis, R., and Wilson, T. (1997) Method of obtaining optical sectioning by using structured light in a conventional microscope, *Opt Lett 22*, 1905-1907.

108. Jones, S. W., Christison, R., Bundell, K., Voyce, C. J., Brockbank, S. M., Newham, P., and Lindsay, M. A. (2005) Characterisation of cell-penetrating peptide-mediated peptide delivery, *Br J Pharmacol 145*, 1093-1102.

109. Sun, X., Fang, H., Li, X., Rossin, R., Welch, M. J., and Taylor, J. S. (2005) MicroPET imaging of MCF-7 tumors in mice via unr mRNA-targeted peptide nucleic acids, *Bioconjug Chem 16*, 294-305.

110. Chauhan, A., Tikoo, A., Kapur, A. K., and Singh, M. (2007) The taming of the cell penetrating domain of the HIV Tat: myths and realities, *J Control Release 117*, 148-162.

111. Gump, J. M., and Dowdy, S. F. (2007) TAT transduction: the molecular mechanism and therapeutic prospects, *Trends Mol Med 13*, 443-448.

112. Futaki, S., Nakase, I., Tadokoro, A., Takeuchi, T., and Jones, A. T. (2007) Arginine-rich peptides and their internalization mechanisms, *Biochem Soc Trans 35*, 784-787.

113. Jia, F., Figueroa, S. D., Gallazzi, F., Balaji, B. S., Hannink, M., Lever, S. Z., Hoffman, T. J., and Lewis, M. R. (2008) Molecular imaging of bcl-2 expression in small lymphocytic lymphoma using 111In-labeled PNA-peptide conjugates, *J Nucl Med 49*, 430-438.

114. Tripathi, S., Chaubey, B., Ganguly, S., Harris, D., Casale, R. A., and Pandey, V. N. (2005) Anti-HIV-1 activity of anti-TAR polyamide nucleic acid conjugated with various membrane transducing peptides, *Nucleic Acids Res 33*, 4345-4356.

115. Morris, M. C., Chaloin, L., Choob, M., Archdeacon, J., Heitz, F., and Divita, G. (2004) Combination of a new generation of PNAs with a peptide-based carrier enables efficient targeting of cell cycle progression, *Gene Ther 11*, 757-764.

116. Abes, S., Williams, D., Prevot, P., Thierry, A., Gait, M. J., and Lebleu, B. (2006) Endosome trapping limits the efficiency of splicing correction by PNA-oligolysine conjugates, *J Control Release 110*, 595-604.

117. Turner, J. J., Ivanova, G. D., Verbeure, B., Williams, D., Arzumanov, A. A., Abes, S., Lebleu, B., and Gait, M. J. (2005) Cell-penetrating peptide conjugates of peptide nucleic acids (PNA) as inhibitors of HIV-1 Tat-dependent trans-activation in cells, *Nucleic Acids Res 33*, 6837-6849.

118. Fischer, P. M. (2007) Cellular uptake mechanisms and potential therapeutic utility of peptidic cell delivery vectors: progress 2001-2006, *Med Res Rev 27*, 755-795.

119. Green, M., and Loewenstein, P. M. (1988) Autonomous functional domains of chemically synthesized human immunodeficiency virus tat trans-activator protein, *Cell 55*, 1179-1188.

120. Frankel, A. D., and Pabo, C. O. (1988) Cellular uptake of the tat protein from human immunodeficiency virus, *Cell 55*, 1189-1193.

121. Joliot, A., Pernelle, C., Deagostini-Bazin, H., and Prochiantz, A. (1991) Antennapedia homeobox peptide regulates neural morphogenesis, *Proc Natl Acad Sci U S A 88*, 1864-1868.

122. Deshayes, S., Morris, M. C., Divita, G., and Heitz, F. (2005) Cell-penetrating peptides: tools for intracellular delivery of therapeutics, *Cell Mol Life Sci 62*, 1839-1849.

123. Wadia, J. S., and Dowdy, S. F. (2002) Protein transduction technology, *Curr Opin Biotechnol 13*, 52-56.

124. Kilic, U., Kilic, E., Dietz, G. P., and Bahr, M. (2003) Intravenous TAT-GDNF is protective after focal cerebral ischemia in mice, *Stroke 34*, 1304-1310.

125. Hotchkiss, R. S., McConnell, K. W., Bullok, K., Davis, C. G., Chang, K. C., Schwulst, S. J., Dunne, J. C., Dietz, G. P., Bahr, M., McDunn, J. E., Karl, I. E., Wagner, T. H., Cobb, J. P., Coopersmith, C. M., and Piwnica-Worms, D. (2006) TAT-BH4 and TAT-Bcl-xL peptides protect against sepsis-induced lymphocyte apoptosis in vivo, *J Immunol 176*, 5471-5477.

126. Bullok, K. E., Dyszlewski, M., Prior, J. L., Pica, C. M., Sharma, V., and Piwnica-Worms, D. (2002) Characterization of novel histidine-tagged Tat-peptide complexes dual-labeled with (99m)Tc-tricarbonyl and fluorescein for scintigraphy and fluorescence microscopy, *Bioconjug Chem 13*, 1226-1237.

127. Leifert, J. A., Harkins, S., and Whitton, J. L. (2002) Full-length proteins attached to the HIV tat protein transduction domain are neither transduced between cells, nor exhibit enhanced immunogenicity, *Gene Ther 9*, 1422-1428.

128. Andrade, D. M., Scherer, S. W., and Minassian, B. A. (2006) Protein therapy for Unverricht-Lundborg disease using cystatin B transduction by TAT-PTD. Is it that simple?, *Epilepsy Res 72*, 75-79.

129. Koppelhus, U., Awasthi, S. K., Zachar, V., Holst, H. U., Ebbesen, P., and Nielsen, P. E. (2002) Cell-dependent differential cellular uptake of PNA, peptides, and PNA-peptide conjugates, *Antisense Nucleic Acid Drug Dev 12*, 51-63.

130. Falnes, P. O., Wesche, J., and Olsnes, S. (2001) Ability of the Tat basic domain and VP22 to mediate cell binding, but not membrane translocation of the diphtheria toxin A-fragment, *Biochemistry 40*, 4349-4358.

131. Fischer, R., Fotin-Mleczek, M., Hufnagel, H., and Brock, R. (2005) Break on through to the other side-biophysics and cell biology shed light on cell-penetrating peptides, *Chembiochem 6*, 2126-2142.

132. Wadia, J. S., Stan, R. V., and Dowdy, S. F. (2004) Transducible TAT-HA fusogenic peptide enhances escape of TAT-fusion proteins after lipid raft macropinocytosis, *Nat Med 10*, 310-315.

133. Yang, S., Coles, D. J., Esposito, A., Mitchell, D. J., Toth, I., and Minchin, R. F. (2009) Cellular uptake of self-assembled cationic peptide-DNA complexes: Multifunctional role of the enhancer chloroquine, *J Control Release*.

134. Shiraishi, T., Pankratova, S., and Nielsen, P. E. (2005) Calcium ions effectively enhance the effect of antisense peptide nucleic acids conjugated to cationic tat and oligoarginine peptides, *Chem Biol 12*, 923-929.

135. Michiue, H., Tomizawa, K., Wei, F. Y., Matsushita, M., Lu, Y. F., Ichikawa, T., Tamiya, T., Date, I., and Matsui, H. (2005) The NH2 terminus of influenza virus hemagglutinin-2 subunit peptides enhances the antitumor potency of polyarginine-mediated p53 protein transduction, *J Biol Chem 280*, 8285-8289.

136. Takeuchi, T., Kosuge, M., Tadokoro, A., Sugiura, Y., Nishi, M., Kawata, M., Sakai, N., Matile, S., and Futaki, S. (2006) Direct and rapid cytosolic delivery using cell-penetrating peptides mediated by pyrenebutyrate, *ACS Chem Biol 1*, 299-303.

137. El-Sayed, A., Futaki, S., and Harashima, H. (2009) Delivery of Macromolecules Using Arginine-Rich Cell-Penetrating Peptides: Ways to Overcome Endosomal Entrapment, *AAPS J*.

138. Chauhan, A., Turchan, J., Pocernich, C., Bruce-Keller, A., Roth, S., Butterfield, D. A., Major, E. O., and Nath, A. (2003) Intracellular human immunodeficiency virus Tat expression in astrocytes promotes astrocyte survival but induces potent neurotoxicity at distant sites via axonal transport, *J Biol Chem 278*, 13512-13519.

139. Brask, J., Chauhan, A., Hill, R. H., Ljunggren, H. G., and Kristensson, K. (2005) Effects on synaptic activity in cultured hippocampal neurons by influenza A viral proteins, *J Neurovirol 11*, 395-402.

140. Lord, J. M., Deeks, E., Marsden, C. J., Moore, K., Pateman, C., Smith, D. C., Spooner, R. A., Watson, P., and Roberts, L. M. (2003) Retrograde transport of toxins across the endoplasmic reticulum membrane, *Biochem Soc Trans 31*, 1260-1262.

141. Rádis-Baptista, G., Kerkis, A., Prieto-Silva, A. R., Hayashi, M. A. F., Kerkis, I., and Yamane, T. (2008) Membrane-translocating Peptides and Toxins: from Nature to Bedside, *Journal of Brazilian Chemical Society 19*, 211-225.

142. Sandvig, K., and van Deurs, B. (2005) Delivery into cells: lessons learned from plant and bacterial toxins, *Gene Ther 12*, 865-872.

143. Ogris, M., Carlisle, R. C., Bettinger, T., and Seymour, L. W. (2001) Melittin enables efficient vesicular escape and enhanced nuclear access of nonviral gene delivery vectors, *J Biol Chem 276*, 47550-47555.

144. Wada, S., Hitora, Y., Tanaka, R., and Urata, H. (2008) Translocation of an Aib-containing peptide through cell membranes, *Bioorg Med Chem Lett 18*, 3999-4001.

145. Kerkis, A., Kerkis, I., Radis-Baptista, G., Oliveira, E. B., Vianna-Morgante, A. M., Pereira, L. V., and Yamane, T. (2004) Crotamine is a novel cell-penetrating protein from the venom of rattlesnake Crotalus durissus terrificus, *FASEB J 18*, 1407-1409.

146. Ugurbil, K., Jha, D., Engelmann, J., Mishra, R., and Wiesmueller, K.-H. (2008) Identification of a novel cysteine-rich cell penetrating peptide.

147. Sahlin, S., Hed, J., and Rundquist, I. (1983) Differentiation between attached and ingested immune complexes by a fluorescence quenching cytofluorometric assay, *J Immunol Methods 60*, 115-124.

148. Engelmann, J., Volk, J., Leyhausen, G., and Geurtsen, W. (2005) ROS formation and glutathione levels in human oral fibroblasts exposed to TEGDMA and camphorquinone, *J Biomed Mater Res B Appl Biomater 75*, 272-276.

149. Andreu, D., Albericio, F., Solé, N. A., Munson, M. C., Ferrer, M., and Barany, G. (1994) *Peptide Synthesis Protocols, Methods in Molecular Biology*, Vol. 35, Humana Press Inc., Totowa, NJ

150. Siedler, F., Weyher, E., and Moroder, L. (1996) Cysteine racemization in peptide synthesis: a new and easy detection method, *J Pept Sci 2*, 271-275.

151. Huang, H., and Rabenstein, D. L. (1999) A cleavage cocktail for methionine-containing peptides, *J Pept Res 53*, 548-553.

152. Wunsch, E., Jaeger, E., Kisfaludy, L., and Low. (1977) Side reactions in peptide synthesis: ter-butylation of tryptophan, *Angew Chem Int Ed Engl 16*, 317-318.

153. Giraud, M., Cavelier, F., and Martinez, J. (1999) A side-reaction in the SPPS of Trp-containing peptides, *J Pept Sci 5*, 457-461.

154. Rueping, M., Mahajan, Y., Sauer, M., and Seebach, D. (2002) Cellular uptake studies with beta-peptides, *Chembiochem 3*, 257-259.

155. Karim, C. B., Paterlini, M. G., Reddy, L. G., Hunter, G. W., Barany, G., and Thomas, D. D. (2001) Role of cysteine residues in structural stability and function of a transmembrane helix bundle, *J Biol Chem 276*, 38814-38819.

156. Moroder, L. (2005) Isosteric replacement of sulfur with other chalcogens in peptides and proteins, *J Pept Sci 11*, 187-214.

157. Dom, G., Shaw-Jackson, C., Matis, C., Bouffioux, O., Picard, J. J., Prochiantz, A., Mingeot-Leclercq, M. P., Brasseur, R., and Rezsohazy, R. (2003) Cellular uptake of Antennapedia Penetratin peptides is a two-step process in which phase transfer precedes a tryptophan-dependent translocation, *Nucleic Acids Res 31*, 556-561.

158. Goncalves, J. M., and Deutsch, H. F. (1956) Ultracentrifugal and zone electrophoresis studies of some crotalidae venoms, *Arch Biochem Biophys 60*, 402-411.

159. Radis-Baptista, G., de la Torre, B. G., and Andreu, D. (2008) A novel cell-penetrating peptide sequence derived by structural minimization of a snake toxin exhibits preferential nucleolar localization, *J Med Chem 51*, 7041-7044.

160. Kim, D., Jeon, C., Kim, J. H., Kim, M. S., Yoon, C. H., Choi, I. S., Kim, S. H., and Bae, Y. S. (2006) Cytoplasmic transduction peptide (CTP): new approach for the delivery of biomolecules into cytoplasm in vitro and in vivo, *Exp Cell Res 312*, 1277-1288.

161. Hariton-Gazal, E., Feder, R., Mor, A., Graessmann, A., Brack-Werner, R., Jans, D., Gilon, C., and Loyter, A. (2002) Targeting of nonkaryophilic cell-permeable peptides into the nuclei of intact cells by covalently attached nuclear localization signals, *Biochemistry 41*, 9208-9214.

162. Bais, M. V., Kumar, S., Tiwari, A. K., Kataria, R. S., Nagaleekar, V. K., Shrivastava, S., and Chindera, K. (2008) Novel Rath peptide for intracellular delivery of protein and nucleic acids, *Biochem Biophys Res Commun 370*, 27-32.

163. Kobayashi, S., Nakase, I., Kawabata, N., Yu, H. H., Pujals, S., Imanishi, M., Giralt, E., and Futaki, S. (2009) Cytosolic Targeting of Macromolecules Using a pH-Dependent Fusogenic Peptide in Combination with Cationic Liposomes, *Bioconjug Chem*.

164. Kosuge, M., Takeuchi, T., Nakase, I., Jones, A. T., and Futaki, S. (2008) Cellular internalization and distribution of arginine-rich peptides as a function of extracellular peptide concentration, serum, and plasma membrane associated proteoglycans, *Bioconjug Chem 19*, 656-664.

165. Scudiero, D. A., Shoemaker, R. H., Paull, K. D., Monks, A., Tierney, S., Nofziger, T. H., Currens, M. J., Seniff, D., and Boyd, M. R. (1988) Evaluation of a soluble tetrazolium/formazan assay for cell growth and drug sensitivity in culture using human and other tumor cell lines, *Cancer Res 48*, 4827-4833.

166. Berridge, M. V., Herst, P. M., and Tan, A. S. (2005) Tetrazolium dyes as tools in cell biology: new insights into their cellular reduction, *Biotechnol Annu Rev 11*, 127-152.

167. Puttonen, K. A., Lehtonen, S., Lampela, P., Mannisto, P. T., and Raasmaja, A. (2008) Different viabilities and toxicity types after 6-OHDA and Ara-C exposure evaluated by four assays in five cell lines, *Toxicol In Vitro 22*, 182-189.

168. Aras, M. A., Hartnett, K. A., and Aizenman, E. (2008) Assessment of cell viability in primary neuronal cultures, *Curr Protoc Neurosci Chapter 7*, Unit 7 18.

169. Hayashi, M. A., Nascimento, F. D., Kerkis, A., Oliveira, V., Oliveira, E. B., Pereira, A., Radis-Baptista, G., Nader, H. B., Yamane, T., Kerkis, I., and Tersariol, I. L. (2008) Cytotoxic effects of crotamine are mediated through lysosomal membrane permeabilization, *Toxicon 52*, 508-517.

170. Palm-Apergi, C., Lorents, A., Padari, K., Pooga, M., and Hallbrink, M. (2009) The membrane repair response masks membrane disturbances caused by cell-penetrating peptide uptake, *FASEB J 23*, 214-223.

171. Nakase, I., Tadokoro, A., Kawabata, N., Takeuchi, T., Katoh, H., Hiramoto, K., Negishi, M., Nomizu, M., Sugiura, Y., and Futaki, S. (2007) Interaction of arginine-rich peptides with membrane-associated proteoglycans is crucial for induction of actin organization and macropinocytosis, *Biochemistry 46*, 492-501.

172. Console, S., Marty, C., Garcia-Echeverria, C., Schwendener, R., and Ballmer-Hofer, K. (2003) Antennapedia and HIV transactivator of transcription (TAT) "protein transduction domains" promote endocytosis of high molecular weight cargo upon binding to cell surface glycosaminoglycans, *J Biol Chem 278*, 35109-35114.

173. Ziegler, A., and Seelig, J. (2004) Interaction of the protein transduction domain of HIV-1 TAT with heparan sulfate: binding mechanism and thermodynamic parameters, *Biophys J 86*, 254-263.

174. Nakase, I., Takeuchi, T., Tanaka, G., and Futaki, S. (2008) Methodological and cellular aspects that govern the internalization mechanisms of arginine-rich cell-penetrating peptides, *Adv Drug Deliv Rev 60*, 598-607.

175. Nascimento, F. D., Hayashi, M. A., Kerkis, A., Oliveira, V., Oliveira, E. B., Radis-Baptista, G., Nader, H. B., Yamane, T., Tersariol, I. L., and Kerkis, I. (2007) Crotamine mediates gene delivery into cells through the binding to heparan sulfate proteoglycans, *J Biol Chem 282*, 21349-21360.

176. Cooper, A. J., and Kristal, B. S. (1997) Multiple roles of glutathione in the central nervous system, *Biol Chem 378*, 793-802.

177. Meister, A. (1995) Glutathione metabolism, *Methods Enzymol 251*, 3-7.

178. Meister, A., and Anderson, M. E. (1983) Glutathione, *Annu Rev Biochem 52*, 711-760.

Publication list

The following articles and manuscripts are based on the work done under this PhD thesis:

I. W. Su, **R. Mishra**, J. Pfeuffer, K. H. Wiesmüller, K. Ugurbil and J. Engelmann: Synthesis and Cellular Uptake of a MR Contrast Agent Coupled to an Antisense Peptide Nucleic Acid - Cell Penetrating Peptide Conjugate. *Contrast Media & Molecular Imaging*, *2*, 42-49 (2007).

II. **R. Mishra**, W. Su, R. Pohmann, M. G. Sauer, J. Pfeuffer, K. Ugurbil and J. Engelmann: Cell Penetrating Peptides and Peptide Nucleic Acid Coupled MRI Contrast Agents: Evaluation of Cellular Delivery and Target Binding. *Bioconjugate Chemistry*, 20, 1860-1868 (2009).

III. **R. Mishra**, D. Jha, K. Ugurbil and J. Engelmann: Novel Cysteine Rich Cell Penetrating Peptide CyLoP-1: Understanding the delivery in cytosol. (In preparation).

IV. D. Jha, **R. Mishra**, K. Ugurbil, M. E. Maier, K. H. Wiesmüller and J. Engelmann: Development of a Novel Cysteine Rich Cell Penetrating Peptide: Efficient Uptake and Access to Cytosol. (In preparation).

The following articles are based on miscellaneous projects performed during the duration of this PhD thesis:

V. A. Mishra, J. Pfeuffer, **R. Mishra**, J. Engelmann, A. K. Mishra, K. Ugurbil and N. K. Logothetis: A New Class of Gd-based DO3A-ethylamine-derived Targeted Contrast Agents for MR and Optical Imaging. *Bioconjugate Chemistry 17*, 773-780 (2006).

VI. R. Joshi, **R. Mishra**, W. Su and J. Engelmann: CPP or cholesterol conjugation to antisense PNA for cellular delivery. *Peptides 2008, Proceedings of the 30th European Peptide Symposium Science, Helsinki, 548-549, electric publication number 4-19-12* (in press) (2009).

Contribution of authors:

R. Mishra: Development and planning of biological studies, data collection, data analysis (I- VI), preparation of chapters for publication (II, III and parts of IV and V).

W. Su: Development and planning of chemistry studies, data collection (I and II and parts of VI), preparation of chapters for publication (I).

D. Jha: Development and planning of chemistry studies, data collection (III and IV), preparation of chapters for publication (IV).

A. Mishra: Development and planning of chemistry studies, data collection (V), preparation of chapters for publication (V).

R. Joshi: Development and planning of chemical studies, data collection (VI), preparation of chapters for publication (VI).

R. Pohmann: Planning of MR studies, data collection (II).

J. Engelmann: Supervision of chemistry and biology studies, participation in experimental analysis, and in manuscript preparation of all studies (I-VI).

K. Ugurbil: Initial ideas and supervision of studies (I-IV and VI).

N. K. Logothetis: Initial ideas and supervision of studies (V).

J. Pfeuffer: Initial idea and planning for MR studies (I, II and V).

M. G. Sauer: Initial idea (II).

K. H. Wiesmüller: Supervision for chemistry (I and IV).

M. E. Maier: Provision of analytical facility (IV).

A. K. Mishra: Support and discussion (V).

Curriculum Vitae

Personal Details

Name	Ritu Mishra
Date and place of birth	April, 18, 1979. Bathinda
Citizenship	Indian
Family Status	Married, have a daughter

Education

PhD thesis (April 2004 till now)

Faculty of Biology, Eberhard Karls Universitaet Tuebingen, Tuebingen, Germany

Master in Science (Biotechnology) (July 2000 to June 2002)

Thapar Institute of Engineering and Technology (Deemed University), Patiala, India.

Score of the exam. 88.6% (9.85 C.G.P.A. out of 10) aggregate

Bachelor in Science (Biotechnology) July 1997 to June 2000.

Mukand Lal National College, Kurukshetra University, Yamunanagar, India.

Score of the exam. 69.4% aggregate

Professional Experience

Research Biologist (August 2002 to February 2004)

Radioligand Enzyme Assay Laboratory, Pharmacology Department, NDDR, Ranbaxy Research Labs. Ltd., Gurgaon, India